Estimation of Transition Probabilities by Laser-Induced Breakdown Spectroscopy for the Expanded Application of Calibration Free Methods

A Thesis Presented for the
Master of Science
Degree
The University of Tennessee, Knoxville

Sawyer Blue Irvine
August 2022

ACKNOWLEDGEMENTS

I would like to acknowledge the incredible support of my wife and my parents during my time preparing for my Masters. My wife has maintained so much responsibility to give me the ability to commit myself fully to this task and the work that was required for this degree. My parents have been ready to pick up their phones and talk to me about my progress and difficulties and encouraged me to keep going despite the challenges that came. I am also incredibly grateful to my advisors Dr. Hunter Andrews, Dr. Jamie Coble, and Dr. Kristian Myhre. I had the unique opportunity to have three advisors during my graduate career. They were more than exceptional in their efforts to see me succeed. I enjoyed my weekly meetings with them and their unending support. This research is supported by the U.S. Department of Energy Isotope Program, managed by the Office of Science for Isotope R&D and Production.

ABSTRACT

Laser-Induced Breakdown Spectroscopy (LIBS) is a versatile technique for compositional analysis for solids, liquids, and gases. LIBS is an asset for the quantitative or qualitative analysis of resource limited materials like actinides and rare earths because it is quasi-nondestructive: typically, only a few nanograms of material are ablated into a plasma for optical emissions. Calibration Free – LIBS (CF-LIBS) is of interest being applied to rare earths; however, it is currently lacking fundamental data needed for application. This fundamental data is transition probabilities, and they allow LIBS to be employed without having to make and use matrix matched standards for a calibration curve. Two studies were employed in this work which aim to utilize the unique qualities of LIBS to prepare a way for transition probabilities to be estimated for resource limited material. Eu pellets were made for the first study and used as a test and validation set. The second study used small amounts of solutions containing a lanthanide and Sr, which acted as an internal reference, dried on Al pellets. In the studies discussed herein, Saha-Boltzmann plots were used to estimate the temperature and electron density of the plasmas generated. This information was then used to calculate previously unknown transition probabilities. Results in the second study showed uncertainties lower than 10% in some cases, while the first study only got down to 35%. In the first study, 8 previously unreported transitions probabilities are reported, and 967 transitions probabilities are reported for the second study. Self-absorption corrections were used in the second study, along with an increase of sampled data which catered to decreasing the uncertainty in the estimations. By calculating new transition probabilities with the methods presented in this thesis, it is possible to complete these estimations with high accuracy and low resource cost, which

suggest it is a viable method to use for resource restricted elements like actinides. CF-LIBS is of interest for the actinides because of its many benefits including in-situ, fast, quasi-nondestructive, remote viewing, and unrequired dilution of samples.

TABLE OF CONTENTS

LIST OF TABLES

LIST OF FIGURES

CHAPTER ONE
INTRODUCTION

1.1 Isotope Production and Application

Production and exploration of radioisotopes is a field of research that offers many benefits and products to the United States and the world. Producing radioisotopes provides materials for reactor startup, radiotherapy, material surveying for airport security, bomb detection, or military ordinance detection to name a few examples. At Oak Ridge National Laboratory (ORNL), many radioisotopes are produced and distributed nationally and internationally through the Department of Energy Isotope Program. One example of the Isotope Production Program at ORNL is the Cf-252 program.[2,3] Production begins with irradiating targets of Am and Cm, which produces a variety of products, including Cf-252. Because of the other products created during the irradiation process, separation techniques are necessary to isolate Cf-252 from everything else. An important aspect of performing these separations is the ability to perform elemental analysis of major and minor components to track the products and ensure maximum purity of the final sample.[4] Laser-induced breakdown spectroscopy (LIBS) offers in-situ analysis as well as measurements before, in the middle (on grab samples), and after separation without having to dilute or perform any type of chemical processes on these samples. Analytical analysis can help maintain quality assurance during production and due to LIBS's ability to be applied remotely and rapidly, it could potentially reduce the risk to employees when working with radioisotopes.

1.2 Benefit of LIBS Techniques

LIBS is a versatile optical emission spectroscopic technique that relies on optical

light emitted from laser generated plasmas to estimate elemental compositions of samples. LIBS typically uses calibration curves made from matrix matched standards to estimate the concentration of analytes in a sample. If matrix matched standards can be made, then the actual analysis process of LIBS is rather straightforward.[5–8] A sample can be analyzed in gas, liquid, or solid forms little to no sample preparation is frequently necessary.[9,10] The laser is focused onto the sample surface and the energy density is high enough that the material ablates and creates a plasma plume. This plasma plume releases characteristic optical light as it cools that can be collected by a spectrometer for analysis. The spectra that are generated have many lines for each lanthanide, with well over a 100 in both the europium and 13-lanthanide studies.[11] The intensities of the sample are compared to the intensities of the calibration standards to determine concentration. This is one of the major benefits of LIBS. There is such an abundance of transitions to choose from when doing analysis, it gives the researcher multiple opportunities to reduce error and confirm calculations. LIBS has also been shown to have detection limits down to 30 ppm.[12] This means that trace elements in samples can be detected and quantitatively analyzed. The ablation process is very fast where the plasma lasts a couple microseconds. The spectrometer's gate width and delay are optimized to observe the plasma after its blackbody radiation has reduced and during a time frame that its optical emissions are visible and under local thermodynamic equilibrium. Once again, all the peaks observed from the plasma give the user ample opportunity to sift through which peaks are the best in terms of signal to noise ratio, self-absorption, and overlap. They will also provide the opportunity to find a peak to represent each analyte present in the sample. Additionally, LIBS can be employed in difficult circumstances such as reduced space or radiation environments.[8,13–

15

LIBS has been employed remotely through telescoping, optic fibers, longer umbilical cords, and periscopes.[13,16,17] Longer umbilical cords, the power supply for the laser head, can be used to employ LIBS inside of hot hoods, glove boxes, and hot cells. Essentially this allows a very small amount of the laser system to be exposed to radiation and takes up less space than having the entire setup (power supply, spectrometer, laser head) in the contained area. The periscope technique is typically suggested for hot cells and can be implemented by drilling a hot cell port and then extending the periscope into the hot cell through the port. The collection optics and focusing optics are at the end of the periscope so samples can be analyzed. Telescoping is used to launch the laser longer distances, like through a glove box window or through the windows of a hot cell and keep all the equipment outside of the environment. This technique often delivers lower signal to noise ratios and is not typically chosen for quantitative methods. The last technique, optic fibers, is one of the most popular techniques for engaging quantitative LIBS in restricted areas. Optic fibers can be fed into hot hoods, glove boxes, or hot cells and keep all the main components of the LIBS system outside of the area of concern. This helps protect systems and ensure longevity of hardware. Usually, one fiber is used to deliver the laser, and then another fiber (or fiber bundle) is used to collect the light from the plasma and transfer it back to the spectrometer. If damage is caused to the fibers over time due to use and exposure to a harmful environment like radiation, then they are relatively cheap to replace when compared to the main laser components. As a summary, LIBS can provide fast, in-situ measurements of samples in any phase at various concentrations.

1.3 Motivation for Developing CF-LIBS

Calibration Free-LIBS (CF-LIBS) is a unique method of LIBS that has inherent benefits over standard LIBS. A feature of LIBS that can be a major drawback is the need for matrix matched standards to analyze your unknown sample. Matrix matched standards are simply standards made to represent the chemical matrix of your sample to be analyzed. They should have the same general mix of material found in the sample. The first difficulty with these standards is that a general knowledge of the sample matrix is not always known, so making the standards can prove to be very difficult due to a lack of information. Another problem with standards is that they require material to make them. The goal of applying LIBS to heavy metals like the actinides means that sometimes samples would be very resource restricted. This is not an analysis problem as the ablation process only uses a few nanograms of material but making enough standards to have quantitative measurements for every possible sample would be very resource intensive. CF-LIBS does not require any matrix matched standards to be made for its analysis. This is achieved by applying some assumptions and working with previously reported data. CF-LIBS assumes that the lines observed in spectra are optically thin and that the plasma was under Local Thermodynamic Equilibrium (LTE) when observed by the spectrometer.[18] When under LTE, the collisional rates exceed the radiative rates of electrons and the primary mechanism for electron excitement between levels is the inelastic collision between electrons and atoms. This allows certain equations to be used which are discussed later that rely on previously reported values called transition probabilities. With transition probabilities acting as the calibration method, standards are no longer needed and can be used to calculate the concentrations of analytes in a sample using the spectrum peaks and Saha-Boltzmann plots

to determine temperature and electron density which are critical for calculating the concentrations. With all the benefit of LIBS combined with the benefits of CF-LIBS, analysis can be done very efficiently and on any sample.

1.4 Enabling CF-LIBS by Producing Transition Probabilities

CF-LIBS as a method is dependent on the user having transitions available for each species and those transitions having corresponding transition probabilities. As mentioned previously and shown later in the text, having the transitions for each species usually is not a problem, due to the multitude of peaks that appear for elements, especially the heavier elements. Having transition probabilities to go with the peaks can be difficult. For many elements across the periodic table, hundreds of transition probabilities are reported for their transitions. However, for the heavy metals, especially some lanthanides and most of the actinides, the number of transition probabilities reported is very low. Not only is the number of transition probabilities reported low, but the number of reported transitions is low as well due to the lower amount of experimentation done with these elements. If the transition probabilities are also missing, CF-LIBS is impossible. The europium and 13-lanthanide studies described in this paper have found a way to employ the benefits of LIBS techniques to calculate transition probabilities for the lanthanides with material on the order of nanograms instead of miligrams, which previously employed methods (e.g., inductively coupled plasma – optical emission spectroscopy (ICP-OES), and laser-induced fluorescence) require. This would potentially enable transition probabilities to be estimated for actinides. If this was done based on the methods presented in the studies below (Chapter Three and Four), then CF-LIBS could be enabled for use in actinide environments. A great advantage of LIBS with actinides is that the samples do not need to be diluted for analysis.

Analysis can take place in the protected environment through the remote analysis mentioned earlier and since the solution will not be diluted, it would be possible to see peeks for trace contaminants present in the samples. The calculations process for transition probabilities using LIBS is quick and a large amount of data can be produced at once. An example of this is represented in Chapter Four where 967 transition probabilities are estimated for 13 lanthanides. The work presented in Chapters Three and Four show how effective this method can be. This may encourage the future use of this process for actinides so that the full advantages of LIBS and CF-LIBS can be employed in actinide production processes.

CHAPTER TWO
LITERATURE REVIEW

2.1 Introduction

LIBS and CF-LIBS are practical in-situ applications of atomic spectroscopy. Both can analyze solids, liquids, and gasses and can be implemented with optic fibers for remote analysis. The goal of this work was to develop a technique to determine the transition probabilities of actinides with little material requirements, thereby enabling CF-LIBS of actinide containing samples. CF-LIBS requires certain fundamental parameters for each element it analyzes in order to avoid making calibration curves that represent the chemical matrices of samples. Self-absorption is often a problem encountered with LIBS and there have been suggestions for how to address it. Two methods to address these challenges are internal reference correction and stark broadening coefficient corrections (internal reference correction is used in Chapter Four). There have been a variety of uses for LIBS and CF-LIBS that will be discussed below, as well as previously used methods for determining transition probabilities.

2.2 LIBS

LIBS has been used for in situ analysis of solids, liquids, and gasses of many materials through a minimally destructive analysis process. The Nd:YAG laser, which has a fundamental wavelength of 1064 nm (though it also has second, third, and fourth harmonics), is a commonly used laser in LIBS instruments, [19–21] which is focused down onto a sample surface such that the power density is great enough that a very small amount of material (on the order of ng) ablates into a plasma. As the plasma cools, it emits optical

light which can then be collected by a spectrometer and converted into a spectrum. The spectra have peaks that correlate with the light emitted which is characteristic of the elemental composition of the plasma. LIBS can also be used for remote (at distance) measurements, which can be accomplished through telescoping the laser or using fiber optics to launch the laser to a desired location. While optical emissions in the visible range are the typical source of information from LIBS spectra, depending on the spectrometer, light from ultra violet (UV) and near infared (NIR) can be rich with spectral information as well.[22,23] LIBS measurements can be made with handheld devices. These handheld devices are typically preprogrammed for handling spectra and identifying elements present in samples. Handheld LIBS is a qualitative tool that can be used to perform rapid in-situ analysis of samples as a first pass to determine if further analysis is needed. Actinides like U have been analyzed with handheld LIBS. U-235 and U-238 could be distinguished from one another in a sample using the 424.437 nm peak.[24] Isotope identification is not a feature explored in this study but it is of interest and is a growing field that requires high resolution with high quality spectrometers.[24] LIBS was shown to have limits of detection in the values of hundredths of precents for certain lanthanide impurities in U samples.[25] The accurate measurement of rare earth elements (REEs) is important in numerous fields, including metal mining, materials processing, nuclear forensics, and nuclear energy.[25]

The appropriate laser wavelength should be determined based on the material type that will be analyzed. UV is typically best for ceramics, stones, and metals. Pulse duration, space and time profile, fluence and irradiance are parameters that need to be considered when choosing a laser as well. LIBS has been used for analysis of solids, liquid, and

gaseous materials. It has successfully been used to analyze metal alloys, biological tissues, archeological samples, geological materials, art samples, polymers, and pharmaceuticals.[26] LIBS has also been used to analyze biological samples such as rice with a laser operating at 400 mJ at 1064 nm and 200 mJ at 532 nm. This laser was able to detect Ni, Cu, Zn, Fe, Ca, Al, Si, Na, K, Ti, Mn, Li, Mo, C, Co, and Mg with 5 ns pulses.[27] Sample environments contribute to the results of LIBS as well and are important to consider when using LIBS. LIBS has been used for space exploration and considered for future work in conditions where pressure and atmosphere are different than ambient conditions on earth. Different gases at different working pressures affect the plasma plume and the type of emissions primarily seen. With ns ablation pulses and in reduced pressures, the spatial distribution of emitting species increases, and neutral line intensities increase and then decrease by reducing the working pressure.[22,23] Different gasses used with the experiment will also contribute its unique lines to the plasma emissions of the sample. This can be of benefit if certain emission lines in ambient air need to be excluded, another gas such as Ar can be used to get rid of N, O, and H lines.

Quantitative LIBS relies on the direct relationship of analyte concentration to the intensity of optical emission peaks. This relationship is typically determined through the measurement of matrix-matched calibration standards. Matrix effects are due to laser characteristics, sample properties, and plasma-particle interaction.[22,23] Multiple standards can be made to represent the matrix effects present in the sample as long as the elemental makeup of the unknown sample is generally known. A peak of the concerned species can be chosen, and its intensity can be measured across the standards. Once a calibration curve

is made from this data, the unknown sample can be shot and compared with the calibration curve to estimate the concentration of the unknown. LIBS can also be used for other applications such as steel age grading by combining LIBS depth profile spectra of steel pipe standards and machine learning to predict age gradings of unknown steel pipes.[28]

There was a unique example of LIBS used by Madhavi Martin.[29] They used Micro-Laser-Induced Breakdown Spectroscopy. The laser system produced 1064 nm which could be frequency doubled and tripled to produce 532 and 355 nm wavelengths. The Quicklaze 200 laser scriber was coupled to a LIBS optical system and placed in a glove box. They produced laser energies less than 1 mJ and were able to produce plasmas and obtain the optical emissions of some rare earths and one transition metal. This is one example of a LIBS system being used in an enclosed environment. The systems are often small enough that adjustments can be made to implement them inside of enclosed conditions. This system used a laser set up on a microscope connected to a laser optical setup to manage its size and then supplied power through the back of the glove box.[29]

It has been reported by manufacturers that LIBS systems can be integrated into confined spaces like hot cells by using extended umbilical cords for the power supply to the laser head so that the laser head is inside the hot cell.[17] Stand-Off LIBS, where measurements are taken at a distance from the sample, can also be used where a telescoping lens is used to launch the laser through the glass barrier of the hot cell and then oblate the sample.[30] The problem with this method is that it can be difficult to set up the spectrometer to receive the emitted light from the plasma with good signal to noise ratios. One of the most practical methods, based on my interaction with LIBS instruments, is to use optic

fibers which has been discussed previously and will be discussed more later (Section 3.2). Essentially fiber optics can be probed into the hot cell environment and deliver the laser pulse as well as receive the emissions of the plasma.[30] There is also a method where the shield wall is plugged with a periscope which can deliver the laser and receive emissions from inside the hot cell at a specific location.[30]

2.3 Advantages of CF-LIBS

CF-LIBS retains all the benefits of LIBS while providing additional ease of sample analysis by foregoing the need for calibration curves. Matrix effects are not considered in CF-LIBS because instead of relying on peak intensity alone, it relies on peak intensity, branching ratios, and fundamental parameters. CF-LIBS accuracy is lower than other analytical techniques and traditional quantitative analysis methods of LIBS. It was first proposed by Ciucci et al. in order to overcome the matrix affects. CF-LIBS is based on several basic assumptions.[31] First, chemometric ablation, which means that the composition of the elements in the plasma are the same as in the sample. Second, LTE which assumes the population of the excited levels obey a Boltzmann distribution. Third, the spectra are optically thin, which means that the lines used for calculation are not affected by self-absorption. There is a fourth assumption in CF-LIBS: that the spectral range of measurement includes measurable lines from all elements present in the sample, which is an experimental requirement.[32]

It has been shown that the accuracy of the measured intensity has a large influence on the final quantitative analysis. Relative efficiency is related to the possible transmission loss and photoelectric conversion efficiency within the spectrometer.[33] Optic fibers are

often used to collect the light from a plasma and transmit it to a spectrometer. Varying fibers can have different transmission and conversion efficiencies for different wavelengths, so it is important to ensure the optic fibers suit the experiment best when being used for remote deployment of a LIBS system. The use of spectral lines requires that the lines are optically thin. The intensity should increase linearly with a percentage increase in the concentration of your analyte. However due to self-absorption a drop off in the intensity would appear as concentration increases if self-absorption was present. Typically, self-absorption is seen less in lower concentrations of analyte due to less material being available to self-absorb and re-emit. Error in the intensity measurement can be made based on the temperature from a Boltzmann plot and the observed broadening, if the thickness of the optically thin peak is known.[19] Self-absorption can often be handled by optimizing the gate width and delay of the spectrometer. LTE, as stated before, is important for CF-LIBS; however, it has been shown that the plasmas generated are typically transient and non-uniform which means that LTE only exist for a certain time (typically around 50 ns) and space range. . While the europium and 13-lanthanide studies used time resolved LIBS, intensified charge coupled devices or ICCDs are typically used with calibration free tactics to ensure a small enough observation window for LTE is upheld. Time resolved LIBS used later in the europium transition probabilities chapter displayed promising results but using ICCDs could help improve the results for future versions.

Peak detection and line identification are also key components in CF-LIBS. It should be noted that for most of this study, both steps were done by hand which is very time consuming. Software was developed to an extent to make these estimations, but it was

not finalized for the project. Other groups have proposed some automatic or semi-automatic recognition procedures. Peak detection is relatively straight forward, however peak identification is more complicated. It is important to consider all the peaks available not just the one being determined, as the presence of other peaks can confirm or oppose the correct identification of one peak. This is because there are so many possible transitions across the elements that some inevitably overlap. This leads to some peaks being misidentified when not enough additional evidence is supporting the identification. The methods for determining which peaks to use are detailed in the europium and lanthanide transition probability chapters. Another way to increase the accuracy of CF-LIBS measurements is to ensure the fundamental data being used to support the calculations like transition probabilities is as accurate as possible. Choosing lines that have associated high accuracy transition probabilities can help yield more confident calculations of temperature and electron density. The use of srontium in the lanthanide transition probability chapter as an internal standard was detailed for this study. There have been algorithms used to correct for self-absorption in peaks, like what was discussed from de Oliviera et al., though these procedures were not used in the europium study.[18,33–35]

Fundamental parameters, such as transition probabilities act as internal calibrations for the samples as they describe the likelihood of a specific transition happening per second. CF-LIBS uses transition probabilities with branching ratios of peaks to compare species concentrations, where species refers to the different ionic states of the same element. One critical component of CF-LIBS is that analysis is performed under local thermodynamic equilibrium or LTE, which is a short lived state that assumes all electronic

transitions and populations are collision governed.[18,20,32,33,36,37] The assumption of LTE is very important for CF-LIBS because it means that the global distribution of the population of all electronic levels of a species can be derived from the population of the upper level of observed transitions. The McWhirter criterion is used often as a requirement for LTE conditions. It states that the rate of collision processes must be dominant over the radiative processes.[18] It is often observed in the early stages of plasma development after a short gate delay. This is also when the electron density is typically on the order of $10^{17} – 10^{18}$ cm^{-3}. A second condition for LTE is that the rate of variation of thermodynamic parameters is small compared to the time scale of establishment of excitation and ionization equilibrium.[38] This condition is more easily achieved in the late stages of a plasma evolution, after the expansion is almost stopped. Therefore, a gate delay is often used for spectrometers when looking at the plasma, to find a balance between looking at the plasma too early and too late.[38] An expanding plasma will often result in more line broadening and self-absorption so optically thin lines can be a sign that the gate timing is properly attuned. A third condition is set such that the length scale of thermodynamic parameters must be larger than the diffusion length of the atoms in the time scale of equilibrium.[32] Theories describing the consistency of LTE for LIBS plasmas are valid for high density plasma where the main mechanism of transition of bound electrons from one level to another level is caused by inelastic electron-atom collisions.[19,21]

Often with CF-LIBS, Boltzmann or Saha-Boltzmann distributions are used to determine the temperature of the plasma. A Boltzmann distribution describes the distribution of a single species among different states. Peak intensities from a spectrum of

a single species, like Eu I, can be used to develop a linear plot and estimate the plasma temperature. The accuracy of the temperature estimation can be improved by using a Saha-Boltzmann plot. Saha-Boltzmann plots relate the population states between two ionization states, like Eu I and Eu II, and thus allows for the peak intensities of both neutral and singly ionized species to be used for a plot which then gives an estimated temperature based on the slope.[1,2,8,13,18–23] The temperature estimated from the Saha-Boltzmann plot along with an estimated electron density, either by Saha-Boltzmann or Stark broadening methods, can be used with the equations previously mentioned and detailed later to calculate species concentrations. The neutral and ionized species distribution in a plasma can be determined by taking measurements along the width and height of the plasma. Doing this can also allow one to map out electron density and temperature.[19] Once the temperature and electron density are determined for the plasma, the CF-LIBS approach optimizes a second parameter in the linear regression of the points in the Boltzmann plane which is the intercept value, which is a function of the number density of the individual species of the plasma. This is also a function of the partition function, which depends on the temperature, and instrument function, which is accounted for before calculations. Typically, the number density is summed over the present states in the plasma, which are most often the neutral and singly ionized state. Once the number density has been calculated for all the elements the relative abundance of the element can be obtained.[32] A benefit of all these methods is that they use very little material. When the lasers used for LIBS and CF-LIBS ablate a target, a very small amount of material is ablated, up to a few nanograms, which makes CF-LIBS an important candidate for the analysis of resource limited materials like actinides. A decent amount of work has been done with the lanthanides to produce

fundamental parameters.[44,45] However, very little work has been produced for the actinides. Actinides are very difficult to work with due to their radioactivity, and how little of these resources are available for research projects. LIBS procedures may use less material than previously reported methods for estimating fundamental parameters, making it a strong candidate for rare materials.

2.4 Self-Absorption

CF-LIBS was performed on frozen aqueous samples by de Oliviera et al.[18] The samples were frozen to provide a solid surface for the sample to oblate which can help provide a better signal and reduce the splashing effects that are native to working with aqueous samples. The state occupation is described by a Boltzmann distribution. They relate this Boltzmann distribution to a linear form and use the intensity of multiple peaks to make a plot and estimate the temperature of the plasma which is a required parameter for CF-LIBS calculations. They also use the stark broadening of the Balmer series Hα line to estimate the electron density, another required parameter for CF-LIBS calculations. Uniquely, de Oliviera et al. used self-absorption corrections to better predict the temperature and electron density. Known Stark broadening coefficients and peaks with known transition probabilities were used to estimate and correct for self-absorption of other lines. Lines with smaller transition probabilities were assumed to be immune from self-absorption affects and were thus used to correct the intensity of larger Ca lines with larger transition probabilities. After the temperature was estimated with the Saha-Boltzmann plot and if the Stark coefficient was known they corrected the spectral line intensity, if it was not, they tried to correct it via transition probability and intensity ratio correction and

repeated these processes until all lines were either analyzed or removed. The Saha-Boltzmann plot was repeated and if the difference between the new temperature and old temperature was less than a predetermined error value then they used the new temperature. After corrections for self-absorption was completed, atom percent and weight precent were calculated for Ca, Mg, Na, K, and Zn.[18]

Two methods are primarily used for self-absorption correction. One method chooses a peak known to be free of self-absorption and uses that as a reference peak to correct others by dividing their intensity equations with a self-absorption correction factor. Another method uses stark broadening values of lines to directly calculate a self-absorption coefficient and then use that to calculate the corrected intensity of a peak. The second method only works if there is stark broadening coefficients for the peaks which are not readily available for the lanthanides studied in Chapter Four, neither are they reported currently for any of the actinides. The first method also requires the availability of a non-self-absorbed peak. Sometimes the number of peaks available for a certain element is restricted in an experimental spectrum, and they could all suffer from self-absorption, which would mean that the ability to correct for self-absorption would be dependent on the peak with the lowest self-absorption. It has also been reported in this method that it is important to use peaks from the same upper energy level or within a certain precent difference of energy level differences.[20,43]

2.5 Previously employed methods to estimate Transition Probabilities

Transition probabilities are fundamental parameters that describe the probability of an electronic transition occurring typically in units of per second. They can be relatively

large or small which can indicate the intensity of the peak being higher or lower, relative to one another. Previous methods of transition probability calculation are often highly dependent on previously reported data or require large amounts of material for the measurements that need to be made.[44–47] Radžiūtė used Dirac Hartree-Fock with multiconfiguration and relativistic configuration-interaction methods to estimate energy levels of astronomically observed transitions. Once these energy levels were calculated, previously reported oscillator strengths were used to estimate transition probabilities for praseodymium through gadolinium.[46] Time resolved LIBS was used to measure radiative lifetimes which can then be related to transition probabilities for Sm, Nd, Pr, Gd, Cu, and Fe.[47] Another popular method for the measurement of fundamental parameters is time resolved laser-induced fluorescence. This was applied for europium and is discussed further on in this paper. An important component of this LIBS process, in contrast to the process in this work, is that it uses a large amount of material, as a europium foil which is sputtered with a large-bore hollow cathode.[44] This is a similar method used from Zhiguo et al. and both require relatively large amounts of material when compared to the current method employed in this paper.[45]

CHAPTER THREE
CALCULATION OF TRANSITION PROBABILITIES FOR EUROPIUM

This chapter discusses eight transition probabilities estimated using LIBS techniques. Two europium oxide pellets were made, one as a test set and one as a validation set. The first pellet was shot with a LIBS system and the optical emissions from the generated plasma were used to estimate the eight new transition probabilities. The second pellet was used with the newly estimated transition probabilities to validate these estimations by comparing the fit of a Saha-Boltzmann plot against previously reported data. The fit compares well to previously reported data, however there is room for improvement on the uncertainties which is discussed and then put into practice in Chapter Four.

The work in this chapter was published in "Journal of Quantitative Spectroscopy & Radiative Transfer," and can be cited as:

Irvine, S.; Andrews, H.; Myhre, K.; Goldstein, K.; Coble, J. Radiative Transition Probabilities of Neutral and Singly Ionized Europium Estimated by Laser-Induced Breakdown Spectroscopy. *J. Quant. Spectrosc. Radiat. Transf.* **2022**, 108184. https://doi.org/10.1016/j.jqsrt.2022.108184.

Sawyer Irvine: Methodology, Investigation, Software, Writing – original draft, Writing – review & editing, Visualization. Hunter Andrews: Conceptualization, Methodology, Investigation, Software, Writing – original draft, Writing – review & editing, Visualization, Funding acquisition, Project administration. Kristian Myhre: Conceptualization, Methodology, Writing – review & editing, Funding acquisition. Kari Goldstein: Investigation. Jamie Coble: Methodology, Writing – review & editing

3.1 Introduction

Optical emission spectroscopy evaluates characteristic light emitted from atoms or molecules in an excited state. Each species emits unique light based on its quantized electronic structure thereby enabling spectral analysis for identification of elements or other species. In the field of astrophysics, the light emitted from stars and galaxies is used to evaluate the elemental abundances of those stellar bodies. Heavy elements and other radioactive materials such as technetium are of particular interest due to their important role in astrophysics phenomenon, such as stellar nucleosynthesis. Tc was discovered in S stars, those with approximately equal quantities of carbon and oxygen in their atmosphere. Due to its longest living isotope having a half-life of 3×10^5 years, and the star being much older, this proved that nucleosynthesis occurred within stars and the products, such as other heavy elements, could reach the surfaces of stars with mass loss and mixing. [48]

Nucleosynthesis occurs through multiple modes including the rapid (r) and slow (s) neutron-capture processes, as well as through the proton-capture (p) process. The r- and s-processes have been shown to contribute to the production of heavier nuclei while the p-process has primarily been shown to produce lighter elements or take very minor roles in heavier element production. europium has been predicted as a near pure r-process nuclide.[49] Efforts to model nucleosynthesis rely on having accurate fundamental optical emission data for key elements (e.g., europium) to predict elemental compositions of stellar bodies and determine the degree of r-process enhancement in stars. R-process studies would also yield a better understanding of the heavy element nucleosynthesis, limits on the age of the galaxy, and the early chemical growth of the galaxy.[44,50–52] The ground state of europium has received more research while reports of its singly and doubly ionized states

are still being produced.[49] Each ionized state persists in stars; therefore, it is important to obtain data representing each state of an element. Stable ion sources for the doubly ionized state are difficult to produce as recombination effects between ions and electrons make highly ionized atoms improbable. Recombination effects can make lifetime values shorter and contribute background light to the sample.[53] Transition probabilities can also be used for galactic elemental abundance, stellar age, and composition predictions.[48,54]

LIBS involves measuring the optical emissions of laser-induced micro plasmas and can provide compositional information. LIBS is predominately used to provide elemental information but has also been demonstrated for isotopic measurements.[22,23] LIBS is performed by firing a focused laser onto a sample such that the energy density at this focal point is enough that a small amount of the sample material is ablated, and a plasma plume is formed. Due to the minute amount of material ablated, LIBS is commonly referred to as being quasi-nondestructive. Light is emitted as the plasma relaxes and optical atomic emissions can be measured with a spectrometer.[26] This provides an elemental fingerprint of the sample material with little-to-no sample preparation. LIBS has gained popularity in the research field due to its high versatility and has been used for analyzing gases, liquids, and solids.[55] Additionally, LIBS can be deployed through fiber optics making it potentially useful for the remote analysis of hazardous materials such as radioactive samples in a hot cell. Traditional LIBS uses calibration curves, made with matrix matched standards, to predict the composition of unknown samples. Making matrix matched standards is difficult when the matrix of your sample is unknown and may require many attempts. The higher accuracy required, the more standard samples need to be made, thus this methodology

requires excessive time and material, which can make the method prohibitive when either of these are lacking.

CF-LIBS, originally proposed by Ciucci et al., provides a way for rapid and accurate sample analysis without the need for complex calibrations, thus providing a cost-effective alternative to traditional LIBS to safely approach elemental analysis of radioactive samples quickly with minimal sample destruction during assay.[31,56] For CF-LIBS to be viable two key assumptions should be true; the plasma exists in a state of LTE, indicating that excitation and de-excitation occur at the same temperature, and is optically thin.[32] Another requirement of CF-LIBS is an accurate database of fundamental properties which allow for an optical emission spectrum to be properly investigated. Measured spectra are often compared with an existing database such as the Atomic Spectra Database maintained by the National Institute of Standards and Technology (NIST) in order to identify photon peaks.[57,58] The ratio of the peak intensities, which represent different species in the plasma, can be used to predict species concentration ratios in the plasma. These predictions require fundamental data, such as transition probabilities, for spontaneous optical transitions.

As previously mentioned, traditional LIBS requires enough material to make multiple matrix matched standards used to produce calibration curves; this becomes troublesome for employing LIBS on actinide samples as this type of material is not widely available. Actinides are all radioactive, some with extremely short half-lives, meaning material is continually lost during manufacturing processes. Californium only exists in tens of milligram quantities in the world. While this is an extreme example, the principle of

restricted resources applies to all transuranic elements. Depending on the environments, there are also limits to how much of an actinide one can work with at a time due to radioactive health and safety regulations. All of this reduces the ability to use standard LIBS for actinide analysis. CF-LIBS would provide a more practical way to analyze radioactive samples by allowing much less material to be used. Unfortunately, many heavier elements including the lanthanides are lacking in their reported fundamental data. For example, singly ionized Er only has 2% of its energy levels well defined.[54] Multiple lanthanides are used in stellar calculations including lanthanum, cerium, praseodymium, europium, terbium, and holmium; each of which have differing amounts of fundamental parameters reported.[59] Based on this, the need to measure fundamental data for rare earths and actinides is evident.

Radžiūtė et al. used multiconfiguration Dirac Hartree-Fock and relativistic configuration-interaction methods to develop energy level descriptions of astronomically observed transitions.[46] This energy level data was then combined with reported oscillator strengths[46] to calculate transition probabilities for the lanthanides praseodymium through gadolinium. In his thesis work Ryder used time resolved LIBS to measure radiative lifetimes and other fundamental parameters such as transition probabilities for samarium, neodymium, praseodymium, gadolinium, copper, and iron.[47] Den Hartog et al. used time-resolved laser-induced fluorescence to measure transition probabilities for neutral europium.[44,50,51] A slow beam of europium ions was produced by sputtering from a large-bore hollow cathode lined with europium foil.[44,50,51] The europium beam was orthogonally crossed with a laser pulse tunable over 205-720 nm. The laser selectively excited a specific

europium energy transition to study and the fluorescence signature was collected. Zhiguo et al. analyzed branching ratios for Eu II and Eu III also using time-resolved laser-induced fluorescence. Radiative lifetimes were first measured using time resolved laser-induced fluorescence and then branching ratios were used from a previous study with the radiative lifetimes measured to calculate transition probabilities. The transition probabilities were also used to calculate oscillator strengths.[45] In the last two example studies from Den Hartog et al. and Zhiguo et al.,[44,45] they produced a large amount of data. However, the methods in the europium and 13-lanthanide studies required less material because Hartog et al. and Zhiguo et al. used sputtering methods.[44,45] The goal was to reduce the resource cost of producing these fundamental parameters for LIBS so they can more realistically be produced to enable routine analysis of far rarer materials like transuranic actinides.

This study focused on the determination of fundamental parameters, specifically transition probabilities, of atomic and ionic europium species critical to analyzing laser-induced plasmas containing Eu. The lanthanide europium was used as a surrogate for actinides which are planned to be evaluated in the future once the methodology is justified. Plasmas were produced by using a LIBS laser to focus light on a sample to ablate it and the spectra collected from the emitted light were used to calculate transition probabilities for europium transitions.

3.2 Experimental

3.2.1 Sample Preparation

The samples used in this study consisted of europium oxide (99.95%, Alfa Aesar) mixed with high purity graphite powder, 99.9995% (metal basis) from Alfa Aesar, and pressed into pellets with approximately 15 ton cm^{-2}. The 1 cm in diameter and nominally

2 mm thick pellets were held under pressure for approximately two minutes after pressure had stabilized. The nominal composition of the first pellet was made to be 1.3 atom% Eu, 96.7 atom% of C, and 2.0 atom% of O. A second pellet with a different europium concentration was made to validate calculated transition probabilities. The composition of the second pellet was made to be 1.6 atom% Eu, 96.0 atom% of C, and 2.4 atom% of O.

3.2.2 LIBS Measurements

All LIBS measurements were performed using an Applied Photonics LIBSCAN 150 laser system with a wavelength of 1064 nm, an energy per pulse of 161 ± 2.25 mJ, a pulse length of 5 ns, a spot size diameter of 500 μm, a laser fluence of 82 J cm^{-2}, a Catalina Scientific Instruments EMU-120/65 echelle spectrometer with a Raptor Falcon Blue EMCCD camera ($\lambda/\Delta\lambda \approx 12000$), and a Quantum Composers pulse generator. The spectrometer integrations were performed with a gate delay of 1 μs and a gate width of 100 μs. The experimental system used in this study was like those previously reported (, Sheng et. al., Umar et. al.).[60,61] Prior to any measurements the spectrometer wavelength was calibrated using a StellarNet, Inc SL2 mercury argon lamp and the spectral efficiency was calculated using a StellarNet, Inc. SL1-CAL tungsten halogen lamp with a certified spectrum. The pellets were tested by positioning them at the laser focal point using a hand adjusted vertical translation stage. Each pellet was shot 20 times, where the first 5 shots were treated as cleaning shots to remove any surface contaminants. Between each pellet sample the stage was cleaned to avoid any cross-contamination. The experimental setup used is shown below in Figure 1. All post experimental data analysis was completed using Python 3 (Rossum, Drake 2009).

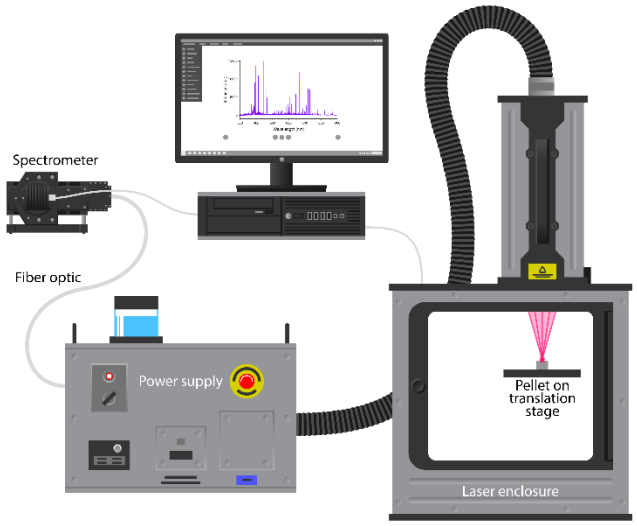

Figure 1. LIBSCAN 150 laser system focused on a transitional stage in the laser enclosure which is mounted with optic fibers connected to the Catalina Scientific Instruments EMU-120/65 echelle spectrometer with a Raptor Falcon Blue EMCCD camera which is then connected to the computer.

3.3 Results and Discussion

Prior to any spectral analysis a relative efficiency function for the optical measurement system including the collimating lens, optical fiber, and spectrometer was calculated by relating the average of ten measured spectra of a calibration lamp to its certified spectrum. The calculated relation was then used to correct measured spectra for differences in wavelength efficiency. Figure 2 (a-c) shows the certified lamp spectrum, the average measured spectrum, and the calculated relative efficiency function, respectively. In addition to efficiency correction, two additional preprocessing steps were employed. First, the measured spectra were background corrected using a process like the method reported by Yaroshchyk and Eberhardt.[62] A list of local minima values was determined by moving through the spectrum in steps of 50 data points (covering 1 nm at a time). Then a polynomial function was fitted through all the minima generating a pseudo-baseline which was subtracted off. Secondly, the spectra intensities were normalized to the 443.56 nm Eu I peak intensity to adjust for shot-to-shot variation in the laser energy. An example spectrum shown throughout the various preprocessing steps is shown in

Figure 3. Spectral peaks of interest were identified after preprocessing and fit with Voigt functions, which are a convolution of Lorentzian and Gaussian functions, using the lmfit package in Python.[63] An example fitted peak is shown in Figure 4. The integral peak intensities used throughout this study were calculated from the fitted Voigt function.

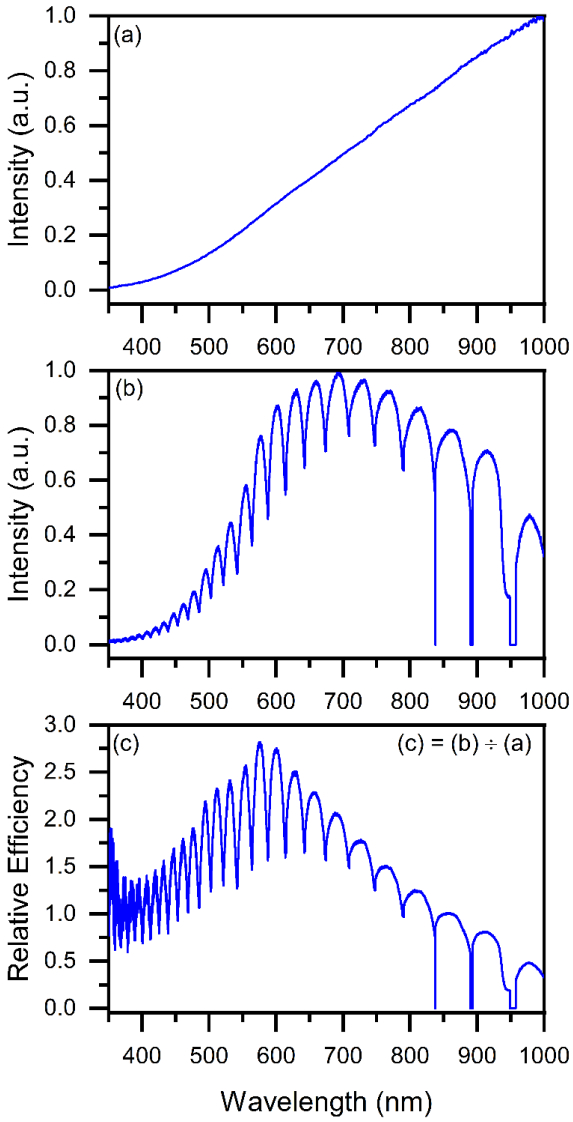

Figure 2. By comparing (a) the certified spectrum of a calibrated lamp source to (b) the measured spectrum of the same lamp, the relative efficiency curve (c) for the experimental setup in this study was calculated.

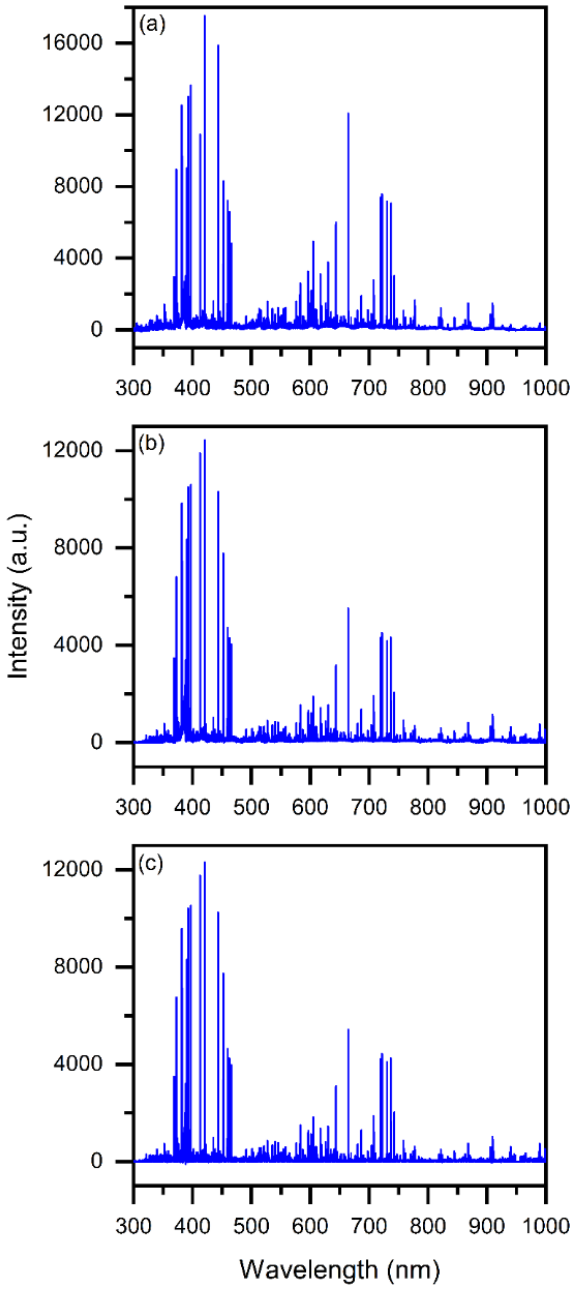

Figure 3. An example spectrum shown (a) as measured, (b) efficiency corrected, and (c) background corrected. Normalizing to the 443.56 nm Eu I peak only changes the vertical scale but has no impact on the spectral shape.

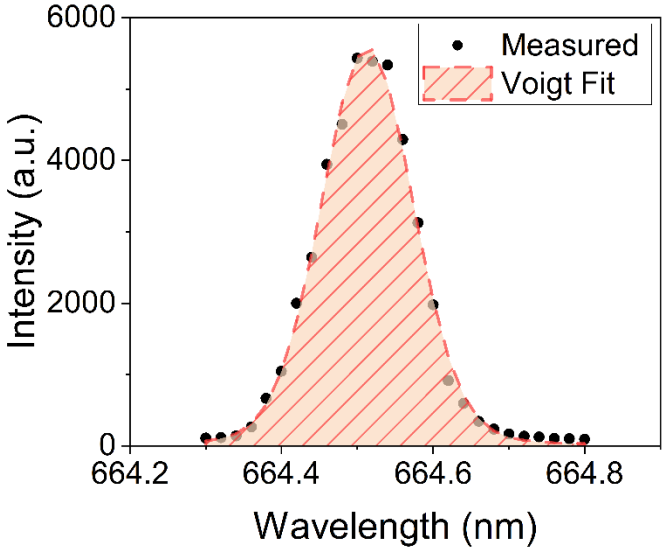

Figure 4. An example of the 664.52 europium peak fitted with a Voigt function.

For optically thin plasmas under LTE conditions, the integral intensity I_{nm} of an electronic transition of species *s* from energy level *n* to *m* can be calculated as a function of several species' parameters and is defined as

$$I_{nm} = F(\lambda) C_s \frac{A_{nm} g_n}{U_s} \exp\left(\frac{-E_n}{T}\right) \quad (1)$$

where $F(\lambda)$ is the instrument function, C_s is the number density of species *s*, *A* is the transition probability, *g* is the level degeneracy, *E* is the ionization energy, *T* is plasma temperature, and $U_s(T)$ is the partition function of species *s* at a given plasma temperature. The instrument function is accounted for through the relative efficiency correction step made previously.

The Saha equation which describes the ratio between the concentration of species at different ionization levels can be written as

$$\frac{C_2}{C_1} = \frac{(2\pi m_e T)^{3/2}}{n_e h^3} \frac{2U_2}{U_1} \exp\left(\frac{-E_{ion}}{T}\right) \quad (2)$$

where 1 and 2 refer to separate upper and lower ionization states, respectively, m_e is the electron mass, n_e is electron density, *h* is Planck's constant, and E_{ion} is the ionization energy.[64,65]

The Saha-Boltzmann plot method allows for both neutral and ionic emissions to be used for temperature and electron density calculation. The Saha-Boltzmann plot parameters can be derived by combining Eqs. (1) and (2). The resulting equation, Eq. (3), can be

transformed into a linear form such as

$$y = mx + b(T) \quad where \begin{cases} m = -\frac{1}{T}, \;\; b(T) = ln\left(\frac{FC_1}{U_1}\right), \\ x = \begin{cases} E_1\,(neutral), \\ E_2 + E_{ion}\,(ionic)\,, \end{cases} \\ y = \begin{cases} \ln\left(\frac{I_1}{g_1 A_1}\right)\,(neutral), \\ \ln\left(\frac{I_2}{g_2 A_2}\right) - \ln\left(\frac{2(2\pi m_e T)^{\frac{3}{2}}}{h^3 n_e}\right)(ionic) \end{cases} \end{cases} \tag{3}$$

The temperature and electron density are required to calculate the vertical coordinates of ionic emissions, as seen in Eq. (3). Therefore, an iterative fitting algorithm was developed in Python to solve for temperature and electron density simultaneously. An initial guess was used to calculate the vertical coordinates of the plot and then a regression line was fitted through the points. A new temperature is calculated from the regression slope, which is then used to calculate the partition functions for neutral and ionized Eu. The partition functions and new temperature were then used with Eq. (2) to calculate the number densities of both neutral and singly ionized species. All this information is then fed into Eq. (3) to calculate a new electron density. With a new electron density and temperature, convergence is checked by calculating the percent difference between the old and new temperatures and electron densities. If the fit was below the designated threshold, which was set to be less than 0.0001%, then it was considered converged.

If the convergence criteria had not been met, then new Saha-Boltzmann plot coordinates were calculated with the new electron density and temperature and the process was repeated. Both high and low initial guesses were given to verify convergence occurs.

It can be seen in Figure 5 that for both temperature and electron density, the convergence occurs from both high and low guesses.

The temperature for the first pellet's plasma was calculated to be 0.452 ± 0.005 eV and the electron density was evaluated to be $1.49 \pm 0.295 \times 10^{15}$ cm^{-3}. The Saha-Boltzmann plot of the first pellet is shown below in Figure 6. Similar temperatures and electron densities were found in other LIBS studies.[38,41] These values also satisfied the McWhirter's criterion which tests if the plasma could be in a state of LTE.[64] It is important to note that fulfillment of the McWhirter criterion is necessary, but not sufficient for assessing the validity of LTE in LIBS plasmas.[37] The current study assumes that the measured spectra reflect an effective state of LTE, despite using a time integrated measurement. The initial period of the plasma lifetime when the system is not in LTE was not measured due to the spectrometer being gated. The assumption that most of the collected signal was emitted during a state of LTE and the contribution to the signal from when the plasma was cooling was minor allows us to assume a state of effective LTE and attempt to apply LTE relationships.

Transition probabilities of observed europium peaks could be calculated from the Saha-Boltzmann line for the first pellet. All possible neutral and singly ionized europium transitions were calculated using the NIST energy level information.[57] Several peaks with unreported transition probabilities were identified in the measured spectra.

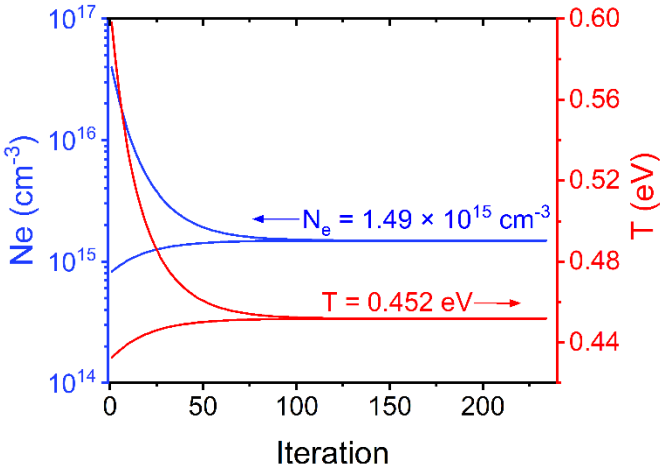

Figure 5. Temperature and electron density convergence occurring at about 0.452 eV and 1.49×10^{15} cm^{-3} for the first pellet, respectively.

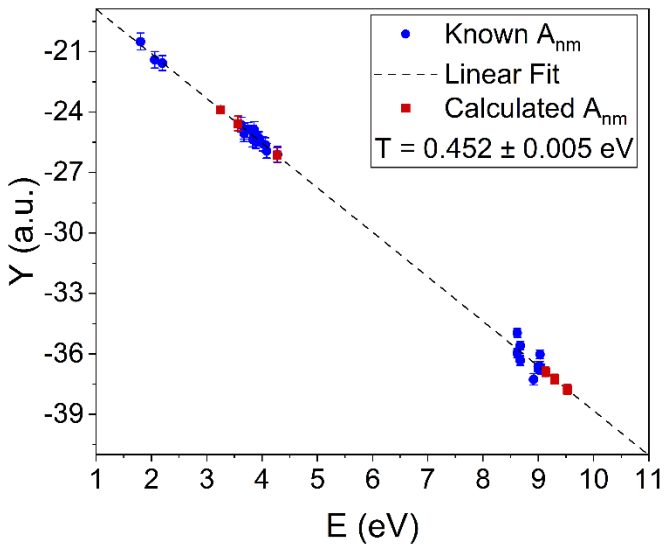

Figure 6. Saha-Boltzmann plot for neutral and singly ionized europium built using known transition probabilities (circles). Data points corresponding to peaks with newly calculated transition probabilities are shown with square markers.

The emission intensity, upper energy level, degeneracy, plasma temperature, electron density, and the fitted Saha-Boltzmann coordinates were then used with Eq. (4) to solve for these transition probabilities.

A leave-one-out cross-validation (LOOCV) approach was used to approximate how well the Saha-Boltzmann plot method would perform for predicting unknown transition probabilities. The LOOCV approach involved systematically leaving one spectral peak out of the Saha-Boltzmann regression model at a time and then the new model built was used to predict the transition probability of the peak left out. This is repeated *n* times, where *n* is the total number of peaks used in the original Saha-Boltzmann model. The root mean squared error of cross-validation (RMSECV) is the metric calculated from the LOOCV to estimate the accuracy of transition probability prediction. RMSECV is defined as

$$RMSECV = \sqrt{\frac{\sum(\hat{y}_i - y_i)^2}{n}} \tag{4}$$

where $\hat{y}_i$ is the predicted transition probability of the peak left out of the model and $y_i$is the reported transition probability of the peak. The RMSECV was 1.07 $\times 10^7$ s^{-1}, corresponding to 41.27% of the mean transition probability value of the peaks used in the analysis. These values provide benchmarks for what the expected uncertainty of the newly estimated transition probabilities. The cross-validation performance supports the application of the effective LTE assumption, but also offers insight that the use of nanosecond exposure times may offer reduced uncertainties in future work.

The newly estimated transition probabilities along with wavelength, ionization state, energy level, and degeneracy information are provided in Table 1. When considering

previously reported data, the NIST database transition probabilities are reported with uncertainties ranging from less than 10% to over 50%, while the average uncertainty of these newly reported values was approximately 45%. This uncertainty level is on par with the results of the cross-validation analysis discussed previously. Potential sources of experimental uncertainty include shot to shot laser energy fluctuation and minor levels of inhomogeneity of the pressed pellets. Due to the transition probabilities calculated in this study being derived from reported values, they also inherit the uncertainty associated with the previously reported values. Future studies would benefit from a larger sample set to allow for population statistics to narrow down uncertainties. To validate these new transition probabilities a second pellet with a different concentration of europium was tested. The electron density and plasma temperature were calculated using the procedure previously detailed and were determined to be $3.73 \pm 0.784 \times 10^{15}$ $_{c}m^{-3}$ and 0.448 ± 0.004 eV, respectively. This electron density and plasma temperature are on par with those of the first pellet and satisfy McWhirter's criterion. Figure 7 shows the Saha-Boltzmann plot of the validation pellet. The Saha-Boltzmann coordinates for the peaks in Table 1 were determined using the transition probabilities calculated using the first pellet. The resulting data points are shown in Figure 7 with red square markers. These Saha-Boltzmann coordinates fall along the europium trend line well, despite a vertical shift in the intercept of the trend due to the increase in europium concentration from the first pellet to the second. This alignment validates the newly estimated transition probabilities.

Table 1. Calculated transition probabilities for neutral and singly ionized europium.

$\lambda_{reported}$ (nm)	$\lambda_{observed}$ (nm)	Ion	E_L (eV)	E_U (eV)	g_L	g_U	A ($\times 10^7$ s^{-1})
490.72	490.72	I	1.74	4.27	8	8	5.24 ± 2.49
491.14	491.14	I	1.74	4.27	8	6	8.09 ± 3.83
680.29	680.27	I	1.74	3.57	8	10	2.15 ± 1.03
758.41	758.39	I	1.93	3.56	12	10	2.58 ± 1.27
581.63*	581.88	I	2.90	3.90	9	7	1.91 ± 0.674
617.08*	617.32	II	1.91	3.85	8	14	1.87 ± 0.739
707.87*	707.71	II	1.75	3.44	10	6	1.63 ± 0.653
730.16*	730.12	II	2.31	3.95	10	12	4.75 ± 1.85

* These peaks did not have reported transition probabilities, degeneracies, or energy levels, only an observed wavelength was reported. Transition wavelengths were calculated from possible transitions using the energy levels of europium then calculated wavelengths were matched to observed wavelengths.

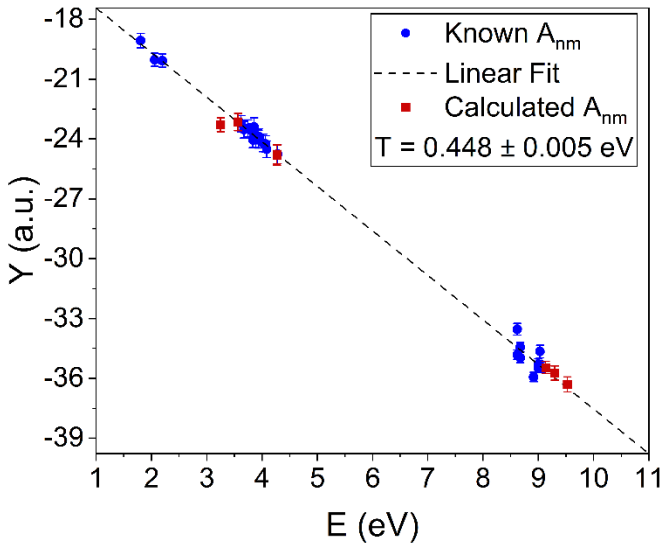

Figure 7. Saha-Boltzmann plot of europium emissions from the second pellet. Data points corresponding to emissions with newly calculated transition probabilities from the first pellet are shown with square markers. The trendline intercept is greater than that of the first pellet, an expected trait due to the increase in europium concentration.

3.4. Conclusions

In this study, eight previously unreported europium transition probabilities were estimated using the Saha-Boltzmann plot method. This information will allow the astrophysics community to make greater use of the spectra they collect from stellar objects by having more peak information. Furthermore, this study has shown that a simple LIBS setup can estimate new transition probabilities by leveraging Saha-Boltzmann plotting methodology to produce fundamental parameters to enable future CF-LIBS. Repeated measurements of these transition probabilities will provide further reduction in their uncertainty. While only a few unreported transition probabilities were calculated in this study, these transitions are of direct relevance to future CF-LIBS applications inherently based on being observed in laser-induced plasmas at relevant temperatures and densities. The procedure presented in this paper will help facilitate the future measurement of fundamental parameters for further REEs and actinides helping to enable the deployment of CF-LIBS for applications involving heavy elements such as those of interest during radioisotope production.

CHAPTER FOUR
CALCULATION OF TRANSITION PROBABILITIES FOR THE REMAINING LANTHANIDE SERIES

The sections below cover a study that discusses methods used for calculating transition probabilities of 13 lanthanides. The methods covered are like what was performed in Chapter Three; however, additional methods are introduced to improve the data statistics and reduce uncertainty. The amount of data produced was greatly increased from the previous chapter. This did not result in a significant amount of material being used which is discussed more in this chapter. Self-absorption correction techniques were also used in this study to further improve the accuracy of our estimations. Saha-Boltzmann plots were used to estimate new transition probabilities. A total of 967 transition probabilities were estimated and are reported in the appendix. Gaussian averages were taken of the estimated transition probabilities across the samples.

The work in this paper was submitted in 2022 and can be cited as:

Irvine, S.; Andrews, H.; Myhre, K.; Coble, J. Radiative Transition Probabilities of Neutral and Singly Ionized Lanthanides (La, Ce, Pr, Nd, Sm, Gd, Tb, Dy, Ho, Er, Tm, Yb, Lu) Estimated by Laser-Induced Breakdown Spectroscopy, Submitted **2022**

Sawyer Irvine: Methodology, Investigation, Software, Writing – original draft, Writing – review & editing, Visualization. Hunter Andrews: Conceptualization, Methodology, Investigation, Software, Writing – original draft, Writing – review & editing, Visualization, Funding acquisition, Project administration. Kristian Myhre: Conceptualization, Methodology, Writing – review & editing, Funding acquisition. Jamie Coble: Methodology, Writing – review & editing

4.1 Introduction

Spectroscopy can be used for many different analysis techniques to characterize and quantitatively analyze samples of various states and compositions. In the nuclear field alpha, neutron, gamma, and optical spectroscopies are used to provide qualitative and quantitative analysis on radioactive samples, such as Ac-227 samples typically being below 3 mCi, which is a standard, or activity limit, set to prevent high dose rates of radiation workers. LIBS can be used to quantify nearly every element in the periodic table including low and high Z elements, as well as both stable and radioactive species. LIBS has been used to analyze REEs in graphite matrices in ranges as low as 30 ppm.[12,66] It has also been used to map out REEs in nuclear glass-ceramic waste from reactors to aid in tracking and cleanup of these materials.[67] These elements are important to study for medical, reactor, and stellar applications.[3,48,68] Radioisotopes are produced through the irradiation of target materials, followed by dissolution and separation. Radioisotopes are used in medicine, used as nuclear reactor startup sources, and power systems for space exploration. Many of these heavy elements are of particular interest in stellar studies to determine the age of the universe and describe the elemental combination and production methods that occur within stellar bodies.[48]

The analysis of radioisotopes can be very difficult due to the inherent risk involved. Solutions must be heavily diluted, handled inside of glove boxes or hot cells, and must be carefully maintained under activity limits to reduce workers' exposure to radiation. Working with samples inside of glove boxes or hot cells can be very restrictive on what type of instruments can be used for analysis due to space restrictions and equipment damage from ionizing radiation. Being able to minimize the time required to make

measurements and restrict the exposure of the instrumentation to radioactivity would decrease the risk towards personal and equipment maintenance costs.

LIBS involves firing a focused laser pulse such that the energy density at the focused location is enough to ablate the material and form a plasma. The generated plasma cools and releases energy as optical light and those emissions are characteristic of the elemental makeup of the sample. One advantage of optical spectroscopy over other forms of analysis such as mass spectrometry is that for mass spectrometry, the lanthanides and actinides have isotopes that share masses and overlap with one another which could interrupt the ability to differentiate elements in a sample. Optical spectroscopy is unique to the electronic structures of the elements so they can be identified from one another. Another advantage of LIBS is that it can be employed remotely through optical fibers, periscope systems, or at large distances through telescope systems so that samples can be analyzed within the contaminated environment.[6–10,13–16,69–73] This remote viewing removes the need to dilute the samples as they no longer need to be removed from shielded areas. This reduces exposure and saves time, as well as preserving a high enough concentration of trace contaminants in the solutions that could be seen with LIBS which has been reported to view many REEs as low as 30 ppm.[12] This would enable more accurate analysis of samples in a short time span due to the rapidness of LIBS analysis. The caveat to the traditional LIBS approach is that it requires matrix matched standards to construct a calibration curve prior to analyzing unknown samples. This generally requires a significant material (~grams) which is very limited for many radionuclides. Additionally, sample preparation increases worker exposure to radiation from the radionuclides, conflicting with

the ‘as low as reasonably achievable’ philosophy.

CF-LIBS, originally proposed by Ciucci et al., could enable more time conservation, material conservation, and lessen exposure time.[31] CF-LIBS relies on the assumption that the plasma is under LTE during the time of data acquisition which has been shown to be accurate under CF-LIBS applied situations.[11,19,32,33] When under LTE conditions, which means that the electron density is high enough that the collisional rates exceed the radiative rates, then the concentration calculations can be dependent on previously known fundamental values such as transition probabilities. Leveraging the calibration on these previously reported values enables the foregoing of calibration curves made with matrix matched samples. This saves time, reduces the resources necessary for measurement, and keeps exposure to a minimum. CF-LIBS can be completed by ablating a sample, collecting the spectra, performing Saha-Boltzmann analysis, and then back calculating your concentrations. As previously stated, this is dependent on the fundamental values being reported.

It does not take many recorded emission lines to perform CF-LIBS, but the problem with many radionuclides and heavy elements is that not many of their transition probabilities have been reported. Another issue is that the typical methods for estimating these values are material intensive such as laser-induced fluorescence using a sputtered source from a hollow cathode tube.[44,45,74] Other methods such as Dirac Hartree-Fock, relativistic configuration interaction methods, and LIBS techniques have been used to produce transition probabilities for praseodymium – gadolinium and copper.[46,47] A method is proposed in this paper to use LIBS techniques with Saha-Boltzmann plots to calculate

transition probabilities. Similar methods were used in our previous study on europium and in a study for neptunium.[11,75] This method has produced a large amount of data and suggest that it could be used for resource restricted materials such as the actinides to enable CF-LIBS inside of hot cells and glove boxes remotely. It has improved upon previous studies by employing self-absorption corrections during the data analysis and using the energy levels of elements to determine as many transitions to calculate new transition probabilities for as possible.

4.2 Experimental

4.2.1 Sample Preparation

Thirteen lanthanide elements were examined during this study including lanthanum, cerium, praseodymium, neodymium, samarium, gadolinium, terbium, dysprosium, holmium, erbium, thulium, ytterbium, and lutecium. Each sample mixture was spiked with strontium as an internal standard. Strontium was selected due to its strong spectral response and well characterized emission peaks (i.e., transition probabilities). Each lanthanide and strontium solution was made from Inorganic Ventures 10,000 μg ml^{-1} ICP Standards. Three different concentrations were made for each lanthanide/strontium combination. The three different molar ratios of the lanthanide to strontium were 10, 5, and 2. Then 10 µl droplets of the mixed solutions were pipetted onto aluminum-6061 pucks. The aluminum pucks were machined to have a small recession in the center where the droplet would rest. The pucks would then be placed on a hot plate, set to low, until the solution had completely dried. Duplicate samples were prepared for each concentration. Both the varied molar ratios and use of duplicate samples were adjustments made from previously reported studies intended to help increase the confidence in the transition

probabilities determined in this study.

4.2.2 LIBS Measurements

All LIBS measurements were performed using a setup like that in our previous work.[11] Blank aluminum pucks were used to optimize the arrangement settings of the translation stage. Each test sample was placed in the LIBS unit on the translation stage and shot in a star pattern in nine different spots, five times at each spot, providing 45 spectra per sample. Every 15 sequential spectra were averaged to provide 6 final spectra per concentration of lanthanide.

4.2.3 Spectra Processing

The analyzed spectra were corrected using a determined relative efficiency function based on the optical arrangement of the system. This included the collection lenses, optical fiber, and the spectrometer itself. The relative efficiency function was determined by relating the average of ten measured spectra of a calibration lamp to its certified spectrum. Additional information about the procedure can be found in our previous work.[11,75] After the efficiency correction was completed, the spectra were background corrected and normalized. The background correction was performed based on the work done by Yaroshchyk and is detailed elsewhere.[11,62]

Lastly, each spectrum was normalized to the 396.26 nm Al I peak. Normalizing the spectra aided in correcting for shot-to-shot variation in the laser energy. Variance in the shot-to-shot laser energy alters the amount of energy distributed into the sample which then impacts the amount of material ablated and the formation of the plasma. Both normalizing and averaging mitigate this variance.

4.2.4 Peak Identification and Fitting

The neutral and singly ionized energy levels of each lanthanide, taken from the Basic Atomic Spectroscopic Database hosted by the NIST, were used to calculate all possible transitions that would result in emissions in the visible spectrum. These emission wavelengths were then plotted against the treated spectra of a blank aluminum puck, a puck with only strontium, and a puck with only a single lanthanide. The spectra were then meticulously scanned to identify lanthanide species' peaks available for further analysis.

After all of the available peaks were identified, the lmfit package in Python was used to fit Voigt functions to the emission peaks.[63] Voigt functions are a combination of Lorentzian and Gaussian functions; this combination is typically used for fitting LIBS peaks.[19] The areas were then determined using the Voigt fits and used in further analysis as the integral intensity.

4.2.5 Saha-Boltzmann Analysis

The integral intensity I_{nm} of an electronic transition in an optically thin plasma under LTE conditions of species *s* from energy level *n* to *m* can be calculated as a function of several species' parameters was covered in our previous work along with the Saha equation which describes the ratio between the concentration of species at different ionization levels.[11,64,65]

As detailed in our previous work, combining the Boltzmann and Saha equations will derive the Saha-Boltzmann relation, which can be written in a linear form as

$$y = mx + b(T) \quad where \begin{cases} m = -\frac{1}{T}, \;\; b(T) = ln\left(\frac{FC_1}{(U_1)}\right), \\ x = \begin{cases} E_1 \, (neutral), \\ E_2 + E_{ion} \, (ionic) \, , \end{cases} \\ y = \begin{cases} \ln\left(\frac{I_1}{g_1 A_1}\right) \, (neutral), \\ \ln\left(\frac{I_2}{g_2 A_2}\right) - \ln\left(\frac{2(2\pi m_e T)^{\frac{3}{2}}}{h^3 n_e}\right) (ionic) \end{cases} \end{cases} \tag{5}$$

where F is the instrument function accounted for by the efficiency correction, C_s is the number density of species s, U_s is the partition function, T is the temperature, E is the upper energy of the transition, E_{ion} is the energy required to ionize the neutral atom, I is the integral intensity of a peak, g is the degeneracy, A is the transition probability of the transition, m_e is the electron mass in eV, n_e is the electron density, h is Planck's constant, and the 1 and 2 subscripts refer to neutral and singly ionized respectively.

The electron density and plasma temperature are needed for the Saha-Boltzmann method. The electron density is obtained using Eq. (6) which relates the stark broadening associated with the Balmer series hydrogen alpha line, which was strongly visible in the spectrum, and its full width half max (Δλ) from de Oliveira Borges.[18] The electron density was calculated for each sample spectrum

$$n_e = \left[\left(\frac{\Delta\lambda}{0.549}\right)^{1.4713}\right] 10^{17} \tag{6}$$

The temperature was calculated through iteratively fitting the Saha-Boltzmann graphs (Eq. 5). An initial temperature guess was provided to a Python script, then Saha-Boltzmann coordinates were calculated, and a line was fitted. A new temperature was determined from the slope of this fitted line. This iterated until the percent difference of

the temperature from the previous iteration and the current one was below 0.0001%. This was done for both the strontium and lanthanide of each sample. It was observed that the strontium temperature was slightly different than each of the lanthanide temperatures and the lanthanide temperatures had more spread in their data.

Given the spectra were efficiency corrected and reproducible, this spread about the Saha-Boltzmann fit was attributed to self-absorption, a common occurrence in LIBS spectra. The preferred method of self-absorption correction is to use stark broadening coefficients when available. This was possible for the two ionized strontium peaks used in this study, both of which showed characteristics of self-absorption. The remaining emissions were corrected using the Internal Reference for Self-Absorption Correction (IRSAC) methodology developed by Sun and Yu.[34] To summarize, IRSAC was performed as follows. The transitions which are affected the most by self-absorption are often ones with large transition probabilities and low upper energy levels. Based on this logic, the neutral and ionized transitions were ranked to identify the emissions with the lowest transition probabilities and highest upper energy levels. Each trait was weighed equally to form an overall rank and the neutral and singly ionized peaks with the highest overall ranks were chosen to be the self-absorption reference peaks. The remaining emission peaks were then adjusted using the self-absorption coefficients calculated as shown in Eq. 7

$$f_\lambda^b = \frac{I_\lambda^{ij} A_{mn} g_m}{I_{\lambda R}^{mn} A_{ij} g_i} e^{\frac{-E_m + E_i}{T}} \tag{7}$$

where R indicates the reference peak, m/n refer to the upper and lower states of the reference line, and i/j refer to the upper and lower states of the line being corrected. The

initial temperature used was from the Saha-Boltzmann iterative fit previously discussed. Once the f-value for each peak was calculated, the intensities of the non-reference peaks were divided by the f-values to provide adjusted integral intensities. Although the reference peaks are assumed to have no self-absorption, there is a possibility of minor levels. If a peak had an f-value greater than one that meant it was experiencing less self-absorption than the reference peaks. When this occurred the f-value was set to one so that the intensity would not be altered. The IRSAC method uses an iterative procedure where the emission peaks were corrected, and a new Saha-Boltzmann plot was calculated. This new plot was then used to correct the emissions again. The process was iterated through until the coefficient of determination (R^2) differences between iterations were less than 0.01%.

4.3 Results and Discussion

The tables containing the reported transition probabilities are given in Appendix A in Tables A1-A13. A total of 78 samples were tested in this study to estimate new transition probabilities for 13 of the 15 lanthanide series elements. The remaining two lanthanides are europium and promethium. Europium, an element relevant to interstellar nucleosynthesis and nuclear processes was tested in a previous study.[11] praseodymium is the only lanthanide element without a stable isotope making it too rare of a material for the current study. Each lanthanide spectrum was parsed to match emission peaks with energy level transitions. The spectra of the lanthanide stock solutions on an aluminum puck, along with the aluminum and strontium spectra, are shown in Figure 8.

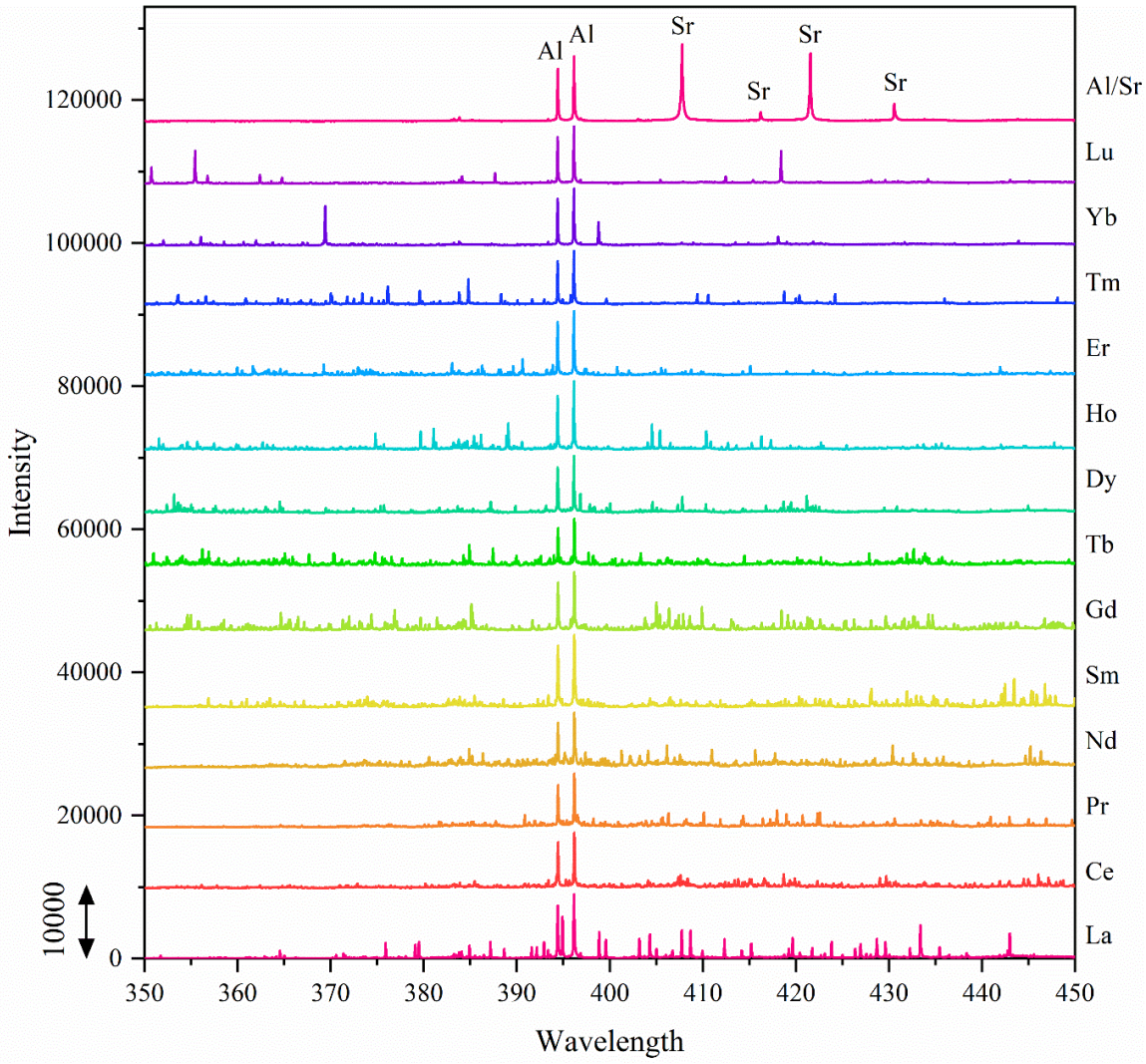

Figure 8. Stacked comparison of lanthanide spectra to the spectrum of the aluminum substrate and strontium standard illustrating the volume of peaks identified in this study.

4.3.1 Value comparisons and Discussion

The emission lines observed in this study ranged between 350 to 650 nm. The lower end of this range was the result of the optical efficiency which was significantly reduced below 350 nm. Lines for oxygen and nitrogen were very prevalent above 650 nm and overwhelmed most of the spectra beyond that point. The lanthanide peaks that were found in this study were primarily ionized peaks, though many neutral peaks were found as well. This behavior is seen in many other studies as the ionized peaks tend to have greater emission intensities than the neutral peaks.[76–80]Figure 9 shows the comparison of neutral versus singly ionized theoretical emission and normalized intensities for lanthanum, cerium, and neodymium. In Figure 9 (a) the ionized emissions are shown to be much more intense than neutral emissions. In Figure 9 both neutral and singly ionized peaks are shown to be in balance with one another for the temperatures seen in this study.

However, because neutral peaks are much lower in their max intensity than ionized peaks, they are much more susceptible to being lost in the background emissions. Future work could intentionally test samples at different laser energies and delay times to measure the plasma at different temperatures to target different ionization states.

The fitted peak areas were used to construct Saha-Boltzmann plots which were then adjusted for self-correction using the IRSAC procedure. These plots are shown in Figure 10 for each element. There is a trend among the Saha-Boltzman plots where the lanthanide lines slowly rise above the strontium lines as the elemental mass increases. The slopes remain similar, but the intercept slowly increases across the series. Each temperature reported is the lanthanide temperature.

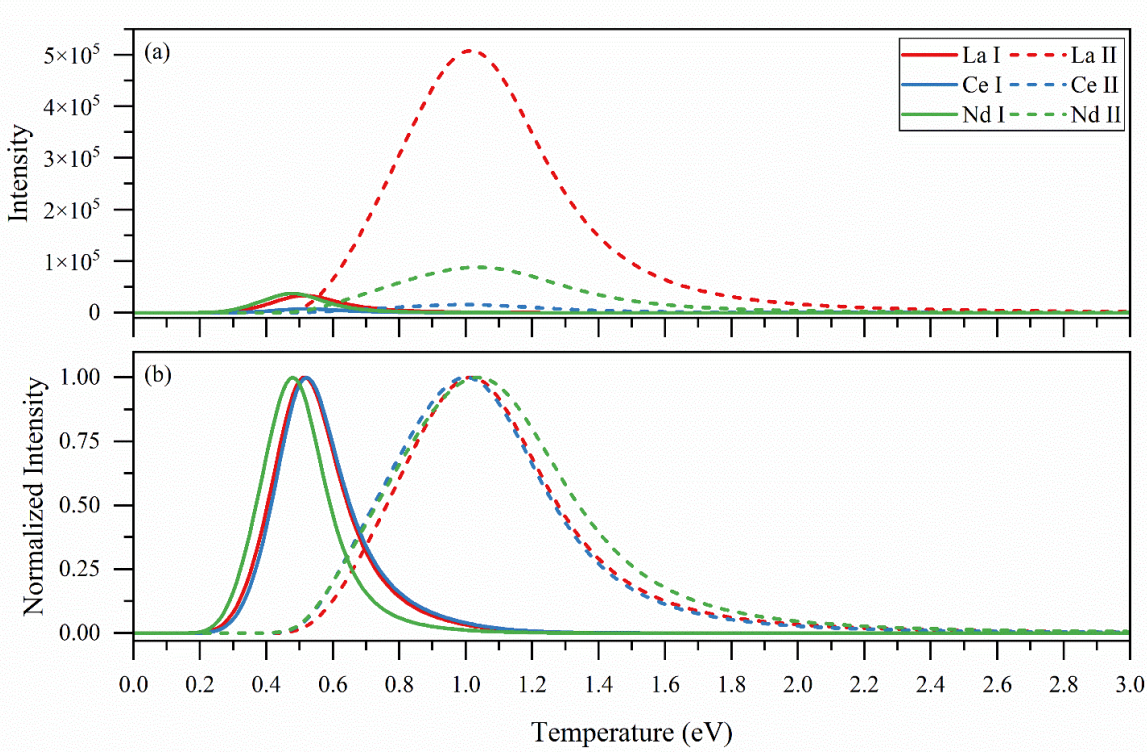

Figure 9. Comparison of neutral versus singly ionized (a) theoretical emission intensities and (b) normalized theoretical emission intensities.

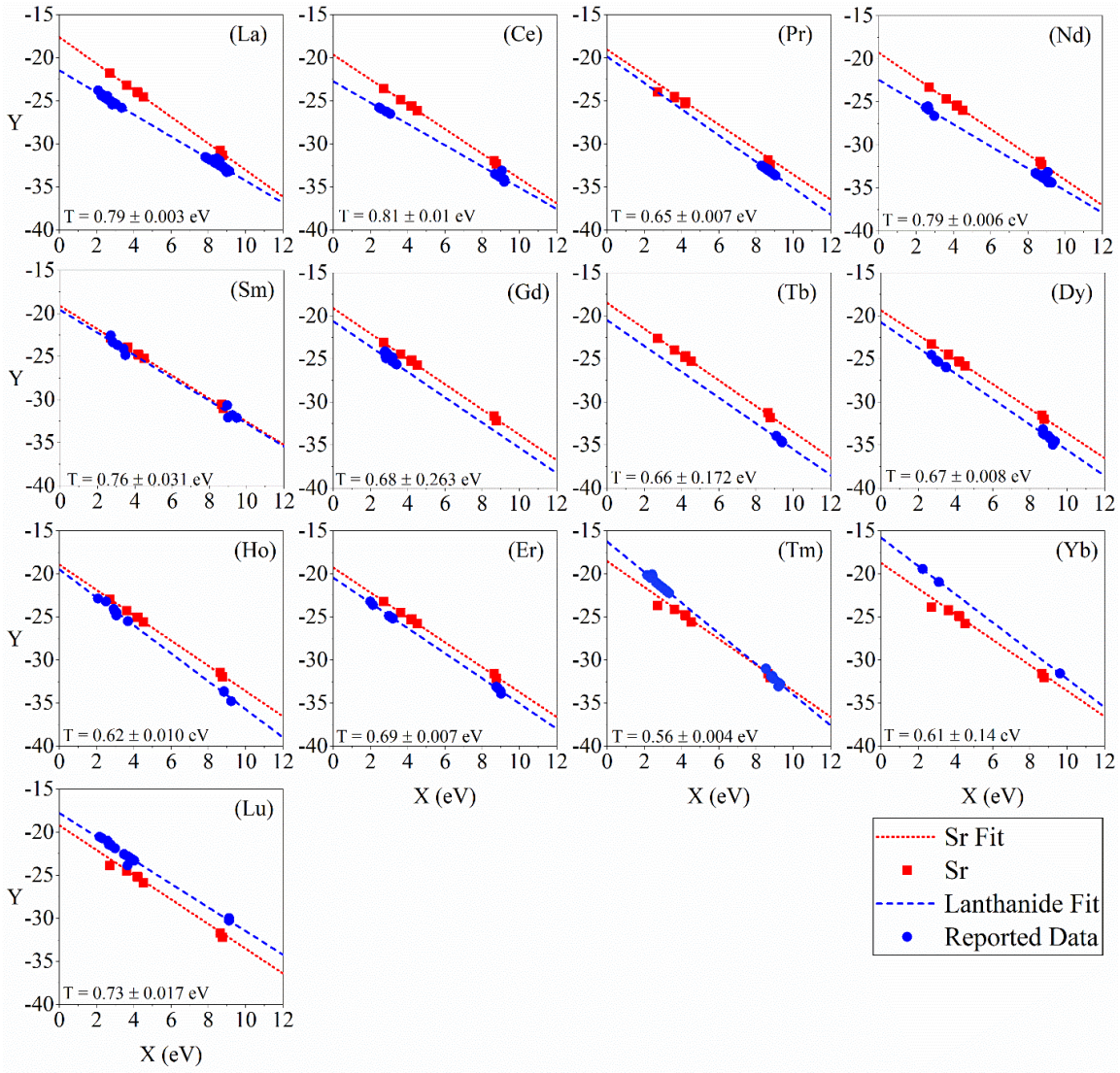

Figure 10. Saha-Boltzmann plots for each lanthanide after self-absorption correction. The shown plots are for the 10:1 lanthanide: strontium molar ratio samples.

For gadolinium and terbium, their slopes were forced to match the strontium slope, as disclosed below, and the temperature is still within good agreement with the other temperatures.

The strontium and lanthanide slopes (temperature) were commonly within 90% of one another in most samples. Although the strontium and lanthanide slopes were typically solved independently of one another, there were exceptions in cases where limited reported transition probabilities were available. For the gadolinium and terbium samples, the plasma temperature was calculated from the strontium slope and the lanthanide intercept was determined using the plasma temperature and the limited terbium lines with reported transition probabilities. This was done based on the assumption that the plasma temperature is homogonous during LTE. Samarium was also missing transition probabilities for one of its states, specifically its neutral state. However, the slope estimated with the ionized values produced a temperature that agreed with the strontium temperature which justified not forcing the samarium's slope to match strontium's slope.

The final Saha-Boltzmann plot fits were used to estimate new transition probabilities and their associated uncertainties. The transition probabilities and uncertainties from the six samples of each lanthanide were combined to get a final value for each emission peak.

Table 2 – 7 show values that were calculated in this study compared to previous works.

Table 2. Ce calculated values compared to reference values.

λ	E_{high}	g_{high}	ion	A	Unc.	Ref[52]	Ref Unc.
(nm)	(eV)			($\times 10^6$ s^{-1})			
484.79	3.51	10	2	4.01	0.86	5.00	0.50
491.29	3.14	6	2	0.64	0.15	0.20	0.03
583.23	3.22	8	2	1.70	0.40	0.54	0.06
539.85	3.51	8	2	2.21	0.51	1.60	0.13
469.89	3.51	10	2	0.76	0.18	0.36	0.05
392.74	3.51	10	2	1.28	0.29	3.40	0.30
404.69	3.51	8	2	9.82	2.17	0.67	0.08
381.49	3.71	10	2	1.43	0.32	2.15	0.16
356.08	4.16	14	2	12.2	2.59	73.00	4.00
357.75	3.93	12	2	8.30	1.77	60.00	4.00
372.84	4.00	16	2	16.5	3.57	43.10	2.90
380.15	4.16	14	2	25.5	5.38	139.00	7.00
468.04	3.51	12	2	4.22	0.89	1.57	0.10
423.26	3.65	12	2	9.91	2.13	5.30	0.30

Table 3. Pr calculated values compared to reference values.

λ	E_{upper}	g_{upper}	ion	A	Unc.	Ref[47]	Ref Unc.
(nm)	(eV)			($\times 10^6$ s^{-1})			
513.34	2.41	12	1	3.89	1.08	38.46	4.64
538.13	2.81	11	2	2.79	0.43	4.61	1.07
504.55	3.00	18	1	7.64	1.90	71.43	8.38
473.67	2.62	8	1	6.39	1.60	52.63	5.09
502.70	2.64	14	1	3.76	1.03	40.00	4.91
435.18	3.06	11	2	10.5	1.71	33.9	58.41
480.11	3.06	11	2	1.61	0.27	5.25	9.06
492.46	2.69	12	1	7.15	2.03	58.82	8.82
494.37	2.99	13	2	0.38	0.07	0.88	1.68
495.14	2.50	10	1	6.65	1.92	81.97	8.96

Table 4. Nd calculated values compared to reference values.

λ	E_{upper}	g_{upper}	ion	A	Unc.	Ref[47]	Ref Unc.
(nm)	(eV)			($\times 10^6$ s^{-1})			
521.32	2.67	13	1	36.8	8.89	21.81	2.30
490.18	2.82	15	1	104	24.8	71.43	7.54

Table 5. Sm calculated values compared to reference values.

λ	E_{upper}	g_{upper}	ion	A	Unc.	Ref[81]	Ref Unc.
(nm)	(eV)			($\times 10^6$ s^{-1})			
426.27	3.29	12	2	3.24	1.52	9.90	0.50
560.09	3.67	14	2	0.794	0.368	2.40	0.30
506.95	3.71	12	2	3.12	1.43	10.50	1.00
505.28	3.83	14	2	3.56	1.65	12.90	1.20
492.04	3.60	10	2	0.762	0.341	3.40	0.30
420.29	3.43	14	2	4.15	1.83	2.82	0.10
425.64	3.29	14	2	4.02	1.84	18.50	1.00
373.92	3.86	12	2	7.60	3.50	21.40	1.10
373.60	3.60	10	2	3.15	1.43	24.80	1.30
371.89	3.71	12	2	2.69	1.35	19.80	1.10
356.83	3.96	16	2	4.91	2.19	63.00	3.00
356.16	3.86	12	2	0.890	0.403	3.14	0.19
380.09	3.54	12	2	1.56	0.712	8.70	0.50
381.21	3.36	4	2	1.57	0.736	8.50	0.50
405.89	3.54	12	2	1.58	0.884	4.68	0.25
404.96	3.31	2	2	6.00	2.70	3.50	0.40
392.24	3.54	12	2	4.85	2.21	19.90	1.00
391.36	3.36	4	2	5.44	2.49	1.18	0.10
388.53	3.67	14	2	6.51	3.01	36.00	1.90
384.13	3.71	14	2	2.32	1.06	0.27	0.05

Table 6. Gd calculated values compared to reference values.

λ	E_{upper}	g_{upper}	ion	A	Unc.	Ref[82]	Ref Unc.	Ref[47]	Ref Unc.
(nm)	(eV)			($\times 10^6$ s^{-1})					
473.26	3.72	8	2	36.9	23.2	10.60	1.00	11.66	2.78
465.38	3.76	12	2	12.2	7.66	0.35	0.05	3.48	0.83
478.69	3.72	10	2	16.9	10.5	2.40	0.30	5.46	1.30
480.11	3.72	6	2	25.5	15.6	10.00	1.00	16.91	4.03
489.43	3.70	4	2	25.1	16.1	5.20	0.50	8.39	2.12
458.26	3.76	12	2	51.6	32.1	7.00	0.80	33.74	3.86
463.90	3.73	12	2	10.1	6.03	2.86	0.26	46.03	5.27
438.77	3.25	6	2	17.6	11.1	6.50	0.40	10.90	2.60
439.75	4.05	14	2	33.9	20.8	10.60	0.60	7.94	1.89
440.82	3.37	10	2	12.8	7.82	6.10	0.40	13.81	3.29
441.90	3.30	8	2	24.6	15.2	8.50	0.50	17.04	1.95

Table 6. Continued.

λ	E_{upper}	g_{upper}	ion	A	Unc.	Ref[82]	Ref Unc.	Ref[47]	Ref Unc.
443.83	3.45	12	2	19.7	12.4	4.30	0.30	12.10	2.88
447.88	3.37	10	2	15.3	9.46	5.00	0.40	9.84	2.34
460.11	3.25	6	2	25.2	15.5	8.20	0.60	16.61	3.80
448.11	3.37	10	2	18.5	11.5	6.00	0.40	9.67	2.30
450.63	3.25	6	2	33.5	21.0	5.10	0.40	13.24	3.16
455.81	3.22	4	2	13.7	8.46	5.20	0.04	8.16	1.95
517.63	3.45	12	2	15.5	9.55	3.80	0.50	4.55	1.08
535.78	3.47	8	2	3.55	2.19	0.61	0.08	1.18	0.28
436.98	3.22	4	2	79.0	48.2	14.30	1.10	25.36	2.91
434.43	3.45	12	2	10.1	6.24	2.49	0.18	7.80	1.86
368.78	3.72	6	2	83.0	50.9	60.00	3.00	48.22	5.52
369.77	3.38	6	2	49.9	29.8	37.30	1.90	22.57	2.58
371.27	3.72	8	2	115	70.8	66.00	3.00	34.25	3.92
371.64	3.37	10	2	19.0	11.7	13.70	0.80	17.23	1.97
373.08	3.70	4	2	141	88.8	70.00	4.00	49.13	5.63
374.35	3.45	12	2	66.8	41.1	48.40	2.40	31.35	3.59
434.22	3.45	12	2	34.2	20.7	15.90	1.10	24.89	2.85
378.76	3.76	12	2	33.9	21.4	19.00	1.40	27.98	3.20
379.64	3.30	8	2	90.2	54.2	61.00	3.00	50.29	5.31
367.12	3.45	12	2	45.1	27.6	25.00	1.40	21.93	2.51
366.23	3.38	6	2	60.8	37.2	24.40	1.30	10.99	2.62
354.94	3.73	12	2	73.2	44.3	85.00	4.00	40.91	4.68
357.19	3.47	8	2	16.0	9.88	10.50	0.60	4.67	1.11
358.50	3.60	10	2	83.8	50.4	96.00	5.00	58.06	6.65
364.62	3.64	14	2	110	68.1	75.00	4.00		
365.46	3.47	8	2	71.5	44.1	52.40	2.70	10.75	2.56
385.10	3.22	4	2	250	155	107.00	5.00	83.02	8.77
404.99	4.05	14	2	310	189	89.00	4.00	45.19	4.77
406.34	4.04	12	2	215	134	72.00	4.00	60.29	6.37
413.23	3.60	10	2	64.7	40.4	27.60	1.80	40.70	4.66
418.43	3.45	12	2	71.2	43.2	31.40	1.80		
420.49	3.47	8	2	34.1	21.0	10.60	0.70	29.58	3.39
423.88	4.05	14	2	50.0	31.1	16.80	0.90	10.30	2.46
425.17	3.30	8	2	59.8	36.7	27.80	1.60	32.94	3.77
425.36	4.04	12	2	119	75.9	27.70	1.50	46.85	4.95
428.05	3.25	6	2	55.8	34.1	19.20	1.10	30.23	3.46
403.73	3.73	12	2	120	74.3	26.50	1.60	30.24	3.46

Table 6. Continued.

λ	E_{upper}	g_{upper}	ion	A	Unc.	Ref[82]	Ref Unc.	Ref[47]	Ref Unc.
385.25	3.25	6	2	96.6	58.0	60.00	3.00	32.44	3.72
386.73	3.70	4	2	110	67.7	8.50	0.50	34.86	3.99
387.55	3.72	8	2	9.99	6.24	4.47	0.29	8.73	2.08
388.19	3.72	6	2	24.7	15.2	1.62	0.14	9.45	2.25
389.52	3.70	4	2	83.9	51.7	9.30	0.60	22.50	2.58
391.38	3.72	10	2	6.07	3.78	1.02	0.11	3.22	0.77
391.66	3.72	8	2	92.2	54.6	0.54	0.08	33.66	3.85
391.82	3.76	12	2	9.92	6.43	1.87	0.15	18.01	4.29
392.32	3.72	6	2	47.9	29.7	9.40	0.60	24.50	2.81
397.40	3.72	8	2	31.6	19.5	14.10	0.80	15.95	3.80
398.30	3.84	14	2	11.6	6.94	2.83	0.25	11.55	2.76
401.40	3.47	8	2	23.8	14.3	1.46	0.14	16.90	1.94

Table 7. Tb calculated values compared to reference values.

λ	E_{upper}	g_{upper}	ion	A	Unc.	Ref[51]	Ref Unc.
(nm)	(eV)			($\times 10^6$ s^{-1})			
414.44	3.12	17	2	35.6	12.2	12.20	0.80
373.24	3.75	15	2	11.3	4.01	16.80	1.10
370.39	3.75	15	2	39.6	13.5	88.00	5.00
374.74	3.71	13	2	96.5	33.0	49.40	2.60
397.68	3.12	17	2	27.7	9.50	20.60	1.20
400.55	3.22	17	2	30.0	10.2	23.40	1.40
377.65	3.71	13	2	59.0	20.2	63.00	3.00
388.18	3.71	13	2	16.9	5.84	9.60	0.70

Transition probabilities calculated in this study are compared to literature values in Table 2 - 7 and are shown in Figure 11. There were limited values available for comparison for the lanthanides; there were no comparison values found for dysprosium, holmium, erbium, thulium, ytterbium, and lutecium. Many of these heavier lanthanides had reported values for transitions not applicable for LIBS (e.g., higher ionization states ((ion > III) or diatomic molecular transitions). LIBS typically produces plasmas containing neutral and singly ionized species. Previous transition probabilities studies done by Den Hartog and Lawler were done with laser-induced fluorescence and Fourier transform spectroscopy for europium, gadolinium, holmium, and cerium.[44,52,74,82] Ryder used a LIBS setup (1064 nm Nd-YAG, Echelle spectrometer with ICCD) to measure branching fractions and then calculate transition probabilities and other fundamental data for neodymium, samarium, and gadolinium.[47] Multiple stages of agreement exist between the values estimated in this study and those reported in literature. For cerium, most of the comparisons are different. There are two cases where our uncertainty barely touches the values of the source. In the praseodymium comparison, three of the reference values have very large errors that do overlap with our values.

The samarium values seem to be mixed. Most of the reference values are above our values but our uncertainty does overlap with a few of the reference values. Gadolinium has an interesting spread. Most of the values seem to be similar and many of our uncertainties overlap the reference values. Many of the terbium values reported overlap their uncertainty with the reference values.

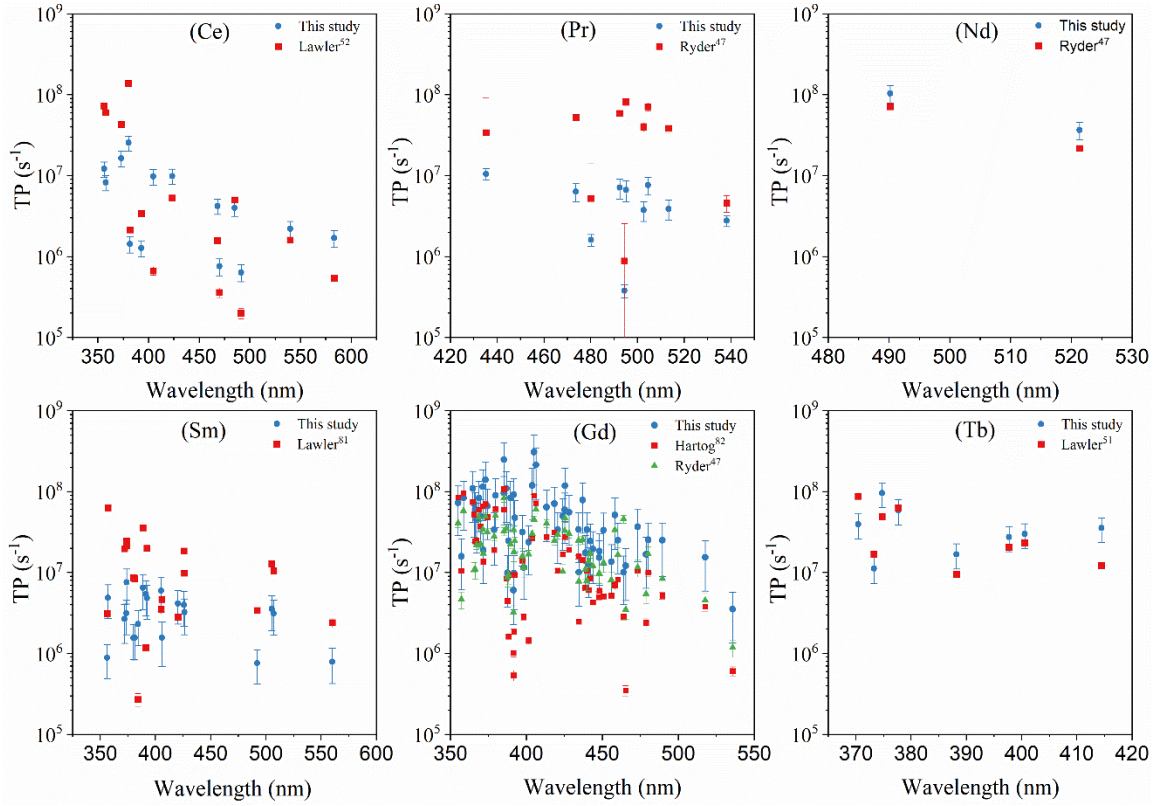

Figure 11. Transition probabilities calculated in this study (blue) compared to other studies (red and green).

While each of these previous studies used different methods from one another, the transition probabilities should be the same regardless of how they were measured. One potential explanation for differing values could be due to a lack of replicate measurements. The literature studies do not detail how many repeated measurements were made for their samples. For the transition probabilities reported in this work, each value represents the conglomeration of six different measurements.

One advantage of using LIBS to directly estimate transition probabilities is the high throughput testing. The volume of data presented in this study could suggest that this method has greater application for producing usable values quickly. Several of the emission peaks with new transition probabilities estimated in this study have been used in previous studies for tradition LIBS (i.e., to build calibration curves). Martin et al. investigated several REEs at low concentrations (30 – 300 ppm) to identify lines which could be used for quantification at that level. Out of the peaks tabulated by Martin et al., this study determined new transition probabilities for the 358.496, 364.619, 374.347, and 418.425 nm Gd II peaks.[12] These REEs are used in an increasing amount of modern electronics.[83] The transitions probabilities estimated in this work open the avenue to apply CF-LIBS to detect low-level REEs in scrap material in order to efficiently recycle electronics. Andrews and Myhre developed a LIBS system to monitor the off-gas stream from a molten salt reactor, a type of advance nuclear reactor in real-time.[84] Many lanthanides are common by products of nuclear fission making them of interest for monitoring. In their study, Andrews and Myhre investigated gadolinium, neodymium, and samarium in an aerosol stream down to parts-per-billion levels.[84] Transitions probabilities were estimated for several of the

peaks listed by Andrews and Myhre: the 404.986, 418.425, and 425.173 nm Gd II peaks and the 442.434 nm Sm II peak.[84]

Another study observed Nd II emissions using LIBS to determine branching ratios. Branching rations or branching fractions essentially compare the intensities of lines against each other to determine the proportion one transition emits over another. Branching ratios, which describe the probability of seeing one transition vs another, can be used to calculate other fundamental parameters like transition probabilities and oscillator strengths. The 463.267 nm Nd II peak was found in both Rehse and Ryder's studies and the current study.[85] A total of 8 transitions for Nd II were identified in Rehse and Ryder's study while in our study we have identified 115 Nd II peaks. These additional peaks provide a larger elemental signature to be used in future studies and help to achieve better statistics.

A comparison plot of the sample values compared to the gaussian averaged value was made and is shown in Figure 12. The residuals show that all sample calculations fall within 1.5 standard deviations of the Gaussian average, most being closer. Praseodymium shows the greatest variation, even though there are values that are within 0.25 standard deviations from the gaussian average. Gadolinium and terbium show a trend of the 10-ratio sample being above and below the other two samples respectively. Overall, Figure 12 shows that the individual data agrees closely with the gaussian average, and that the data supports each other.

Compared to the previous lanthanide LIBS works mentioned in this section, this paper reports transition probabilities for far more peaks for each of these elements which increases the breadth of data available.

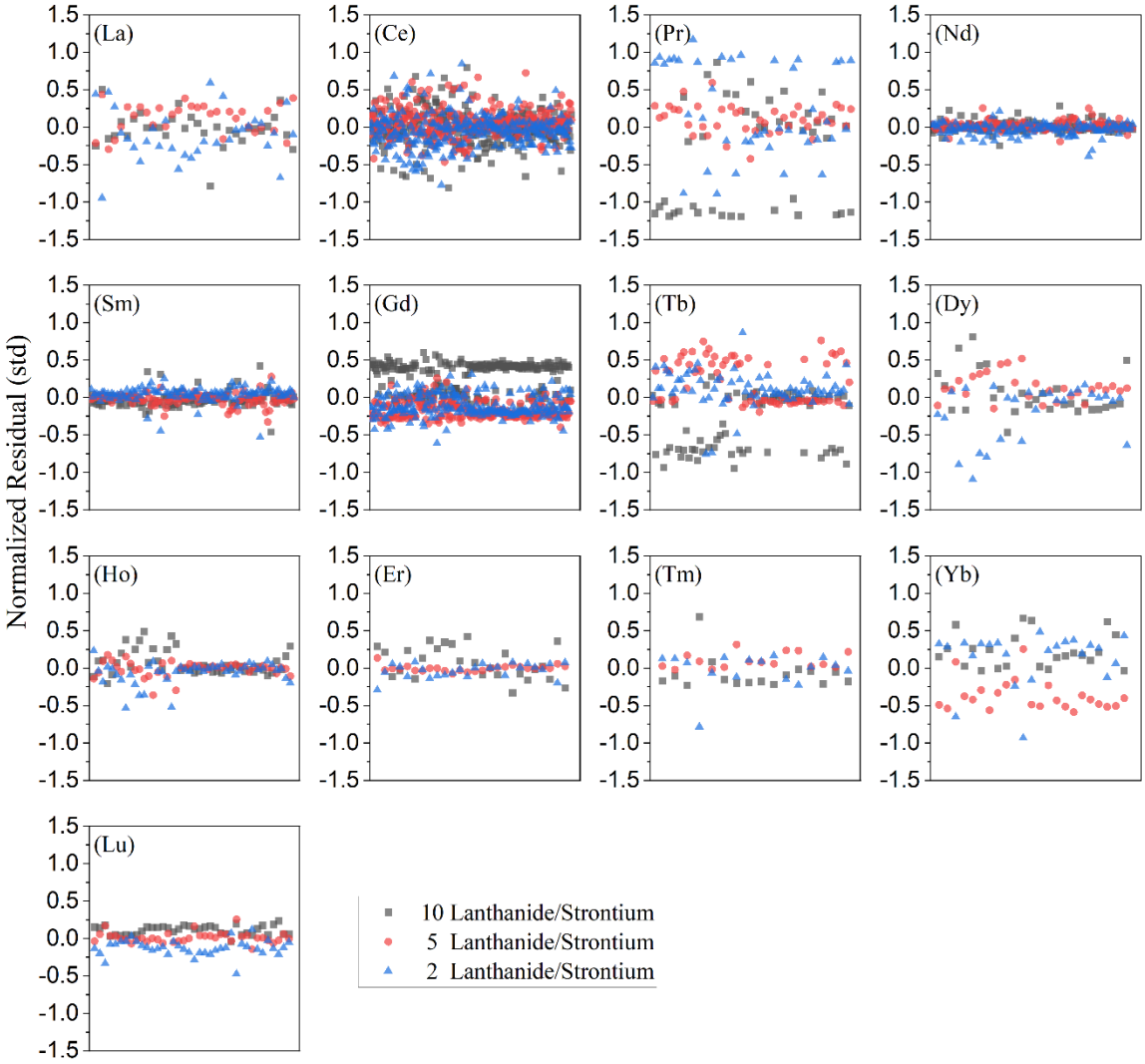

Figure 12. Normalized residual plot of the three samples versus the Gaussian average.

Overall, these studies provide examples of how newly calculated transition probabilities can enable CF-LIBS applications for elemental quantification in nuclear reactor off-gas streams, nuclear waste forms, archeological artifacts, and raw materials for electronics.[8,12,66,67,84]

4.4 Conclusions

In this study, 967 new transition probabilities were estimated using the Saha-Boltzmann plot method. The fundamental parameters reported in this study will contribute to the astrophysics community so that the spectra collected from stellar objects can be interpreted more thoroughly. More importantly, this study has shown that LIBS methods can be used to estimate new transition probabilities with high throughput with uncertainties as low as 10%. It was found in this study that neutral peaks typically result in lower uncertainty than ionized peaks, which is likely due to ionized peaks having much greater intensities that are more subject to self-absorption. Depending on the number of replicates made and the ability to collect well behaved data from the spectra, it is possible to reduce uncertainty significantly as seen when comparing this study's levels to our previous europium study.[11]

This has confirmed that increasing the number of samples allows the uncertainty in the transition probabilities to be reduced. Even though the number of samples was increased in this study, the amount of analyte used was still very low. This suggest that transition probabilities with reasonable uncertainties could be estimated using this method for actinides in the future. Performing a study on all possible transitions using the known energy levels of each element was a significant advantage for determining more transitions

available for Saha-Boltzmann plots and the necessary information for calculating transition probabilities. It is suggested that this method be used in future studies, especially with the actinides, to maximize the amount of data one can work with.

Chapter Five

CONCLUSIONS

From both the europium and 13-lanthanide studies it is suggested that transition probabilities can be successfully calculated using LIBS and Saha-Boltzmann methods. Introducing CF-LIBS as an analytical technique into the world of REEs, like the actinides, is a significant challenge because of the lack of fundamental data available for these elements, specifically transition probabilities. In the studies discussed above two similar methods were shown to use LIBS techniques along with Saha-Boltzmann plots to calculate these missing transition probabilities.

It has also been discussed that the analysis of actinides can be improved through using methods like optic fibers to analyze the materials in their native environments at labs, without the need to dilute them. Producing transition probabilities using these methods reduces exposure time to radiation for workers and allows for a minimal amount of material to be used. These are both significant advantages for working with these resource restricted and radioactive elements. CF-LIBS would provide a new way to monitor actinides and their use/production. These studies suggest that using LIBS and Saha-Boltzmann methods could be used as methods for producing the needed fundamental data for actinides to enable CF-LIBS for safer and more cost-effective analysis techniques. Besides looking at the actinides of interest for a study, LIBS and CF-LIBS could be used to track impurities in a sample as it passes through purification steps, and it could be used to track the ingrowth of daughter isotopes from a parent.

One aspect of work that was never made viable enough to use in the studies reported in this paper was the development of automatic peak finding and classifying software. This

has been explored throughout the time these studies took place and some progress was made on identifying peaks and classifying them. Having a background knowledge of what should be in the sample is helpful in narrowing down what peaks the software must look at. Overall, it is suggested that this type of software be explored as it would greatly decrease the time it takes to pick and sort peaks. It would be requisite to teach the program how to use multiple peaks as arguments for validating a certain species being present in the sample. Random Forest methods have been discussed and investigated to categorize peaks and then use the forest of decisions it makes across the entire spectrum to assign classifications to individual peaks. This was never fully implanted as stated before and is something that could be studied in the future of this work.

This method does seem to carry more uncertainty for certain transitions (ionized peaks) than other previously employed techniques (laser-induced fluorescence, Fourier transform spectroscopy, ICP-OES), however, this method typically uses less material and is able to complete its measurements faster than these previous methods. It has been stated in previous studies that using a purge gas over samples, specifically argon, would help increase signal to noise ratios. This was not used in this study but is another step that could be taken to better the results in future works. Potentially even purging the spectrometers with gasses could help increase signal yield. Estimation of transitions via the available reported energy levels for the neutral and singly ionized species of interest enabled matching peaks in the spectra and calculating more transitions probabilities. The reported transitions would also yield more data for future studies to use as references for evaluating spectra.

LIST OF REFERENCES

(1) Irvine, S. Estimation of Transition Probabilities by Laser-Induced Breakdown Spectroscopy for the Expanded Application of Calibration Free Methods, University of Tennessee - Knoxville, 2022.

(2) Martin, R. C.; Knauer, J. B.; Balo, P. A. Production, Distribution and Applications of Californium-252 Neutron Sources. *Appl. Radiat. Isot.* **2000**, *53* (4), 785–792. https://doi.org/10.1016/S0969-8043(00)00214-1.

(3) Boll, R. A.; Van Cleve, S. M.; Sims, N. J.; Felker, L. K.; Burns, J. D.; Owen, G. D.; Smith, E. H.; White, C. S.; Ezold, J. G. Californium Electrodepositions at Oak Ridge National Laboratory. *J. Radioanal. Nucl. Chem.* **2015**, *305* (3), 921–926. https://doi.org/10.1007/s10967-015-4148-8.

(4) Mayes, R. T.; VanCleve, S. M.; Kehn, J. S.; Delashmitt, J.; Langley, J. T.; Lester, B. P.; Du, M.; Felker, L. K.; Delmau, L. H. Combination of DGA and LN Columns: A Versatile Option for Isotope Production and Purification at Oak Ridge National Laboratory. *Solvent Extr. Ion Exch.* **2021**, *39* (2), 166–183. https://doi.org/10.1080/07366299.2020.1831244.

(5) Griffiths, T. L.; Woodbury, S. E.; Brooks, A.; Pinon, V.; Giakoumaki, A.; Whitehouse, A. I. A Study of the Effects of Gamma Radiation on Optical Components Used in Specially Constructed Hot Cell Laser-Induced Breakdown Spectroscopy (LIBS) Instruments. *Spectrochim. Acta Part B At. Spectrosc.* **2021**, *180*, 106205. https://doi.org/10.1016/j.sab.2021.106205.

(6) Saeki, M.; Iwanade, A.; Ito, C.; Wakaida, I.; Thornton, B.; Sakka, T.; Ohba, H. Development of a Fiber-Coupled Laser-Induced Breakdown Spectroscopy

Instrument for Analysis of Underwater Debris in a Nuclear Reactor Core. *J. Nucl. Sci. Technol.* **2014**, *51* (7–8), 930–938. https://doi.org/10.1080/00223131.2014.917996.

(7) Nakanishi, R.; Saeki, M.; Wakaida, I.; Ohba, H. Detection of Gadolinium in Surrogate Nuclear Fuel Debris Using Fiber-Optic Laser-Induced Breakdown Spectroscopy under Gamma Irradiation. *Appl. Sci.* **2020**, *10* (24), 8985. https://doi.org/10.3390/app10248985.

(8) Guirado, S.; Fortes, F. J.; Lazic, V.; Laserna, J. J. Chemical Analysis of Archeological Materials in Submarine Environments Using Laser-Induced Breakdown Spectroscopy. On-Site Trials in the Mediterranean Sea. *Spectrochim. Acta Part B At. Spectrosc.* **2012**, *74–75*, 137–143. https://doi.org/10.1016/j.sab.2012.06.032.

(9) Beddows, D. C. S.; Samek, O.; Liška, M.; Telle, H. H. Single-Pulse Laser-Induced Breakdown Spectroscopy of Samples Submerged in Water Using a Single-Fibre Light Delivery System. *Spectrochim. Acta Part B At. Spectrosc.* **2002**, *57* (9), 1461–1471. https://doi.org/10.1016/S0584-8547(02)00083-6.

(10) Fortes, F. J.; Laserna, J. J. The Development of Fieldable Laser-Induced Breakdown Spectrometer: No Limits on the Horizon. *Spectrochim. Acta Part B At. Spectrosc.* **2010**, *65* (12), 975–990. https://doi.org/10.1016/j.sab.2010.11.009.

(11) Irvine, S.; Andrews, H.; Myhre, K.; Goldstein, K.; Coble, J. Radiative Transition Probabilities of Neutral and Singly Ionized Europium Estimated by Laser-Induced Breakdown Spectroscopy. *J. Quant. Spectrosc. Radiat. Transf.* **2022**, 108184. https://doi.org/10.1016/j.jqsrt.2022.108184.

(12) Martin, M.; Martin, R. C.; Andrews, H. B.; Allman, S.; Brice, D.; Martin, S.; Nicolas, A. Quantification of Rare Earth Elements in the Parts Per Million Range_ A Novel

Approach in the Application of Laser-Induced Breakdown Spectroscopy.Pdf. *Appl. Spectrosc.* **2022**, *0*, 1–9. https://doi.org/10.1177/00037028221092051.

(13) Whitehouse, A. I.; Young, J.; Botheroyd, I. M.; Lawson, S.; Evans, C. P.; Wright, J. Remote Material Analysis of Nuclear Power Station Steam Generator Tubes by Laser-Induced Breakdown Spectroscopy ଌ. *At. Spectrosc.* **2001**, 10.

(14) Fobar, D. G.; Xiao, X.; Burger, M.; Le Berre, S.; Motta, A. T.; Jovanovic, I. Robotic Delivery of Laser-Induced Breakdown Spectroscopy for Sensitive Chlorine Measurement in Dry Cask Storage Systems. *Prog. Nucl. Energy* **2018**, *109*, 188–194. https://doi.org/10.1016/j.pnucene.2018.08.001.

(15) Neuhauser, R. E.; Panne, U.; Niessner, R. Utilization of Fiber Optics for Remote Sensing by Laser-Induced Plasma Spectroscopy (LIPS). *Appl. Spectrosc.* **2000**, *54* (6), 923–927. https://doi.org/10.1366/0003702001950337.

(16) Cremers, D. A.; Barefield, J. E.; Koskelo, A. C. Remote Elemental Analysis by Laser-Induced Breakdown Spectroscopy Using a Fiber-Optic Cable. *Appl. Spectrosc.* **1995**, *49* (6), 857–860. https://doi.org/10.1366/0003702953964589.

(17) Griffiths, T. L.; Woodbury, S. E.; Brooks, A.; Pinon, V.; Giakoumaki, A.; Whitehouse, A. I. A Study of the Effects of Gamma Radiation on Optical Components Used in Specially Constructed Hot Cell Laser-Induced Breakdown Spectroscopy (LIBS) Instruments. *Spectrochim. Acta Part B At. Spectrosc.* **2021**, *180*, 106205. https://doi.org/10.1016/j.sab.2021.106205.

(18) de Oliveira Borges, F.; Ospina, J. U.; de Holanda Cavalcanti, G.; Farias, E. E.; Rocha, A. A.; Ferreira, P. I. L. B.; Gomes, G. C.; Mello, A. CF-LIBS Analysis of Frozen Aqueous Solution Samples by Using a Standard Internal Reference and Correcting

the Self-Absorption Effect. *J. Anal. At. Spectrom.* **2018**, *33* (4), 629–641. https://doi.org/10.1039/C7JA00299H.

(19) Aguilera, J. A.; Aragón, C. Characterization of a Laser-Induced Plasma by Spatially Resolved Spectroscopy of Neutral Atom and Ion Emissions. *Spectrochim. Acta Part B At. Spectrosc.* **2004**, *59* (12), 1861–1876. https://doi.org/10.1016/j.sab.2004.08.003.

(20) Yang, Y.; Hao, X.; Ren, L. Correction of Self-Absorption Effect in Calibration-Free Laser-Induced Breakdown Spectroscopy(CF-LIBS) by Considering Plasma Temperature and Electron Density. *Optik* **2020**, *208*, 163702. https://doi.org/10.1016/j.ijleo.2019.163702.

(21) Capitelli, M.; Capitelli, F.; Eletskii, A. Non-Equilibrium and Equilibrium Problems in Laser-Induced Plasmas. *Spectrochim. Acta Part B At. Spectrosc.* **2000**, *55* (6), 559–574. https://doi.org/10.1016/S0584-8547(00)00168-3.

(22) Hahn, D. W.; Omenetto, N. Laser-Induced Breakdown Spectroscopy (LIBS), Part I: Review of Basic Diagnostics and Plasma–Particle Interactions: Still-Challenging Issues Within the Analytical Plasma Community. **2010**, 32.

(23) Hahn, D. W.; Omenetto, N. Laser-Induced Breakdown Spectroscopy (LIBS), Part II: Review of Instrumental and Methodological Approaches to Material Analysis and Applications to Different Fields. *Appl. Spectrosc.* **2012**, *66* (4), 347–419. https://doi.org/10.1366/11-06574.

(24) Cremers, D. A.; Beddingfield, A.; Smithwick, R.; Chinni, R. C.; Jones, C. R.; Beardsley, B.; Karch, L. Monitoring Uranium, Hydrogen, and Lithium and Their Isotopes Using a Compact Laser-Induced Breakdown Spectroscopy (LIBS) Probe and

High-Resolution Spectrometer. *Appl. Spectrosc.* **2012**, *66* (3), 250–261. https://doi.org/10.1366/11-06314.

(25) Manard, B. T.; Wylie, E. M.; Willson, S. P. Analysis of Rare Earth Elements in Uranium Using Handheld Laser-Induced Breakdown Spectroscopy (HH LIBS). *Appl. Spectrosc.* **2018**, *72* (11), 1653–1660. https://doi.org/10.1177/0003702818775431.

(26) Horňáčková, M.; Horňáček, M.; Rakovský, J.; Hudec, P.; Veis, P. Determination of Si/Al Molar Ratios in Microporous Zeolites Using Calibration-Free Laser Induced Breakdown Spectroscopy. *Spectrochim. Acta Part B At. Spectrosc.* **2013**, *88*, 69–74. https://doi.org/10.1016/j.sab.2013.03.006.

(27) JABBAR, A. Elemental Composition of Rice Using Calibration Free La- Ser Induced Breakdown Spectroscopy. **2019**, *15* (1). https://doi.org/10.1007/s11801-019-8099-0.

(28) Zhang, Y.; Dong, M.; Cai, J.; Chen, Y.; Chen, H.; Liu, C.; Yoo, J. H.; Lu, J. Study on the Evaluation of the Aging Grade for Industrial Heat-Resistant Steel by Laser-Induced Breakdown Spectroscopy. *J. Anal. At. Spectrom.* **2021**. https://doi.org/10.1039/D1JA00331C.

(29) Martin, M.; Hamm, D.; Martin, S.; Allman, S.; Bell, G.; Martin, R. Micro-Laser-Induced Breakdown Spectroscopy: A Novel Approach Used in the Detection of Six Rare Earths and One Transition Metal. *Minerals* **2019**, *9* (2), 103. https://doi.org/10.3390/min9020103.

(30) Applied Photonics.

(31) Ciucci, A.; Corsi, M.; Palleschi, V.; Rastelli, S.; Salvetti, A.; Tognoni, E. New Procedure for Quantitative Elemental Analysis by Laser-Induced Plasma

Spectroscopy. *Appl. Spectrosc.* **1999**, *53* (8), 960–964. https://doi.org/10.1366/0003702991947612.

(32) Tognoni, E.; Cristoforetti, G.; Legnaioli, S.; Palleschi, V. Calibration-Free Laser-Induced Breakdown Spectroscopy: State of the Art. *Spectrochim. Acta Part B At. Spectrosc.* **2010**, *65* (1), 1–14. https://doi.org/10.1016/j.sab.2009.11.006.

(33) Fu, H.; Ni, Z.; Wang, H.; Jia, J.; Dong, F. Accuracy Improvement of Calibration-Free Laser-Induced Breakdown Spectroscopy. *Plasma Sci. Technol.* **2019**, *21* (3), 034001. https://doi.org/10.1088/2058-6272/aaead6.

(34) Sun, L.; Yu, H. Correction of Self-Absorption Effect in Calibration-Free Laser-Induced Breakdown Spectroscopy by an Internal Reference Method. *Talanta* **2009**, *79* (2), 388–395. https://doi.org/10.1016/j.talanta.2009.03.066.

(35) Purić, J.; Platiša, M.; Konjević, N. Stark Broadening of Singly Ionized Strontium and Calcium Lines. *Z. Für Phys. Hadrons Nucl.* **1971**, *247* (3), 216–222. https://doi.org/10.1007/BF01402491.

(36) Hu, Z.; Chen, F.; Zhang, D.; Chu, Y.; Wang, W.; Tang, Y.; Guo, L. A Method for Improving the Accuracy of Calibration-Free Laser-Induced Breakdown Spectroscopy by Exploiting Self-Absorption. *Anal. Chim. Acta* **2021**, *1183*, 339008. https://doi.org/10.1016/j.aca.2021.339008.

(37) Cristoforetti, G.; De Giacomo, A.; Dell'Aglio, M.; Legnaioli, S.; Tognoni, E.; Palleschi, V.; Omenetto, N. Local Thermodynamic Equilibrium in Laser-Induced Breakdown Spectroscopy: Beyond the McWhirter Criterion. *Spectrochim. Acta Part B At. Spectrosc.* **2010**, *65* (1), 86–95. https://doi.org/10.1016/j.sab.2009.11.005.

(38) Unnikrishnan, V. K.; Alti, K.; Kartha, V. B.; Santhosh, C.; Gupta, G. P.; Suri, B. M. Measurements of Plasma Temperature and Electron Density in Laser-Induced Copper Plasma by Time-Resolved Spectroscopy of Neutral Atom and Ion Emissions. *Pramana* **2010**, *74* (6), 983–993. https://doi.org/10.1007/s12043-010-0089-5.

(39) Borduchi, L. C. L.; Milori, D. M. B. P.; Villas-Boas, P. R. One-Point Calibration of Saha-Boltzmann Plot to Improve Accuracy and Precision of Quantitative Analysis Using Laser-Induced Breakdown Spectroscopy. *Spectrochim. Acta Part B At. Spectrosc.* **2019**, *160*, 105692. https://doi.org/10.1016/j.sab.2019.105692.

(40) Bye, C. A.; Scheeline, A. Saha-Boltzmann Statistics for Determination of Electron Temperature and Density in Spark Discharges Using an Echelle/CCD System. *Appl. Spectrosc.* **1993**, *47* (12), 2022–2030. https://doi.org/10.1366/0003702934066217.

(41) Ohno, N.; Razzak, M. A.; Ukai, H.; Takamura, S.; Uesugi, Y. Validity of Electron Temperature Measurement by Using Boltzmann Plot Method in Radio Frequency Inductive Discharge in the Atmospheric Pressure Range. *Plasma Fusion Res.* **2006**, *1*, 028–028. https://doi.org/10.1585/pfr.1.028.

(42) Naoi, Y.; Iwata, M.; Yokota, D.; Gaigalas, G.; Kato, D.; Murakami, I.; Sakaue, H. A.; Sekiguchi, Y.; Tanaka, M.; Tanuma, H.; Wanajo, S.; Nakamura, N. Laser Induced Breakdown Spectroscopy of Er II for Transition Probability Measurements. *Appl. Sci.* **2022**, *12* (4), 2219. https://doi.org/10.3390/app12042219.

(43) Messaoud Aberkane, S.; Safi, A.; Botto, A.; Campanella, B.; Legnaioli, S.; Poggialini, F.; Raneri, S.; Rezaei, F.; Palleschi, V. Laser-Induced Breakdown Spectroscopy for Determination of Spectral Fundamental Parameters. *Appl. Sci.* **2020**, *10* (14), 4973. https://doi.org/10.3390/app10144973.

(44) Den Hartog, E. A.; Wickliffe, M. E.; Lawler, J. E. Radiative Lifetimes of Eu and Transition Probabilities of Eu. *Astrophys. J. Suppl. Ser.* **2002**, *141* (1), 255–265. https://doi.org/10.1086/340039.

(45) Zhiguo, Z.; Li, Z. S.; Lundberg, H.; Zhang, K. Y.; Dai, Z. W.; Zhankui, J.; Svanberg, S. Radiative Properties of Eu II and Eu III Obtained from Lifetime and Branching Ratio Measurements. *J. Phys. B At. Mol. Opt. Phys.* **2000**, *33* (3), 521–526. https://doi.org/10.1088/0953-4075/33/3/319.

(46) Radžiūtė, L.; Gaigalas, G.; Kato, D.; Rynkun, P.; Tanaka, M. Extended Calculations of Energy Levels and Transition Rates for Singly Ionized Lanthanide Elements. I. Pr–Gd. *Astrophys. J. Suppl. Ser.* **2020**, *248* (1), 17. https://doi.org/10.3847/1538-4365/ab8312.

(47) Ryder, C. Oscillator Strength Measurements in Singly-Ionized, Doubly-Ionized and Neutral Lanthanides and Transition Elements (Sm, Nd, Pr, Gd, Cu, and Fe) Using Laser-Induced Breakdown Spectroscopy. **2011**, 555.

(48) Wallerstein, G.; Iben, I.; Parker, P.; Boesgaard, A. M.; Hale, G. M.; Champagne, A. E.; Barnes, C. A.; Käppeler, F.; Smith, V. V.; Hoffman, R. D.; Timmes, F. X.; Sneden, C.; Boyd, R. N.; Meyer, B. S.; Lambert, D. L. Synthesis of the Elements in Stars: Forty Years of Progress. *Rev. Mod. Phys.* **1997**, *69* (4), 995–1084. https://doi.org/10.1103/RevModPhys.69.995.

(49) Tian, Y.; Wang, X.; Liu, C.; Yu, Q.; Dai, Z. Measurements of Radiative Lifetimes, Branching Fractions, Transition Probabilities, and Oscillator Strengths for Eu II and Eu III Levels. *Mon. Not. R. Astron. Soc.* **2019**, *485* (4), 4485–4491. https://doi.org/10.1093/mnras/stz562.

(50) Wickli, M. E. Atomic Transition Probabilities for Dy I and Dy II. **2000**, 42.

(51) Lawler, J. E.; Wickliffe, M. E.; Cowley, C. R.; Sneden, C. *ATOMIC TRANSITION PROBABILITIES IN Tb II WITH APPLICATIONS TO SOLAR AND STELLAR SPECTRA*. https://iopscience.iop.org/article/10.1086/323001/pdf (accessed 2022-04-29).

(52) Lawler, J. E.; Sneden, C.; Cowan, J. J.; Ivans, I. I.; Den Hartog, E. A. IMPROVED LABORATORY TRANSITION PROBABILITIES FOR Ce II, APPLICATION TO THE CERIUM ABUNDANCES OF THE SUN AND FIVE *r*- PROCESS-RICH, METAL-POOR STARS, AND RARE EARTH LAB DATA SUMMARY. *Astrophys. J. Suppl. Ser.* **2009**, *182* (1), 51–79. https://doi.org/10.1088/0067-0049/182/1/51.

(53) Zhang, Z. G.; Svanberg, S.; Quinet, P.; Palmeri, P.; Biémont, E. Time-Resolved Laser Spectroscopy of Multiply Ionized Atoms: Natural Radiative Lifetimes in Ce IV. *Phys. Rev. Lett.* **2001**, *87* (27), 273001. https://doi.org/10.1103/PhysRevLett.87.273001.

(54) Biémont, É. Recent Advances and Difficulties in Oscillator Strength Determination for Rare-Earth Elements and Ions. *Phys. Scr.* **2005**, *T119*, 55–60. https://doi.org/10.1088/0031-8949/2005/T119/010.

(55) Ortiz, M.; Mayo, R.; Biémont, É.; Quinet, P.; Malcheva, G.; Blagoev, K. Radiative Parameters for Some Transitions Arising from the 3d94d and 3d84s2electronic Configurations in Cu II Spectrum. *J. Phys. B At. Mol. Opt. Phys.* **2006**, *40* (1), 167–176. https://doi.org/10.1088/0953-4075/40/1/015.

(56) Zaitun; Prasetyo, S.; Suliyanti, M. M.; Isnaeni; Herbani, Y. Quantitative Analysis of Titanium Concentration Using Calibration-Free Laser-Induced Breakdown

Spectroscopy (LIBS). *J. Phys. Conf. Ser.* **2018**, *985* (1), 12010-. https://doi.org/10.1088/1742-6596/985/1/012010.

(57) Ralchenko, Y.; Kramida, A. Development of NIST Atomic Databases and Online Tools. *Atoms* **2020**, *8* (3), 56. https://doi.org/10.3390/atoms8030056.

(58) *Determination of excitation temperature in laser-induced plasmas using columnar density Saha-Boltzmann plot | Elsevier Enhanced Reader*. https://reader.elsevier.com/reader/sd/pii/S2090123219300098?token=C2F0046711BFD2479879F9D52EBCCB86F56A75A30F655FAA646B460D9EFD2A1E3E66CA71D5B874A2BE2BA85698B7143A&originRegion=us-east-1&originCreation=20210615193540 (accessed 2021-06-15). https://doi.org/10.1016/j.jare.2019.01.008.

(59) Wahlgren, G. M. The Lanthanide Elements in Stellar and Laboratory Spectra. *Phys. Scr.* **2002**, *T100* (1), 22. https://doi.org/10.1238/Physica.Topical.100a00022.

(60) Umar, Z. A.; Liaqat, U.; Ahmed, R.; Hedwig, R.; Ramli, M.; Marpaung, M. A.; Kurniawan, K. H.; Pardede, M.; Baig, M. A. Determination of Micronutrients and Toxic Elements in Moringa Oleifera Leaves by Calibration Free Laser-Induced Breakdown Spectroscopy (LIBS). *Anal. Lett.* **2022**, *55* (5), 755–769. https://doi.org/10.1080/00032719.2021.1966794.

(61) Sheng, L.; Zhang, T.; Wang, K.; Tang, H.; Li, H. Quantitative Analysis of Fe Content in Iron Ore via External Calibration in Conjunction with Internal Standardization Method Coupled with LIBS. *Chem. Res. Chin. Univ.* **2015**, *31* (1), 107–111. https://doi.org/10.1007/s40242-014-4318-1.

(62) Yaroshchyk, P.; Eberhardt, J. E. Automatic Correction of Continuum Background in Laser-Induced Breakdown Spectroscopy Using a Model-Free Algorithm. *Spectrochim. Acta Part B At. Spectrosc.* **2014**, *99*, 138–149. https://doi.org/10.1016/j.sab.2014.06.020.

(63) Newville, M.; Stensitzki, T.; Allen, D. B.; Ingargiola, A. *LMFIT: Non-Linear Least-Square Minimization and Curve-Fitting for Python*; Zenodo, 2014. https://doi.org/10.5281/zenodo.11813.

(64) Farooq, Z.; Ali, R.; Qurashi, U. S.; Mahmood, M. H.; Yaseen, M.; Qayyum, M. A.; Hussain, M. N.; Shah, S. M.; Jan, T. Spectroscopic Studies of Laser Produced Plasma of Doped Nano-Structured Material by Laser Induced Breakdown Spectroscopy. *Phys. Plasmas* **2018**, *25* (9), 093106. https://doi.org/10.1063/1.5031828.

(65) Tognoni, E.; Cristoforetti, G.; Legnaioli, S.; Palleschi, V. A Numerical Study of Expected Accuracy and Precision in Calibration-Free Laser-Induced Breakdown Spectroscopy in the Assumption of Ideal Analytical Plasma. *Spectrochim. Acta Part B* **2007**, *62*, 1287–1302.

(66) Martin, M.; Martin, R. C.; Allman, S.; Brice, D.; Wymore, A.; Andre, N. Quantification of Rare Earth Elements Using Laser-Induced Breakdown Spectroscopy. *Spectrochim. Acta Part B At. Spectrosc.* **2015**, *114*, 65–73. https://doi.org/10.1016/j.sab.2015.10.005.

(67) Wang, X.; Motto-Ros, V.; Panczer, G.; De Ligny, D.; Yu, J.; Benoit, J. M.; Dussossoy, J. L.; Peuget, S. Mapping of Rare Earth Elements in Nuclear Waste Glass–Ceramic Using Micro Laser-Induced Breakdown Spectroscopy. *Spectrochim.*

Acta Part B At. Spectrosc. **2013**, *87*, 139–146. https://doi.org/10.1016/j.sab.2013.05.022.

(68) Knapp Jr., F. f.; Mirzadeh, S.; Beets, A. l.; Du, M. Production of Therapeutic Radioisotopes in the ORNL High Flux Isotope Reactor (HFIR) for Applications in Nuclear Medicine, Oncologyand Interventional Cardiology. *J. Radioanal. Nucl. Chem.* **2005**, *263* (2), 503–509. https://doi.org/10.1007/s10967-005-0083-4.

(69) Marquardt, B. J.; Goode, S. R.; Angel, S. M. In Situ Determination of Lead in Paint by Laser-Induced Breakdown Spectroscopy Using a Fiber-Optic Probe. *Anal. Chem.* **1996**, *68* (6), 977–981. https://doi.org/10.1021/ac950828h.

(70) Sasazawa, S.; Kakino, S.; Matsuura, Y. Optical-Fiber-Based Laser-Induced Breakdown Spectroscopy for Detection of Early Caries. *J. Biomed. Opt.* **2015**, *20* (6), 065002. https://doi.org/10.1117/1.JBO.20.6.065002.

(71) Rai, A. K.; Zhang, H.; Yueh, F. Y.; Singh, J. P.; Weisberg, A. Parametric Study of a Fiber-Optic Laser-Induced Breakdown Spectroscopy Probe for Analysis of Aluminum Alloys. *Spectrochim. Acta Part B At. Spectrosc.* **2001**, *56* (12), 2371–2383. https://doi.org/10.1016/S0584-8547(01)00299-3.

(72) Wu, J.; Qiu, Y.; Li, X.; Yu, H.; Zhang, Z.; Qiu, A. Progress of Laser-Induced Breakdown Spectroscopy in Nuclear Industry Applications. *J. Phys. Appl. Phys.* **2020**, *53* (2), 023001. https://doi.org/10.1088/1361-6463/ab477a.

(73) Davies, C. M.; Telle, H. H.; Montgomery, D. J.; Corbett, R. E. Quantitative Analysis Using Remote Laser-Induced Breakdown Spectroscopy (LIBS). *Spectrochim. Acta Part B At. Spectrosc.* **1995**, *50* (9), 1059–1075. https://doi.org/10.1016/0584-8547(95)01314-5.

(74) Den Hartog, E. A.; Wiese, L. M.; Lawler, J. E. Radiative Lifetimes of HoI and HoII. *J. Opt. Soc. Am. B* **1999**, *16* (12), 2278. https://doi.org/10.1364/JOSAB.16.002278.

(75) Andrews, H. B.; Sadergaski, L. R.; Myhre, K. G. Neptunium Transition Probabilities Estimated through Laser Induced Breakdown Spectroscopy (LIBS) Measurements. *J. Anal. At. Spectrom.* **2022**, *37* (4), 768–774. https://doi.org/10.1039/D1JA00423A.

(76) Andrews, H.; Phongikaroon, S. Development of an Experimental Routine for Electrochemical and Laser-Induced Breakdown Spectroscopy Composition Measurements of $SmCl_3$ in LiCl-KCl Eutectic Salt Systems. *Nucl. Technol.* **2019**, *205* (7), 891–904. https://doi.org/10.1080/00295450.2018.1551988.

(77) Abedin, K. M.; Haider, A. F. M. Y.; Rony, M. A.; Khan, Z. H. Identification of Multiple Rare Earths and Associated Elements in Raw Monazite Sands by Laser-Induced Breakdown Spectroscopy. *Opt. Laser Technol.* **2011**, *43* (1), 45–49. https://doi.org/10.1016/j.optlastec.2010.05.003.

(78) Alamelu, D.; Sarkar, A.; Aggarwal, S. K. Laser-Induced Breakdown Spectroscopy for Simultaneous Determination of Sm, Eu and Gd in Aqueous Solution. *Talanta* **2008**, *77* (1), 256–261. https://doi.org/10.1016/j.talanta.2008.06.021.

(79) Jung, E. C.; Lee, D. H.; Yun, J.-I.; Kim, J. G.; Yeon, J. W.; Song, K. Quantitative Determination of Uranium and Europium in Glass Matrix by Laser-Induced Breakdown Spectroscopy. *Spectrochim. Acta Part B At. Spectrosc.* **2011**, *66* (9–10), 761–764. https://doi.org/10.1016/j.sab.2011.09.002.

(80) Hotokezaka, H.; Tanaka, S.; Suzuki, A.; Nagasaki, S. Speciation Analysis on Europium(III) Using Laser-Induced Breakdown Spectroscopy. *Radiochim. Acta* **2000**, *88* (9–11), 645–650. https://doi.org/10.1524/ract.2000.88.9-11.645.

(81) Lawler, J. E.; Hartog, E. A. D.; Sneden, C.; Cowan, J. J. Sm Transition Probabilities and Abundances. arXiv October 19, 2005.

(82) Den Hartog, E. A.; Lawler, J. E.; Sneden, C.; Cowan, J. J. Improved Laboratory Transition Probabilities for Gd II and Application to the Gadolinium Abundances of the Sun and Three *r* -Process Rich, Metal-poor Stars. *Astrophys. J. Suppl. Ser.* **2006**, *167* (2), 292–314. https://doi.org/10.1086/508262.

(83) Penchoff, D. A.; Sims, C. B.; Windus, T. L. Rare Earth Elements and Critical Materials: Uses and Availability. In *ACS Symposium Series*; Penchoff, D. A., Windus, T. L., Peterson, C. C., Eds.; American Chemical Society: Washington, DC, 2021; Vol. 1388, pp 63–74. https://doi.org/10.1021/bk-2021-1388.ch003.

(84) Andrews, H. B.; Myhre, K. G. Quantification of Lanthanides in a Molten Salt Reactor Surrogate Off-Gas Stream Using Laser-Induced Breakdown Spectroscopy. *Appl. Spectrosc.* **2022**, 00037028211070323. https://doi.org/10.1177/00037028211070323.

(85) Steven J. Rehse; Caleb A. Ryder. Laser-Induced Breakdown Spectroscopy for Branching Ratio and Atomic Lifetime Measurements in Singly-Ionized Neodymium and Gallium. *Spectrochim. Acta Part B* **2009**, *64*, 974–980.

APPENDIX

A.1 La Estimated Transition Probabilities

Table 8 La transition probabilities and their associated energy level details.

$\lambda_{Reported}$ (nm)		$\lambda_{Observed}$ (nm)	Ion	E_{low} (eV)	E_{upper} (eV)	g_{low}	g_{upper}	A (s^{-1})	Uncertainty (s^{-1})
365.02		365.02	2	0.00	3.40	5	5	5.21×10^{6}	8.91×10^{5}
371.55		371.54	2	0.32	3.66	5	5	7.00×10^{6}	1.23×10^{6}
378.07		378.07	2	0.71	3.99	3	3	1.77×10^{7}	2.84×10^{6}
383.51		383.51	2	0.71	3.94	3	1	2.81×10^{7}	4.77×10^{6}
384.60		384.60	2	0.17	3.40	5	5	3.30×10^{6}	6.14×10^{5}
385.49		385.49	2	0.77	3.99	5	3	1.32×10^{7}	2.50×10^{6}
404.29		404.30	2	0.93	3.99	9	7	9.16×10^{7}	1.53×10^{7}
404.95		405.01	2	0.93	3.99	9	3	6.89×10^{7}	1.11×10^{7}
414.38		414.39	2	0.77	3.76	5	3	2.90×10^{6}	7.76×10^{5}
419.22		419.24	1	0.51	3.47	10	4	3.00×10^{8}	5.86×10^{7}
420.40		420.41	2	0.71	3.66	3	5	8.99×10^{6}	1.74×10^{6}
426.38		426.36	2	0.13	3.03	7	5	1.16×10^{7}	1.91×10^{6}
429.61		429.61	2	0.77	3.66	5	5	3.97×10^{7}	6.69×10^{6}
431.59		431.59	2	0.40	3.27	7	5	1.00×10^{6}	2.13×10^{5}
435.44		435.44	2	0.92	3.76	1	3	4.87×10^{7}	8.41×10^{6}
436.47		436.47	2	0.65	3.49	1	3	6.73×10^{6}	1.20×10^{6}
445.58		445.58	2	0.71	3.49	3	3	4.26×10^{6}	8.04×10^{5}
471.29		471.30	2	0.40	3.03	7	5	8.15×10^{5}	1.63×10^{5}
472.44		472.44	2	0.77	3.40	5	5	1.18×10^{6}	2.11×10^{5}
485.06		485.07	2	0.77	3.33	5	7	2.20×10^{6}	4.62×10^{5}
493.48		493.49	2	1.25	3.76	5	3	1.57×10^{7}	2.65×10^{6}
495.24		495.21	2	0.77	3.27	5	5	3.20×10^{6}	5.19×10^{5}
546.44		546.45	2	0.77	3.04	5	7	4.10×10^{5}	8.60×10^{4}
571.24		571.24	2	0.17	2.34	5	5	1.59×10^{5}	4.35×10^{4}
580.83		580.83	2	0.00	2.13	5	5	3.19×10^{5}	7.08×10^{4}
632.04		632.04	2	0.17	2.13	5	5	5.57×10^{5}	1.21×10^{5}
639.89		639.91	1	0.95	2.89	6	8	1.56×10^{7}	2.68×10^{6}

A.2 Ce Estimated Transition Probabilities

Table 9. Ce transition probabilities and their associated energy level details.

$\lambda_{Reported}$ (nm)	$\lambda_{Observed}$ (nm)	Ion	E_{low} (eV)	E_{upper} (eV)	g_{low}	g_{upper}	A (s^{-1})	Uncertainty (s^{-1})
351.78	351.82	2	0.48	4.00	8	16	3.94×10^{6}	8.33×10^{5}
352.82	352.82	2	0.00	3.51	8	10	9.65×10^{5}	2.09×10^{5}
353.44	353.46	2	0.32	3.82	12	16	3.88×10^{6}	8.28×10^{5}
353.93	353.90	2	0.65	4.16	2	14	3.96×10^{6}	8.23×10^{5}
356.11	356.08	2	0.68	4.16	16	14	1.23×10^{7}	2.59×10^{6}
356.40	356.41	2	0.54	4.01	6	10	1.88×10^{6}	3.90×10^{5}
357.30	357.33	2	0.42	3.89	6	14	9.95×10^{5}	2.08×10^{5}
357.78	357.75	2	0.47	3.93	14	12	8.30×10^{6}	1.77×10^{6}
360.79	360.75	2	0.72	4.16	10	14	2.94×10^{6}	6.92×10^{5}
361.64	361.65	2	0.43	3.86	2	12	1.40×10^{6}	3.14×10^{5}
362.25	362.28	2	0.46	3.89	4	14	2.76×10^{6}	5.87×10^{5}
362.41	362.46	2	0.43	3.85	2	12	6.94×10^{6}	1.56×10^{6}
365.61	365.60	2	0.46	3.85	4	12	8.51×10^{6}	1.81×10^{6}
366.83	366.82	2	0.63	4.01	6	10	6.02×10^{6}	1.34×10^{6}
370.99	370.99	2	0.52	3.86	14	12	1.94×10^{7}	4.10×10^{6}
371.86	371.85	2	0.53	3.86	8	12	4.93×10^{6}	1.14×10^{6}
372.60	372.62	2	0.56	3.89	6	14	1.91×10^{6}	4.41×10^{5}
372.86	372.84	2	0.68	4.00	16	16	1.66×10^{7}	3.57×10^{6}
375.17	375.20	2	0.52	3.82	4	16	2.40×10^{6}	5.36×10^{5}
375.58	375.58	2	0.70	4.00	12	16	4.68×10^{6}	9.91×10^{5}
376.09	376.11	2	0.53	3.82	8	16	5.30×10^{5}	1.11×10^{5}
376.32	376.30	2	0.56	3.85	10	12	2.37×10^{6}	5.13×10^{5}
376.92	376.91	2	0.54	3.82	6	16	2.59×10^{6}	5.44×10^{5}
377.29	377.31	2	0.60	3.89	4	14	1.53×10^{6}	3.27×10^{5}
378.28	378.26	2	0.61	3.89	12	14	1.29×10^{6}	3.25×10^{5}
378.70	378.67	2	0.43	3.71	2	10	4.54×10^{6}	1.02×10^{6}
380.18	380.15	2	0.90	4.16	12	14	2.56×10^{7}	5.38×10^{6}
380.35	380.37	2	0.68	3.93	16	12	7.66×10^{6}	1.62×10^{6}
380.84	380.81	2	0.90	4.16	4	14	1.06×10^{7}	2.33×10^{6}
380.96	380.98	2	0.61	3.86	12	12	5.50×10^{6}	1.14×10^{6}
381.25	381.26	2	0.63	3.89	6	14	8.49×10^{5}	1.88×10^{5}
381.53	381.49	2	0.46	3.71	8	10	1.43×10^{6}	3.24×10^{5}
381.79	381.77	2	0.27	3.51	2	12	1.49×10^{6}	3.67×10^{5}
382.42	382.44	2	0.62	3.86	6	12	7.89×10^{6}	1.77×10^{6}
385.35	385.32	2	0.30	3.51	10	12	3.93×10^{6}	8.82×10^{5}

Table 9. Continued.

$\lambda_{Reported}$ (nm)	$\lambda_{Observed}$ (nm)	Ion	E_{low} (eV)	E_{upper} (eV)	g_{low}	g_{upper}	A (s^{-1})	Uncertainty (s^{-1})
385.46	385.46	2	0.61	3.82	12	16	1.30×10^{7}	2.77×10^{6}
386.73	386.72	2	0.81	4.01	4	10	2.55×10^{6}	5.26×10^{5}
388.27	388.27	2	0.81	4.00	4	16	1.24×10^{7}	2.91×10^{6}
388.69	388.70	2	0.81	4.00	6	16	1.00×10^{6}	2.53×10^{5}
389.71	389.71	2	0.98	4.16	8	14	7.17×10^{6}	1.58×10^{6}
390.76	390.75	2	0.48	3.65	8	12	8.58×10^{6}	1.89×10^{6}
390.88	390.88	2	0.68	3.85	12	12	1.23×10^{7}	2.65×10^{6}
392.01	392.04	2	0.70	3.86	12	12	5.74×10^{6}	1.23×10^{6}
392.49	392.46	2	0.70	3.85	10	12	5.50×10^{6}	1.24×10^{6}
392.77	392.74	2	0.36	3.51	12	10	1.28×10^{6}	2.92×10^{5}
392.91	392.92	2	0.50	3.65	8	12	2.96×10^{5}	1.08×10^{5}
393.84	393.81	2	0.56	3.71	10	10	1.05×10^{7}	2.21×10^{6}
395.29	395.27	2	0.27	3.40	2	10	1.40×10^{7}	3.12×10^{6}
395.65	395.60	2	0.72	3.85	10	12	2.51×10^{7}	5.41×10^{6}
397.22	397.18	2	0.89	4.01	6	10	1.63×10^{7}	3.45×10^{6}
397.90	397.90	2	0.74	3.85	8	12	5.31×10^{6}	1.14×10^{6}
398.13	398.09	1	0.29	3.41	5	13	7.41×10^{7}	1.52×10^{7}
400.41	400.45	2	0.52	3.62	4	10	7.31×10^{6}	1.61×10^{6}
401.52	401.52	2	0.62	3.71	6	10	6.24×10^{6}	1.35×10^{6}
402.28	402.28	2	0.32	3.40	10	10	3.30×10^{6}	7.22×10^{5}
402.50	402.51	2	0.32	3.40	4	10	5.97×10^{6}	1.40×10^{6}
402.65	402.64	2	1.08	4.16	4	14	7.91×10^{5}	1.95×10^{5}
402.85	402.88	2	0.92	4.00	4	16	1.53×10^{7}	3.37×10^{6}
403.16	403.14	2	0.33	3.40	6	10	5.19×10^{6}	1.12×10^{6}
403.82	403.81	2	1.09	4.16	10	14	1.30×10^{7}	2.71×10^{6}
404.11	404.12	2	0.33	3.39	8	12	1.22×10^{7}	2.62×10^{6}
404.29	404.30	2	1.09	4.16	10	14	1.76×10^{7}	3.75×10^{6}
404.56	404.56	1	0.30	3.37	9	15	3.49×10^{7}	9.07×10^{6}
404.66	404.69	2	0.45	3.51	10	8	9.82×10^{6}	2.17×10^{6}
405.54	405.55	2	0.46	3.52	4	6	9.41×10^{6}	2.09×10^{6}
410.21	410.19	2	0.12	3.14	10	6	8.88×10^{6}	1.90×10^{6}
411.57	411.54	2	0.70	3.71	10	10	9.72×10^{6}	2.13×10^{6}
412.41	412.40	2	1.01	4.01	10	10	5.16×10^{7}	1.10×10^{7}
413.12	413.16	2	1.01	4.01	6	10	2.41×10^{7}	5.31×10^{6}
413.41	413.38	2	0.86	3.86	14	12	3.75×10^{7}	7.81×10^{6}
414.28	414.27	2	0.52	3.51	10	8	2.60×10^{7}	5.62×10^{6}
415.03	415.00	2	0.88	3.86	2	12	2.19×10^{7}	4.76×10^{6}

Table 9. Continued.

$\lambda_{Reported}$ (nm)	$\lambda_{Observed}$ (nm)	Ion	E_{low} (eV)	E_{upper} (eV)	g_{low}	g_{upper}	A (s^{-1})	Uncertainty (s^{-1})
415.23	415.20	2	0.87	3.85	10	12	2.47×10^{7}	5.27×10^{6}
415.34	415.35	2	0.42	3.40	6	10	1.09×10^{6}	2.92×10^{5}
416.60	416.59	2	0.88	3.85	12	12	2.19×10^{7}	4.63×10^{6}
416.72	416.70	2	1.03	4.00	12	16	8.45×10^{6}	1.87×10^{6}
417.69	417.71	2	0.86	3.82	14	16	9.11×10^{6}	2.07×10^{6}
419.36	419.36	2	0.45	3.40	10	10	1.86×10^{7}	4.08×10^{6}
419.52	419.51	2	0.90	3.85	8	12	2.26×10^{6}	5.69×10^{5}
419.66	419.66	2	0.70	3.65	10	12	6.32×10^{6}	1.40×10^{6}
419.88	419.91	2	1.21	4.16	10	14	5.07×10^{7}	1.14×10^{7}
422.81	422.82	2	0.89	3.82	6	16	1.15×10^{7}	2.40×10^{6}
423.23	423.26	2	0.72	3.65	10	12	9.91×10^{6}	2.13×10^{6}
423.47	423.48	2	1.01	3.93	10	12	3.25×10^{6}	7.27×10^{5}
424.30	424.33	2	0.59	3.51	6	8	8.33×10^{6}	1.77×10^{6}
424.48	424.48	2	0.60	3.52	4	6	1.35×10^{6}	3.89×10^{5}
424.90	424.94	2	0.48	3.39	8	12	1.22×10^{7}	2.62×10^{6}
425.62	425.59	2	0.60	3.51	4	10	7.94×10^{6}	1.73×10^{6}
426.14	426.13	2	1.03	3.93	12	12	2.36×10^{6}	5.35×10^{5}
426.42	426.41	2	1.11	4.01	12	10	1.92×10^{7}	4.09×10^{6}
429.02	429.02	1	0.17	3.06	7	13	2.58×10^{8}	5.16×10^{7}
429.31	429.31	2	0.62	3.51	6	8	6.72×10^{6}	1.45×10^{6}
431.57	431.57	2	1.01	3.89	6	14	6.30×10^{6}	1.33×10^{6}
432.11	432.15	2	0.96	3.82	10	16	5.91×10^{6}	1.30×10^{6}
432.51	432.52	2	0.53	3.39	8	12	2.57×10^{6}	5.98×10^{5}
432.72	432.73	2	1.15	4.01	2	10	3.10×10^{6}	7.88×10^{5}
433.66	433.64	1	0.03	2.89	5	17	2.62×10^{7}	5.67×10^{6}
433.81	433.83	2	0.65	3.51	2	12	8.34×10^{6}	1.86×10^{6}
433.96	433.98	2	1.08	3.93	4	12	9.04×10^{6}	1.98×10^{6}
435.01	435.00	2	1.01	3.86	4	12	1.51×10^{7}	3.16×10^{6}
435.34	435.33	2	1.09	3.93	10	12	2.11×10^{7}	4.49×10^{6}
436.20	436.18	2	1.01	3.85	4	12	2.05×10^{6}	4.90×10^{5}
436.50	436.47	2	0.42	3.26	6	8	1.07×10^{7}	2.30×10^{6}
436.75	436.75	2	1.32	4.16	6	14	2.48×10^{6}	5.39×10^{5}
436.95	436.96	2	0.68	3.51	16	10	9.78×10^{5}	2.40×10^{5}
438.25	438.25	2	1.03	3.85	12	12	2.49×10^{7}	5.27×10^{6}
439.71	439.70	1	0.55	3.37	13	11	9.97×10^{6}	2.90×10^{6}
440.36	440.35	2	1.05	3.86	6	12	2.21×10^{6}	5.07×10^{5}
441.11	441.10	2	0.56	3.37	10	8	8.42×10^{6}	1.78×10^{6}

Table 9. Continued.

$\lambda_{Reported}$ (nm)	$\lambda_{Observed}$ (nm)	Ion	E_{low} (eV)	E_{upper} (eV)	g_{low}	g_{upper}	A (s^{-1})	Uncertainty (s^{-1})
441.61	441.61	2	1.08	3.89	4	14	6.74×10^{5}	1.65×10^{5}
441.91	441.92	1	0.16	2.96	9	9	2.93×10^{8}	6.09×10^{7}
443.34	443.31	2	1.09	3.89	6	14	2.57×10^{6}	5.18×10^{5}
444.15	444.16	2	0.72	3.51	10	12	2.39×10^{6}	5.50×10^{5}
444.49	444.51	2	1.21	4.00	6	16	2.55×10^{7}	5.41×10^{6}
455.58	455.61	2	0.67	3.39	8	12	4.17×10^{6}	8.81×10^{5}
456.09	456.08	1	0.69	3.41	9	13	2.61×10^{8}	5.54×10^{7}
456.62	456.62	1	0.17	2.89	7	17	4.79×10^{7}	1.03×10^{7}
457.95	457.92	2	0.81	3.51	6	8	9.16×10^{6}	1.99×10^{6}
458.29	458.30	2	0.81	3.51	4	10	9.42×10^{6}	2.01×10^{6}
459.16	459.16	2	1.16	3.85	8	12	4.37×10^{6}	9.61×10^{5}
459.43	459.47	2	0.82	3.52	10	6	3.40×10^{7}	7.25×10^{6}
462.52	462.52	2	1.21	3.89	8	14	1.25×10^{7}	2.66×10^{6}
462.85	462.87	2	1.18	3.85	2	12	3.65×10^{7}	7.59×10^{6}
468.05	468.04	2	0.86	3.51	14	12	4.22×10^{6}	8.86×10^{5}
468.51	468.52	2	0.87	3.51	10	8	7.48×10^{6}	1.62×10^{6}
469.53	469.56	2	0.88	3.51	10	8	4.04×10^{6}	9.89×10^{5}
469.90	469.89	2	0.88	3.51	10	10	7.56×10^{5}	1.76×10^{5}
471.44	471.45	2	0.88	3.51	12	8	2.69×10^{6}	5.90×10^{5}
472.54	472.51	2	0.52	3.14	4	6	3.87×10^{6}	8.82×10^{5}
473.06	473.08	2	0.89	3.51	6	10	1.69×10^{6}	3.73×10^{5}
473.40	473.36	2	1.09	3.71	6	10	3.92×10^{6}	8.84×10^{5}
473.76	473.75	2	0.90	3.52	14	6	1.39×10^{7}	3.00×10^{6}
473.99	474.01	2	0.90	3.51	8	8	4.16×10^{6}	9.21×10^{5}
474.53	474.52	2	0.90	3.51	8	12	1.67×10^{6}	3.89×10^{5}
474.97	474.97	2	0.90	3.51	4	12	1.93×10^{5}	6.61×10^{4}
475.25	475.22	2	0.54	3.14	6	6	1.78×10^{6}	3.89×10^{5}
475.31	475.11	1	0.16	2.77	9	13	2.30×10^{6}	1.28×10^{6}
475.83	475.86	2	0.91	3.51	12	8	4.09×10^{6}	8.43×10^{5}
478.06	478.02	1	0.29	2.89	7	17	5.02×10^{6}	9.86×10^{5}
478.72	478.73	2	0.81	3.40	6	10	3.95×10^{5}	1.10×10^{5}
479.36	479.36	2	1.12	3.71	8	10	2.25×10^{6}	5.11×10^{5}
479.96	479.94	2	0.81	3.39	6	12	5.37×10^{5}	1.30×10^{5}
480.50	480.53	2	0.93	3.51	2	12	2.73×10^{5}	1.12×10^{5}
482.08	482.11	2	1.08	3.65	4	12	3.54×10^{5}	9.64×10^{4}
484.00	484.01	1	0.85	3.41	5	13	3.02×10^{6}	1.33×10^{6}
484.83	484.79	2	0.96	3.51	10	10	4.01×10^{6}	8.62×10^{5}

Table 9. Continued

$\lambda_{Reported}$ (nm)	$\lambda_{Observed}$ (nm)	Ion	E_{low} (eV)	E_{upper} (eV)	g_{low}	g_{upper}	A (s^{-1})	Uncertainty (s^{-1})
485.06	485.08	1	0.40	2.95	11	11	6.60×10^{7}	1.44×10^{7}
485.90	485.89	2	0.96	3.51	6	8	2.11×10^{6}	4.99×10^{5}
488.29	488.35	2	0.98	3.51	8	8	1.08×10^{7}	2.35×10^{6}
489.62	489.64	2	1.18	3.71	2	10	1.09×10^{6}	2.35×10^{5}
490.04	490.05	1	0.21	2.74	7	15	1.04×10^{7}	2.26×10^{6}
490.68	490.68	1	0.49	3.02	13	19	4.40×10^{6}	1.19×10^{6}
491.28	491.29	2	0.62	3.14	6	6	6.42×10^{5}	1.50×10^{5}
491.56	491.59	1	0.17	2.69	7	11	3.93×10^{7}	7.98×10^{6}
492.47	492.49	2	0.74	3.26	12	8	1.40×10^{6}	3.37×10^{5}
494.06	494.04	1	0.55	3.06	13	13	9.37×10^{6}	2.58×10^{6}
494.28	494.26	2	1.01	3.52	4	6	4.22×10^{5}	1.10×10^{5}
494.40	494.38	2	0.96	3.46	10	10	2.75×10^{6}	6.17×10^{5}
494.98	494.93	2	0.90	3.40	12	10	2.85×10^{5}	8.11×10^{4}
498.49	498.50	1	0.38	2.87	9	7	3.03×10^{7}	6.86×10^{6}
500.33	500.35	2	0.74	3.22	8	8	1.53×10^{6}	3.38×10^{5}
501.21	501.19	2	1.04	3.51	8	8	4.09×10^{6}	8.64×10^{5}
501.61	501.65	1	0.59	3.06	9	13	4.61×10^{6}	1.33×10^{6}
502.19	502.17	2	0.90	3.37	4	8	6.83×10^{5}	1.84×10^{5}
502.32	502.35	2	1.05	3.51	6	8	5.44×10^{6}	1.17×10^{6}
503.82	503.80	1	0.49	2.95	13	11	2.75×10^{7}	5.88×10^{6}
504.45	504.45	2	1.06	3.51	8	8	9.07×10^{6}	1.90×10^{6}
506.65	506.65	2	0.92	3.37	4	8	9.88×10^{5}	2.15×10^{5}
508.02	507.97	2	1.38	3.82	18	16	1.39×10^{7}	2.93×10^{6}
508.39	508.39	2	0.93	3.37	2	8	6.69×10^{5}	1.53×10^{5}
508.81	508.84	2	1.08	3.51	4	8	7.80×10^{5}	1.91×10^{5}
509.16	509.18	2	0.96	3.39	6	12	9.43×10^{5}	2.01×10^{5}
510.59	510.56	2	1.46	3.89	12	14	1.66×10^{6}	3.68×10^{5}
511.60	511.61	2	0.72	3.14	10	6	2.98×10^{6}	6.83×10^{5}
511.76	511.83	2	1.19	3.62	4	10	4.81×10^{6}	1.08×10^{6}
513.36	513.36	2	0.96	3.37	10	8	2.92×10^{5}	7.13×10^{4}
513.54	513.61	2	0.96	3.37	6	8	1.72×10^{6}	4.75×10^{5}
515.24	515.24	2	1.06	3.46	8	10	2.32×10^{5}	5.41×10^{4}
516.02	515.97	1	0.66	3.06	15	13	1.30×10^{7}	2.91×10^{6}
516.18	516.15	1	0.96	3.37	13	15	5.53×10^{7}	1.14×10^{7}
516.49	516.48	1	0.29	2.69	7	11	2.36×10^{6}	5.68×10^{5}
516.94	516.94	1	0.97	3.37	3	11	9.28×10^{6}	2.46×10^{6}
518.18	518.20	1	0.52	2.91	7	15	2.14×10^{7}	4.50×10^{6}

Table 9. Continued.

$\lambda_{Reported}$ (nm)	$\lambda_{Observed}$ (nm)	Ion	E_{low} (eV)	E_{upper} (eV)	g_{low}	g_{upper}	A (s^{-1})	Uncertainty (s^{-1})
519.21	519.17	1	1.02	3.41	5	13	1.30×10^{8}	2.67×10^{7}
520.29	520.27	1	0.98	3.37	11	15	1.74×10^{7}	4.00×10^{6}
524.62	524.63	2	1.01	3.37	10	8	2.02×10^{6}	4.63×10^{5}
525.32	525.34	2	1.04	3.40	8	10	7.85×10^{5}	1.63×10^{5}
526.33	526.32	1	0.52	2.87	7	7	6.06×10^{6}	1.30×10^{6}
526.48	526.47	2	0.90	3.26	4	8	9.77×10^{5}	2.13×10^{5}
526.61	526.61	2	1.05	3.40	6	10	3.34×10^{6}	7.24×10^{5}
526.99	527.01	2	0.79	3.14	10	6	2.56×10^{5}	7.07×10^{4}
527.22	527.19	1	0.38	2.74	9	15	8.80×10^{6}	1.82×10^{6}
528.60	528.58	1	1.02	3.37	5	15	1.66×10^{6}	4.26×10^{5}
529.43	529.41	2	0.88	3.22	2	8	4.33×10^{5}	9.61×10^{4}
530.89	530.90	1	0.68	3.02	7	19	1.23×10^{7}	2.83×10^{6}
531.49	531.49	2	0.81	3.14	6	6	4.24×10^{6}	9.48×10^{5}
531.85	531.84	2	1.32	3.65	6	12	2.28×10^{5}	7.90×10^{4}
532.23	532.21	2	1.04	3.37	8	8	3.21×10^{5}	7.09×10^{4}
533.64	533.60	2	1.33	3.65	10	12	2.07×10^{6}	4.68×10^{5}
534.45	534.48	2	0.88	3.19	2	10	1.50×10^{5}	5.33×10^{4}
535.40	535.39	2	1.21	3.52	10	6	3.26×10^{7}	6.86×10^{6}
537.27	537.31	2	1.09	3.39	10	12	3.38×10^{5}	1.03×10^{5}
539.82	539.85	2	1.21	3.51	6	8	2.21×10^{6}	5.12×10^{5}
540.98	540.94	1	0.38	2.68	9	11	8.09×10^{7}	1.63×10^{7}
542.09	542.06	2	1.18	3.46	2	10	1.05×10^{6}	2.35×10^{5}
543.08	543.08	1	0.55	2.83	13	17	4.28×10^{6}	1.04×10^{6}
544.52	544.50	2	1.24	3.52	12	6	2.78×10^{5}	9.25×10^{4}
545.68	545.69	1	0.79	3.06	7	17	1.76×10^{6}	5.11×10^{5}
545.97	545.96	2	0.92	3.19	4	10	2.42×10^{6}	5.57×10^{5}
546.33	546.32	2	1.24	3.51	12	10	3.94×10^{5}	1.09×10^{5}
547.10	547.10	2	1.38	3.65	18	12	1.26×10^{5}	4.87×10^{4}
547.28	547.27	2	0.88	3.14	12	6	5.71×10^{6}	1.23×10^{6}
548.96	548.96	2	1.21	3.46	10	10	1.67×10^{5}	4.26×10^{4}
551.25	551.21	1	0.66	2.91	15	15	6.93×10^{7}	1.47×10^{7}
551.89	551.85	1	0.77	3.02	7	19	1.34×10^{7}	3.09×10^{6}
552.88	552.88	2	1.28	3.52	10	6	7.17×10^{5}	1.85×10^{5}
554.94	554.94	1	0.46	2.69	3	11	6.57×10^{6}	1.92×10^{6}
555.71	555.71	2	1.03	3.26	12	8	4.13×10^{6}	9.09×10^{5}
556.99	557.00	2	0.97	3.19	4	10	1.30×10^{5}	4.41×10^{4}
558.51	558.54	2	1.24	3.46	12	10	1.15×10^{6}	2.47×10^{5}

Table 9. Continued.

$\lambda_{Reported}$ (nm)	$\lambda_{Observed}$ (nm)	Ion	E_{low} (eV)	E_{upper} (eV)	g_{low}	g_{upper}	A (s^{-1})	Uncertainty (s^{-1})
558.86	558.86	2	1.18	3.39	2	12	5.10×10^{5}	1.11×10^{5}
559.22	559.24	2	1.25	3.46	14	10	1.75×10^{5}	6.03×10^{4}
561.10	561.09	1	0.47	2.68	11	11	2.76×10^{7}	5.71×10^{6}
561.65	561.62	1	0.85	3.06	9	17	2.19×10^{6}	7.99×10^{5}
562.35	562.41	2	1.01	3.22	4	8	1.15×10^{6}	2.53×10^{5}
562.70	562.71	1	0.63	2.83	3	17	1.10×10^{6}	3.80×10^{5}
563.29	563.25	1	0.49	2.69	13	11	1.43×10^{6}	5.19×10^{5}
565.18	565.22	1	0.83	3.02	11	19	1.64×10^{6}	6.12×10^{5}
567.00	567.01	2	1.33	3.51	10	10	8.46×10^{6}	1.79×10^{6}
568.39	568.33	2	1.01	3.19	6	10	1.99×10^{5}	4.70×10^{4}
568.62	568.64	1	0.77	2.95	11	11	1.69×10^{7}	3.88×10^{6}
569.33	569.30	1	0.50	2.68	3	11	6.47×10^{6}	1.44×10^{6}
569.97	569.92	1	0.84	3.02	17	19	3.31×10^{7}	7.09×10^{6}
570.83	570.82	1	0.85	3.02	5	19	1.97×10^{6}	5.01×10^{5}
571.45	571.46	2	1.09	3.26	10	8	1.66×10^{5}	4.31×10^{4}
571.58	571.54	1	0.38	2.55	9	13	5.77×10^{6}	1.22×10^{6}
571.94	571.93	1	0.70	2.87	3	7	9.33×10^{7}	2.00×10^{7}
572.44	572.45	2	1.09	3.26	10	8	1.13×10^{5}	3.05×10^{4}
574.10	574.10	2	1.06	3.22	8	8	4.49×10^{5}	9.93×10^{4}
574.66	574.65	2	1.24	3.40	12	10	1.84×10^{5}	4.05×10^{4}
575.25	575.26	1	0.73	2.89	5	17	1.11×10^{6}	2.93×10^{5}
575.42	575.39	2	1.25	3.40	14	10	3.12×10^{5}	9.11×10^{4}
576.12	576.12	1	0.72	2.87	15	7	1.79×10^{7}	4.68×10^{6}
577.35	577.39	1	0.62	2.77	7	13	3.83×10^{7}	8.46×10^{6}
578.86	578.89	1	0.55	2.69	13	11	2.67×10^{7}	5.81×10^{6}
579.50	579.53	1	0.73	2.87	5	7	2.93×10^{6}	1.12×10^{6}
580.02	580.01	1	0.55	2.68	11	15	9.94×10^{6}	2.09×10^{6}
581.34	581.30	1	0.82	2.95	7	11	2.91×10^{7}	6.61×10^{6}
583.24	583.23	2	1.09	3.22	10	8	1.70×10^{6}	3.95×10^{5}
583.63	583.65	2	1.25	3.37	14	8	1.65×10^{6}	3.94×10^{5}
585.26	585.26	2	1.03	3.14	12	6	3.39×10^{5}	7.43×10^{4}
587.20	587.22	2	1.40	3.51	16	10	1.29×10^{6}	2.97×10^{5}
587.52	587.48	2	1.40	3.51	16	12	1.85×10^{5}	7.72×10^{4}
591.05	591.00	1	0.77	2.87	11	7	3.88×10^{7}	1.02×10^{7}
591.33	591.29	1	0.59	2.68	13	15	8.09×10^{6}	1.76×10^{6}
597.63	597.65	1	0.89	2.96	9	9	4.50×10^{7}	9.33×10^{6}
622.95	622.93	1	0.97	2.96	3	9	1.93×10^{7}	4.52×10^{6}

Table 9. Continued.

$\lambda_{Reported}$ (nm)	$\lambda_{Observed}$ (nm)	Ion	E_{low} (eV)	E_{upper} (eV)	g_{low}	g_{upper}	A (s^{-1})	Uncertainty (s^{-1})
629.45	629.42	1	0.55	2.52	13	11	3.22×10^{6}	7.38×10^{5}
632.20	632.22	1	1.00	2.96	5	9	1.10×10^{7}	2.54×10^{6}

A.3 Pr Estimated Transition Probabilties

Table 10. Pr transition probabilities and their associated energy level details.

$\lambda_{Reported}$ (nm)	$\lambda_{Observed}$ (nm)	Ion	E_{low} (eV)	E_{upper} (eV)	g_{low}	g_{upper}	A (s^{-1})	Uncertainty (s^{-1})
374.58	374.62	2	0.05	3.36	11	17	1.30×10^{6}	2.28×10^{5}
376.52	376.50	2	0.20	3.50	13	17	5.06×10^{6}	6.48×10^{5}
386.58	386.57	2	0.22	3.42	11	13	1.04×10^{7}	1.49×10^{6}
387.23	387.22	2	0.37	3.57	15	19	2.86×10^{5}	7.03×10^{4}
401.10	401.13	2	0.48	3.57	13	19	7.74×10^{6}	1.18×10^{6}
413.10	413.08	2	0.42	3.42	13	13	5.29×10^{6}	8.48×10^{5}
435.22	435.18	2	0.22	3.06	11	11	1.06×10^{7}	1.71×10^{6}
435.38	435.39	2	0.73	3.57	13	19	1.10×10^{6}	1.35×10^{5}
444.12	444.13	1	0.00	2.79	10	10	6.61×10^{5}	1.35×10^{5}
445.87	445.83	2	0.55	3.33	17	15	1.42×10^{6}	2.44×10^{5}
456.49	456.46	2	0.65	3.36	13	17	2.45×10^{5}	4.99×10^{4}
462.92	462.92	2	0.80	3.47	15	15	6.23×10^{6}	1.05×10^{6}
464.02	463.95	1	0.17	2.84	12	10	5.25×10^{6}	1.33×10^{6}
467.50	467.47	1	0.17	2.82	12	16	1.37×10^{6}	2.68×10^{5}
473.10	473.08	2	0.55	3.17	17	15	1.90×10^{6}	2.92×10^{5}
473.70	473.67	1	0.00	2.62	10	8	6.39×10^{6}	1.60×10^{6}
475.83	475.82	2	0.97	3.57	19	19	1.55×10^{6}	2.44×10^{5}
480.16	480.11	2	0.48	3.06	13	11	1.61×10^{6}	2.70×10^{5}
484.89	484.87	2	0.51	3.06	11	11	2.89×10^{6}	3.56×10^{5}
490.19	490.15	2	0.97	3.50	19	17	9.06×10^{5}	1.89×10^{5}
491.45	491.44	2	0.65	3.17	13	15	2.04×10^{6}	3.15×10^{5}
492.51	492.46	1	0.17	2.69	12	12	7.15×10^{6}	2.03×10^{6}
494.03	493.97	1	0.35	2.86	14	14	1.24×10^{7}	3.32×10^{6}
494.39	494.37	2	0.48	2.99	13	13	3.76×10^{5}	6.68×10^{4}
495.17	495.14	1	0.00	2.50	10	10	6.65×10^{6}	1.92×10^{6}
499.45	499.41	2	0.51	2.99	11	13	3.47×10^{5}	5.29×10^{4}
502.73	502.70	1	0.17	2.64	12	14	3.76×10^{6}	1.03×10^{6}
504.59	504.55	1	0.54	3.00	16	18	7.63×10^{6}	1.90×10^{6}

Table 10. Continued.

$\lambda_{Reported}$ (nm)	$\lambda_{Observed}$ (nm)	Ion	E_{low} (eV)	E_{upper} (eV)	g_{low}	g_{upper}	A (s^{-1})	Uncertainty (s^{-1})
513.39	513.34	1	0.00	2.41	10	12	3.89×10^{6}	1.07×10^{6}
538.18	538.13	2	0.51	2.81	11	11	2.79×10^{6}	4.32×10^{5}
544.85	544.82	2	1.15	3.42	21	13	2.12×10^{5}	6.08×10^{4}
553.02	553.03	1	0.55	2.79	10	10	3.06×10^{5}	1.01×10^{5}
559.34	559.35	2	1.15	3.36	21	17	2.78×10^{5}	6.04×10^{4}
564.76	564.77	2	0.80	2.99	15	13	7.20×10^{4}	2.60×10^{4}
566.67	566.64	1	0.60	2.79	12	10	5.73×10^{5}	1.24×10^{5}
567.01	566.98	1	0.60	2.79	12	16	1.19×10^{6}	3.47×10^{5}
569.15	569.09	2	0.63	2.81	15	11	2.84×10^{5}	6.16×10^{4}
577.97	578.01	1	0.54	2.69	16	12	1.99×10^{6}	5.66×10^{5}
579.17	579.14	1	0.72	2.86	10	14	1.87×10^{6}	4.87×10^{5}
609.69	609.69	1	0.60	2.64	12	14	5.82×10^{5}	1.49×10^{5}
626.31	626.26	1	0.81	2.79	8	16	5.30×10^{5}	1.48×10^{5}
629.93	629.96	1	0.85	2.82	12	16	6.97×10^{5}	1.87×10^{5}

A.4 Nd Estimated Transition Probabilities

Table 11. Nd transition probabilities and their associated energy level details.

$\lambda_{Reported}$ (nm)	$\lambda_{Observed}$ (nm)	Ion	E_{low} (eV)	E_{upper} (eV)	g_{low}	g_{upper}	A (s^{-1})	Uncertainty (s^{-1})
351.77	351.78	2	0.00	3.52	8	18	3.34×10^{5}	7.98×10^{4}
358.05	358.05	2	0.00	3.46	8	10	1.26×10^{6}	3.06×10^{5}
358.30	358.25	2	0.06	3.52	10	18	1.31×10^{6}	4.18×10^{5}
359.83	359.82	2	0.20	3.65	10	14	1.75×10^{6}	4.42×10^{5}
359.98	359.97	2	0.06	3.51	10	12	5.93×10^{5}	1.64×10^{5}
364.59	364.64	2	0.32	3.72	14	20	1.72×10^{6}	4.61×10^{5}
365.07	365.04	2	0.18	3.58	12	16	1.21×10^{6}	4.15×10^{5}
367.82	367.81	2	0.38	3.75	12	18	2.05×10^{6}	5.01×10^{5}
370.95	370.97	2	0.18	3.52	12	18	1.06×10^{6}	2.88×10^{5}
371.16	371.15	2	0.38	3.72	12	20	1.87×10^{6}	5.15×10^{5}
372.38	372.35	2	0.32	3.65	14	14	3.14×10^{6}	8.55×10^{5}
374.16	374.20	2	0.55	3.86	12	14	5.90×10^{6}	1.62×10^{6}
380.57	380.56	2	0.55	3.81	12	16	2.14×10^{7}	5.30×10^{6}
383.08	383.12	2	0.20	3.44	10	14	4.30×10^{6}	1.22×10^{6}
385.20	385.17	2	0.18	3.40	12	10	2.09×10^{7}	5.20×10^{6}
386.94	386.98	2	0.32	3.52	14	18	3.62×10^{6}	9.91×10^{5}
387.62	387.64	2	0.38	3.58	12	16	5.15×10^{6}	1.42×10^{6}

Table 11. Continued.

$\lambda_{Reported}$ (nm)	$\lambda_{Observed}$ (nm)	Ion	E_{low} (eV)	E_{upper} (eV)	g_{low}	g_{upper}	A (s^{-1})	Uncertainty (s^{-1})
387.88	387.87	2	0.20	3.40	10	10	2.77×10^{6}	8.18×10^{5}
389.50	389.51	2	0.68	3.86	14	14	5.67×10^{6}	1.38×10^{6}
390.22	390.18	2	0.63	3.81	18	16	1.29×10^{7}	3.24×10^{6}
404.38	404.39	2	0.74	3.81	16	16	6.07×10^{6}	1.58×10^{6}
410.47	410.42	2	0.38	3.40	12	10	3.59×10^{6}	9.80×10^{5}
412.10	412.06	2	0.74	3.75	16	18	2.74×10^{6}	6.14×10^{5}
412.42	412.40	2	0.74	3.75	10	18	3.89×10^{6}	9.65×10^{5}
414.48	414.49	2	0.47	3.46	16	10	4.15×10^{6}	1.10×10^{6}
414.78	414.76	2	0.55	3.54	12	16	6.63×10^{5}	1.60×10^{5}
417.49	417.48	2	0.68	3.65	14	14	2.07×10^{6}	5.85×10^{5}
418.74	418.74	2	0.20	3.16	10	14	6.48×10^{5}	1.62×10^{5}
425.45	425.43	2	0.74	3.66	16	12	1.66×10^{6}	4.08×10^{5}
426.23	426.22	2	0.63	3.54	18	16	7.16×10^{6}	1.79×10^{6}
426.41	426.34	2	0.74	3.65	16	14	5.83×10^{6}	1.48×10^{6}
426.71	426.70	2	0.74	3.65	10	14	8.37×10^{6}	1.97×10^{6}
427.09	427.07	2	0.56	3.46	14	10	3.29×10^{6}	8.14×10^{5}
427.31	427.33	2	0.20	3.11	10	8	2.43×10^{6}	6.31×10^{5}
427.76	427.79	2	0.68	3.58	14	16	8.37×10^{5}	2.17×10^{5}
429.13	429.09	2	1.14	4.02	20	16	6.87×10^{6}	2.02×10^{6}
432.61	432.65	2	1.16	4.02	12	16	2.53×10^{7}	6.20×10^{6}
434.24	434.21	2	0.06	2.92	10	10	1.94×10^{6}	5.06×10^{5}
437.53	437.57	2	0.82	3.66	16	12	9.06×10^{6}	2.32×10^{6}
438.31	438.29	2	0.38	3.21	12	6	1.28×10^{6}	3.77×10^{5}
439.24	439.22	1	0.00	2.82	9	15	8.88×10^{6}	2.08×10^{6}
445.67	445.69	2	0.86	3.64	12	16	1.03×10^{7}	2.69×10^{6}
447.13	447.15	2	1.09	3.86	6	14	7.94×10^{6}	2.20×10^{6}
451.67	451.68	2	0.98	3.72	18	20	6.28×10^{6}	1.57×10^{6}
454.87	454.88	2	0.38	3.11	12	8	1.92×10^{6}	5.35×10^{5}
456.81	456.76	2	0.20	2.92	10	10	1.50×10^{6}	3.77×10^{5}
458.69	458.67	2	1.16	3.86	12	14	5.26×10^{6}	1.37×10^{6}
459.49	459.46	2	0.74	3.44	16	14	2.80×10^{6}	7.64×10^{5}
462.45	462.50	2	0.98	3.66	18	12	2.31×10^{6}	5.92×10^{5}
463.30	463.27	2	0.20	2.88	10	10	4.68×10^{5}	1.22×10^{5}
465.27	465.26	2	0.86	3.52	12	18	7.71×10^{5}	1.89×10^{5}
465.51	465.53	2	0.99	3.66	14	12	5.88×10^{6}	1.37×10^{6}
469.67	469.66	2	1.08	3.72	4	20	1.20×10^{6}	3.22×10^{5}
473.21	473.24	2	0.63	3.25	18	14	2.68×10^{6}	6.46×10^{5}

Table 11. Continued.

$\lambda_{Reported}$ (nm)	$\lambda_{Observed}$ (nm)	Ion	E_{low} (eV)	E_{upper} (eV)	g_{low}	g_{upper}	A (s^{-1})	Uncertainty (s^{-1})
475.00	474.96	2	1.14	3.75	8	18	5.76×10^{6}	1.49×10^{6}
477.72	477.71	2	0.74	3.34	16	16	1.16×10^{5}	4.12×10^{4}
479.75	479.80	2	1.14	3.72	20	20	3.71×10^{6}	9.96×10^{5}
481.38	481.37	2	1.08	3.66	4	12	3.99×10^{5}	1.66×10^{5}
482.58	482.54	2	1.08	3.65	4	14	1.58×10^{7}	3.92×10^{6}
485.94	485.96	2	1.20	3.75	6	18	1.19×10^{7}	3.00×10^{6}
488.03	487.98	2	1.32	3.86	8	14	1.62×10^{6}	4.44×10^{5}
488.42	488.41	2	0.99	3.52	14	18	7.51×10^{6}	1.84×10^{6}
488.96	488.99	1	0.14	2.67	11	7	4.70×10^{7}	1.25×10^{7}
490.22	490.18	1	0.29	2.82	13	15	1.05×10^{8}	2.49×10^{7}
490.79	490.78	2	1.28	3.81	14	16	4.36×10^{6}	1.05×10^{6}
491.77	491.81	2	1.20	3.72	6	20	6.14×10^{5}	1.69×10^{5}
492.11	492.11	1	0.46	2.98	15	13	1.16×10^{8}	2.78×10^{7}
492.80	492.81	2	1.14	3.66	8	12	1.28×10^{6}	3.10×10^{5}
493.25	493.25	2	1.14	3.65	20	14	7.70×10^{5}	2.82×10^{5}
495.52	495.57	2	1.36	3.86	18	14	7.65×10^{6}	2.00×10^{6}
498.33	498.35	2	1.09	3.58	6	16	1.08×10^{6}	3.36×10^{5}
501.51	501.54	2	0.56	3.03	14	12	1.45×10^{6}	3.46×10^{5}
504.77	504.30	2	1.35	3.81	10	16	1.94×10^{5}	1.06×10^{5}
506.72	506.70	2	1.30	3.75	22	18	1.15×10^{6}	2.89×10^{5}
507.71	507.71	2	1.14	3.58	20	16	4.47×10^{6}	1.23×10^{6}
510.58	510.58	2	1.32	3.75	8	18	2.38×10^{6}	6.85×10^{5}
512.19	512.17	2	0.74	3.16	10	14	3.00×10^{5}	9.16×10^{4}
512.76	512.73	2	1.12	3.54	16	16	1.07×10^{6}	2.59×10^{5}
516.81	516.85	2	1.14	3.54	8	16	2.48×10^{6}	5.76×10^{5}
521.28	521.32	1	0.29	2.67	13	13	3.68×10^{7}	8.89×10^{6}
521.60	521.62	2	1.65	4.02	14	16	2.79×10^{6}	7.64×10^{5}
527.03	526.98	2	1.17	3.52	16	18	3.44×10^{6}	9.22×10^{5}
527.39	527.34	2	0.68	3.03	14	12	6.91×10^{6}	1.74×10^{6}
527.74	527.70	2	0.86	3.21	12	6	6.46×10^{6}	1.63×10^{6}
530.69	530.71	2	1.17	3.51	16	12	1.91×10^{6}	5.07×10^{5}
531.19	531.21	2	1.53	3.86	14	14	5.98×10^{6}	1.54×10^{6}
534.38	534.37	2	1.08	3.40	4	10	8.54×10^{5}	1.81×10^{5}
534.60	534.57	2	1.12	3.44	16	14	2.19×10^{6}	5.73×10^{5}
535.00	535.01	2	0.93	3.25	8	14	8.37×10^{5}	2.33×10^{5}
541.70	541.75	2	1.36	3.65	18	14	2.05×10^{6}	5.06×10^{5}
542.20	542.15	2	0.74	3.03	10	12	1.09×10^{6}	2.71×10^{5}

Table 11. Continued.

$\lambda_{Reported}$ (nm)	$\lambda_{Observed}$ (nm)	Ion	E_{low} (eV)	E_{upper} (eV)	g_{low}	g_{upper}	A (s^{-1})	Uncertainty (s^{-1})
544.79	544.76	2	1.04	3.32	10	12	1.66×10^{6}	4.44×10^{5}
547.53	547.53	2	1.14	3.40	20	10	2.51×10^{6}	6.78×10^{5}
549.44	549.41	2	1.08	3.34	4	16	1.14×10^{6}	2.66×10^{5}
552.62	552.61	2	1.26	3.51	18	12	1.36×10^{6}	4.65×10^{5}
552.91	552.89	2	1.28	3.52	14	18	1.47×10^{6}	3.61×10^{5}
554.65	554.66	2	1.30	3.54	22	16	8.18×10^{5}	2.14×10^{5}
555.80	555.74	2	1.41	3.64	16	16	1.15×10^{6}	2.94×10^{5}
556.17	556.15	2	1.09	3.32	6	12	5.52×10^{5}	2.14×10^{5}
557.06	556.99	2	1.28	3.51	14	12	1.54×10^{6}	3.73×10^{5}
559.31	559.31	2	1.32	3.54	8	16	4.19×10^{5}	1.32×10^{5}
559.49	559.52	2	0.99	3.21	14	10	5.29×10^{6}	1.39×10^{6}
568.90	568.87	2	1.14	3.32	8	12	5.04×10^{6}	1.30×10^{6}
569.58	569.58	2	0.74	2.92	16	10	4.92×10^{5}	1.26×10^{5}
570.66	570.62	2	0.93	3.11	8	8	1.18×10^{6}	2.96×10^{5}
570.87	570.83	2	0.86	3.03	12	12	2.22×10^{6}	5.84×10^{5}
572.45	572.43	2	1.17	3.34	16	16	2.77×10^{5}	7.37×10^{4}
572.73	572.70	2	1.04	3.21	10	6	2.96×10^{6}	7.69×10^{5}
574.13	574.13	2	1.49	3.65	12	14	1.98×10^{6}	4.77×10^{5}
574.50	574.50	2	1.56	3.72	20	20	1.73×10^{6}	4.19×10^{5}
577.66	577.71	2	1.36	3.51	18	12	1.18×10^{6}	2.94×10^{5}
579.76	579.74	2	0.74	2.88	16	10	2.28×10^{5}	7.32×10^{4}
582.65	582.59	2	1.08	3.21	4	6	4.54×10^{6}	1.21×10^{6}
584.64	584.63	2	1.53	3.65	14	14	4.29×10^{5}	1.16×10^{5}
622.38	622.35	2	1.65	3.64	14	16	1.81×10^{6}	4.83×10^{5}
634.18	634.15	2	1.80	3.75	16	18	1.66×10^{6}	4.20×10^{5}

A.5 Sm Estimated Transition Probabilities

Table 12. Sm transition probabilities and their associated energy level details.

$\lambda_{Reported}$ (nm)	$\lambda_{Observed}$ (nm)	Ion	E_{low} (eV)	E_{upper} (eV)	g_{low}	g_{upper}	A (s^{-1})	Uncertainty (s^{-1})
356.20	356.16	2	0.38	3.86	12	12	8.90×10^{5}	4.03×10^{5}
356.86	356.83	2	0.48	3.96	14	16	4.91×10^{6}	2.19×10^{6}
360.98	360.96	2	0.00	3.43	2	14	3.11×10^{6}	1.43×10^{6}
362.97	363.00	2	0.54	3.96	10	16	2.69×10^{5}	1.27×10^{5}
364.57	364.52	1	0.00	3.40	1	7	3.24×10^{7}	1.47×10^{7}
370.72	370.72	1	0.39	3.73	11	13	2.53×10^{7}	1.14×10^{7}

Table 12. Continued.

$\lambda_{Reported}$ (nm)	$\lambda_{Observed}$ (nm)	Ion	E_{low} (eV)	E_{upper} (eV)	g_{low}	g_{upper}	A (s^{-1})	Uncertainty (s^{-1})
370.89	370.93	2	0.33	3.67	6	14	2.84×10^{6}	1.33×10^{6}
371.19	371.14	2	0.04	3.38	4	16	3.80×10^{5}	1.79×10^{5}
371.91	371.89	2	0.38	3.71	12	12	2.96×10^{6}	1.35×10^{6}
372.21	372.23	2	0.10	3.43	6	14	1.61×10^{6}	7.40×10^{5}
373.15	373.21	1	0.00	3.32	1	5	4.73×10^{7}	2.14×10^{7}
373.63	373.60	2	0.28	3.60	10	10	3.15×10^{6}	1.43×10^{6}
373.76	373.71	1	0.28	3.60	9	11	1.54×10^{7}	6.70×10^{6}
373.95	373.92	2	0.54	3.86	10	12	7.60×10^{6}	3.50×10^{6}
375.67	375.64	1	0.10	3.40	5	7	2.23×10^{7}	1.03×10^{7}
376.78	376.73	2	0.25	3.54	4	12	3.13×10^{6}	1.44×10^{6}
377.64	377.60	1	0.10	3.38	5	15	1.07×10^{6}	5.26×10^{5}
378.11	378.17	2	0.43	3.71	8	12	2.76×10^{6}	1.27×10^{6}
379.98	380.00	2	0.33	3.60	6	10	1.11×10^{6}	5.09×10^{5}
380.11	380.09	2	0.28	3.54	10	12	1.56×10^{6}	7.12×10^{5}
381.23	381.21	2	0.10	3.36	6	4	1.57×10^{6}	7.36×10^{5}
381.40	381.37	2	0.04	3.29	4	14	5.94×10^{5}	2.69×10^{5}
381.48	381.47	2	0.18	3.43	8	14	1.02×10^{5}	6.16×10^{4}
382.46	382.43	2	0.43	3.67	8	14	2.51×10^{6}	1.11×10^{6}
384.07	384.13	2	0.48	3.71	14	12	2.32×10^{6}	1.06×10^{6}
384.91	384.88	1	0.10	3.32	5	5	1.82×10^{7}	8.52×10^{6}
385.46	385.46	1	0.18	3.40	7	7	4.82×10^{7}	2.15×10^{7}
386.04	386.01	1	0.39	3.60	11	11	1.82×10^{7}	8.40×10^{6}
387.57	387.52	1	0.18	3.38	7	15	1.16×10^{7}	5.21×10^{6}
388.56	388.53	2	0.48	3.67	14	14	6.51×10^{6}	3.01×10^{6}
388.94	388.97	2	0.10	3.29	6	14	7.60×10^{5}	3.34×10^{5}
391.37	391.36	2	0.19	3.36	2	4	5.44×10^{6}	2.49×10^{6}
392.27	392.24	2	0.38	3.54	12	12	4.85×10^{6}	2.21×10^{6}
392.56	392.52	1	0.10	3.26	5	3	1.95×10^{7}	8.99×10^{6}
392.69	392.69	2	0.28	3.43	10	14	1.60×10^{5}	7.53×10^{4}
397.49	397.46	1	0.28	3.40	9	7	2.47×10^{7}	1.10×10^{7}
399.54	399.54	2	0.19	3.29	2	14	1.22×10^{5}	6.35×10^{4}
399.86	399.83	1	0.50	3.60	13	11	3.29×10^{6}	1.53×10^{6}
404.88	404.89	1	0.18	3.25	7	13	3.29×10^{6}	1.53×10^{6}
405.00	404.96	2	0.25	3.31	4	2	6.00×10^{6}	2.70×10^{6}
405.80	405.83	1	0.00	3.05	1	9	1.58×10^{6}	8.84×10^{5}
405.92	405.89	2	0.48	3.54	14	12	1.49×10^{6}	6.66×10^{5}
410.77	410.71	1	0.04	3.05	3	9	1.33×10^{7}	6.00×10^{6}

Table 12. Continued.

$\lambda_{Reported}$ (nm)	$\lambda_{Observed}$ (nm)	Ion	E_{low} (eV)	E_{upper} (eV)	g_{low}	g_{upper}	A (s^{-1})	Uncertainty (s^{-1})
411.42	411.41	1	0.39	3.40	11	7	1.78×10^{7}	7.99×10^{6}
412.95	412.93	2	0.38	3.38	12	16	5.67×10^{5}	2.62×10^{5}
418.14	418.16	1	0.28	3.25	9	13	9.96×10^{6}	4.60×10^{6}
420.34	420.29	2	0.48	3.43	14	14	4.15×10^{6}	1.83×10^{6}
425.21	425.20	1	0.10	3.02	5	11	4.62×10^{6}	2.16×10^{6}
425.67	425.64	2	0.38	3.29	12	14	4.02×10^{6}	1.84×10^{6}
426.30	426.27	2	0.38	3.29	12	12	3.24×10^{6}	1.52×10^{6}
431.93	431.95	1	0.18	3.05	7	9	3.96×10^{7}	1.80×10^{7}
433.65	433.61	1	0.39	3.25	11	13	1.15×10^{7}	5.29×10^{6}
437.03	436.99	2	0.54	3.38	10	16	8.95×10^{5}	4.24×10^{5}
437.85	437.83	2	1.00	3.83	8	14	3.23×10^{6}	1.46×10^{6}
439.12	439.13	1	0.50	3.32	13	5	6.95×10^{7}	3.16×10^{7}
441.80	441.76	2	0.48	3.29	14	14	1.27×10^{6}	5.82×10^{5}
442.47	442.43	2	0.48	3.29	14	12	9.04×10^{6}	4.22×10^{6}
443.45	443.46	2	1.06	3.86	4	12	2.60×10^{7}	1.19×10^{7}
444.24	444.21	2	0.88	3.67	4	14	4.29×10^{6}	2.00×10^{6}
445.50	445.45	2	1.08	3.86	10	12	8.67×10^{6}	4.04×10^{6}
446.77	446.73	2	0.66	3.43	12	14	7.30×10^{6}	3.25×10^{6}
447.12	447.09	1	0.28	3.05	9	9	1.07×10^{7}	5.03×10^{6}
447.55	447.51	1	0.04	2.81	3	7	2.06×10^{6}	9.25×10^{5}
450.37	450.31	2	1.08	3.83	10	14	1.86×10^{6}	8.74×10^{5}
451.21	451.26	2	0.54	3.29	10	14	3.15×10^{6}	1.46×10^{6}
453.41	453.38	1	0.28	3.02	9	11	3.67×10^{6}	1.68×10^{6}
459.71	459.73	2	0.66	3.36	12	4	2.29×10^{6}	1.10×10^{6}
464.58	464.54	1	0.04	2.70	3	5	7.01×10^{6}	3.25×10^{6}
464.83	464.81	1	0.39	3.05	11	9	8.76×10^{6}	4.01×10^{6}
465.55	465.57	2	1.17	3.83	12	14	1.72×10^{6}	8.11×10^{5}
467.73	467.75	2	0.66	3.31	12	2	2.08×10^{7}	9.49×10^{6}
468.91	468.87	1	0.28	2.93	9	9	6.57×10^{6}	3.00×10^{6}
471.10	471.06	2	0.66	3.29	12	14	5.37×10^{5}	2.45×10^{5}
488.43	488.40	1	0.39	2.93	11	9	2.76×10^{7}	1.26×10^{7}
490.54	490.50	1	0.10	2.63	5	3	1.22×10^{7}	5.54×10^{6}
491.08	491.04	1	0.28	2.81	9	7	1.58×10^{7}	7.17×10^{6}
491.94	491.90	1	0.18	2.70	7	5	1.24×10^{7}	5.68×10^{6}
492.08	492.04	2	1.08	3.60	10	10	7.62×10^{5}	3.41×10^{5}
492.43	492.40	1	0.50	3.02	13	11	6.67×10^{6}	3.02×10^{6}
502.88	502.84	2	1.49	3.96	18	16	2.88×10^{6}	1.35×10^{6}

Table 12. Continued.

$\lambda_{Reported}$ (nm)	$\lambda_{Observed}$ (nm)	Ion	E_{low} (eV)	E_{upper} (eV)	g_{low}	g_{upper}	A (s^{-1})	Uncertainty (s^{-1})
503.40	503.36	2	1.08	3.54	10	12	9.47×10^{4}	4.77×10^{4}
505.32	505.28	2	1.38	3.83	16	14	3.56×10^{6}	1.65×10^{6}
506.99	506.95	2	1.27	3.71	14	12	3.12×10^{6}	1.43×10^{6}
511.27	511.23	2	0.88	3.31	4	2	3.39×10^{6}	1.60×10^{6}
528.33	528.38	1	0.28	2.63	9	3	1.85×10^{7}	8.59×10^{6}
531.26	531.30	2	1.26	3.60	8	10	5.62×10^{5}	2.66×10^{5}
534.92	534.96	1	0.39	2.70	11	5	4.90×10^{6}	2.38×10^{6}
539.05	539.04	2	1.38	3.67	16	14	4.30×10^{4}	2.30×10^{4}
540.56	540.56	2	1.00	3.29	8	14	7.55×10^{5}	3.57×10^{5}
540.83	540.84	2	1.06	3.36	4	4	3.62×10^{5}	2.91×10^{5}
546.72	546.72	2	1.17	3.43	6	14	1.31×10^{6}	6.15×10^{5}
555.08	555.06	2	1.08	3.31	10	2	5.97×10^{6}	2.79×10^{6}
558.86	558.83	2	1.49	3.71	18	12	4.76×10^{5}	2.24×10^{5}
560.13	560.09	2	1.46	3.67	12	14	7.94×10^{5}	3.68×10^{5}
568.72	568.67	2	1.36	3.54	10	12	4.01×10^{5}	1.87×10^{5}
573.00	573.04	2	1.38	3.54	16	12	2.51×10^{5}	1.22×10^{5}
584.65	584.67	2	1.17	3.29	12	12	3.72×10^{4}	2.00×10^{4}
592.15	592.16	2	1.26	3.36	8	4	1.19×10^{5}	6.14×10^{4}
593.29	593.35	2	1.27	3.36	14	4	1.60×10^{6}	7.43×10^{5}
611.11	611.10	2	1.26	3.29	8	14	3.71×10^{5}	1.70×10^{5}
635.39	635.33	1	1.54	3.49	11	9	3.28×10^{6}	1.51×10^{6}

A.6 Gd Estimated Transition Probabilities

Table 13. Gd transition probabilities and their associated energy level details.

$\lambda_{Reported}$ (nm)	$\lambda_{Observed}$ (nm)	Ion	E_{low} (eV)	E_{upper} (eV)	g_{low}	g_{upper}	A (s^{-1})	Uncertainty (s^{-1})
354.31	354.29	1	0.03	3.53	7	19	2.99×10^{7}	1.11×10^{7}
354.61	354.59	2	0.56	4.05	8	14	9.78×10^{7}	6.11×10^{7}
354.97	354.94	2	0.24	3.73	14	12	7.32×10^{7}	4.43×10^{7}
355.86	355.87	2	0.24	3.72	14	10	3.25×10^{7}	1.98×10^{7}
357.22	357.19	2	0.00	3.47	6	8	1.60×10^{7}	9.88×10^{6}
358.53	358.50	2	0.14	3.60	12	10	8.38×10^{7}	5.04×10^{7}
359.30	359.28	2	0.60	4.05	10	14	5.68×10^{7}	3.58×10^{7}
360.91	360.89	2	0.43	3.86	8	16	2.37×10^{7}	1.45×10^{7}
364.64	364.62	2	0.24	3.64	14	14	1.10×10^{8}	6.81×10^{7}
365.49	365.46	2	0.08	3.47	10	8	7.15×10^{7}	4.41×10^{7}

Table 13. Continued.

$\lambda_{Reported}$ (nm)	$\lambda_{Observed}$ (nm)	Ion	E_{low} (eV)	E_{upper} (eV)	g_{low}	g_{upper}	A (s^{-1})	Uncertainty (s^{-1})
365.65	365.69	2	0.66	4.05	12	14	8.94×10^{7}	5.58×10^{7}
366.25	366.23	2	0.00	3.38	6	6	6.08×10^{7}	3.72×10^{7}
367.15	367.12	2	0.08	3.45	10	12	4.51×10^{7}	2.76×10^{7}
367.44	367.41	1	0.03	3.40	7	9	3.71×10^{7}	1.35×10^{7}
368.66	368.65	2	0.50	3.86	4	16	1.22×10^{7}	7.28×10^{6}
368.80	368.78	2	0.35	3.72	4	6	8.30×10^{7}	5.09×10^{7}
369.80	369.77	2	0.03	3.38	8	6	4.99×10^{7}	2.98×10^{7}
370.00	370.00	2	0.38	3.73	6	12	3.48×10^{7}	2.15×10^{7}
371.30	371.27	2	0.38	3.72	6	8	1.15×10^{8}	7.08×10^{7}
371.67	371.64	2	0.03	3.37	8	10	1.90×10^{7}	1.17×10^{7}
371.98	371.99	1	0.03	3.36	7	1	1.59×10^{9}	5.95×10^{8}
372.58	372.55	1	0.00	3.33	5	3	7.01×10^{7}	2.78×10^{7}
373.12	373.08	2	0.38	3.70	6	4	1.41×10^{8}	8.88×10^{7}
373.33	373.30	2	0.73	4.05	14	14	5.38×10^{7}	3.35×10^{7}
374.38	374.35	2	0.14	3.45	12	12	6.68×10^{7}	4.11×10^{7}
374.91	374.92	2	0.08	3.38	10	6	9.56×10^{6}	5.85×10^{6}
375.58	375.56	1	0.03	3.33	7	3	4.48×10^{7}	1.69×10^{7}
376.11	376.09	2	0.42	3.72	8	8	5.61×10^{7}	3.47×10^{7}
376.45	376.44	1	0.07	3.36	9	1	4.51×10^{8}	1.71×10^{8}
376.74	376.72	1	0.12	3.41	11	17	2.46×10^{7}	9.38×10^{6}
376.87	376.84	2	0.08	3.37	10	10	8.01×10^{7}	4.96×10^{7}
377.10	377.07	2	0.56	3.84	8	14	6.55×10^{7}	4.02×10^{7}
378.79	378.76	2	0.49	3.76	10	12	3.39×10^{7}	2.14×10^{7}
379.66	379.64	2	0.03	3.30	8	8	9.02×10^{7}	5.42×10^{7}
380.16	380.22	2	0.60	3.86	10	16	3.89×10^{7}	2.43×10^{7}
380.57	380.54	2	0.38	3.64	6	14	4.12×10^{7}	2.56×10^{7}
381.43	381.40	2	0.00	3.25	6	6	1.00×10^{8}	6.01×10^{7}
381.70	381.74	2	0.35	3.60	4	10	2.46×10^{7}	1.54×10^{7}
382.76	382.71	1	0.03	3.27	7	13	1.36×10^{7}	5.19×10^{6}
383.99	384.03	1	0.03	3.25	7	7	8.67×10^{7}	3.23×10^{7}
384.49	384.50	2	0.50	3.72	4	10	5.45×10^{7}	3.44×10^{7}
385.12	385.10	2	0.00	3.22	6	4	2.50×10^{8}	1.55×10^{8}
385.28	385.25	2	0.03	3.25	8	6	9.66×10^{7}	5.80×10^{7}
385.59	385.60	2	0.42	3.64	8	14	1.53×10^{7}	9.48×10^{6}
386.14	386.16	2	0.52	3.73	6	12	8.82×10^{6}	5.37×10^{6}
386.74	386.73	2	0.50	3.70	4	4	1.10×10^{8}	6.77×10^{7}
387.18	387.18	1	0.00	3.20	5	9	7.03×10^{6}	2.97×10^{6}

Table 13. Continued.

$\lambda_{Reported}$ (nm)	$\lambda_{Observed}$ (nm)	Ion	E_{low} (eV)	E_{upper} (eV)	g_{low}	g_{upper}	A (s^{-1})	Uncertainty (s^{-1})
387.57	387.55	2	0.52	3.72	6	8	9.99×10^{6}	6.24×10^{6}
388.21	388.19	2	0.52	3.72	6	6	2.47×10^{7}	1.52×10^{7}
389.51	389.52	2	0.52	3.70	6	4	8.39×10^{7}	5.17×10^{7}
389.60	389.58	1	0.00	3.18	5	13	1.53×10^{7}	5.64×10^{6}
390.27	390.25	2	0.56	3.73	8	12	3.11×10^{7}	1.92×10^{7}
390.44	390.43	1	0.03	3.20	7	9	6.22×10^{6}	2.22×10^{6}
391.43	391.38	2	0.56	3.72	8	10	6.07×10^{6}	3.78×10^{6}
391.68	391.66	2	0.56	3.72	8	8	9.22×10^{7}	5.46×10^{7}
391.83	391.82	2	0.60	3.76	10	12	9.92×10^{6}	6.43×10^{6}
392.36	392.32	2	0.56	3.72	8	6	4.79×10^{7}	2.97×10^{7}
393.51	393.48	1	0.07	3.22	9	11	3.39×10^{7}	1.35×10^{7}
393.68	393.68	2	0.56	3.70	8	4	7.10×10^{6}	4.67×10^{6}
397.43	397.40	2	0.60	3.72	10	8	3.16×10^{7}	1.95×10^{7}
398.33	398.30	2	0.73	3.84	14	14	1.16×10^{7}	6.94×10^{6}
398.76	398.78	1	0.00	3.11	5	3	1.21×10^{8}	4.52×10^{7}
399.45	399.45	2	0.66	3.76	12	12	1.69×10^{7}	1.06×10^{7}
399.81	399.76	2	0.35	3.45	4	12	9.11×10^{6}	5.53×10^{6}
401.41	401.40	2	0.38	3.47	6	8	2.38×10^{7}	1.43×10^{7}
402.35	402.33	1	0.07	3.15	9	11	2.52×10^{7}	9.81×10^{6}
403.38	403.40	2	0.38	3.45	6	12	1.23×10^{7}	7.81×10^{6}
403.79	403.73	2	0.66	3.73	12	12	1.20×10^{8}	7.43×10^{7}
405.00	404.99	2	0.99	4.05	14	14	3.10×10^{8}	1.89×10^{8}
405.85	405.87	1	0.07	3.12	9	5	9.52×10^{7}	3.57×10^{7}
406.36	406.34	2	0.99	4.04	14	12	2.15×10^{8}	1.34×10^{8}
409.08	409.10	2	0.42	3.45	8	12	8.97×10^{6}	5.75×10^{6}
409.90	409.86	2	0.82	3.84	16	14	1.71×10^{8}	1.06×10^{8}
413.07	413.04	2	0.73	3.73	14	12	8.00×10^{7}	4.92×10^{7}
413.26	413.23	2	0.60	3.60	10	10	6.47×10^{7}	4.04×10^{7}
413.74	413.70	1	0.12	3.12	11	5	8.09×10^{7}	3.00×10^{7}
415.39	415.36	2	0.73	3.72	14	6	2.37×10^{7}	1.44×10^{7}
417.22	417.23	2	0.50	3.47	4	8	5.44×10^{6}	3.58×10^{6}
418.46	418.43	2	0.49	3.45	10	12	7.12×10^{7}	4.32×10^{7}
419.14	419.12	1	0.21	3.17	13	9	1.60×10^{8}	6.08×10^{7}
419.35	419.39	2	0.50	3.45	4	12	3.13×10^{6}	1.92×10^{6}
420.29	420.32	1	0.03	2.98	7	11	9.33×10^{6}	3.52×10^{6}
420.52	420.49	2	0.52	3.47	6	8	3.41×10^{7}	2.10×10^{7}
423.91	423.88	2	1.13	4.05	12	14	5.00×10^{7}	3.11×10^{7}

Table 13. Continued.

$\lambda_{Reported}$ (nm)	$\lambda_{Observed}$ (nm)	Ion	E_{low} (eV)	E_{upper} (eV)	g_{low}	g_{upper}	A (s^{-1})	Uncertainty (s^{-1})
425.21	425.17	2	0.38	3.30	6	8	5.98×10^{7}	3.67×10^{7}
425.38	425.36	2	1.13	4.04	12	12	1.19×10^{8}	7.59×10^{7}
426.05	426.01	1	0.07	2.98	9	11	9.58×10^{6}	3.58×10^{6}
426.24	426.21	2	0.73	3.64	14	14	7.01×10^{7}	4.35×10^{7}
426.71	426.66	1	0.12	3.03	11	13	2.54×10^{7}	9.65×10^{6}
427.47	427.42	1	0.00	2.90	5	7	2.29×10^{7}	8.06×10^{6}
428.08	428.05	2	0.35	3.25	4	6	5.58×10^{7}	3.41×10^{7}
428.63	428.61	1	0.21	3.10	13	11	2.52×10^{7}	9.53×10^{6}
432.14	432.12	2	0.50	3.37	4	10	2.58×10^{7}	1.65×10^{7}
434.25	434.22	2	0.60	3.45	12	12	3.42×10^{7}	2.07×10^{7}
434.47	434.43	2	0.60	3.45	10	12	1.01×10^{7}	6.24×10^{6}
434.69	434.65	1	0.12	2.98	11	11	7.53×10^{7}	2.78×10^{7}
437.02	436.98	2	0.38	3.22	6	4	7.90×10^{7}	4.82×10^{7}
437.42	437.38	1	0.07	2.90	9	7	3.87×10^{7}	1.48×10^{7}
438.11	438.07	1	0.00	2.83	5	9	1.31×10^{7}	4.88×10^{6}
438.79	438.77	2	0.42	3.25	8	6	1.76×10^{7}	1.11×10^{7}
439.78	439.75	2	1.23	4.05	12	14	3.39×10^{7}	2.08×10^{7}
440.86	440.82	2	0.56	3.37	8	10	1.28×10^{7}	7.82×10^{6}
441.15	441.12	1	0.07	2.88	9	11	1.32×10^{7}	5.00×10^{6}
441.94	441.90	2	0.49	3.30	10	8	2.46×10^{7}	1.52×10^{7}
443.66	443.67	2	0.42	3.22	8	4	4.62×10^{7}	2.88×10^{7}
443.86	443.83	2	0.66	3.45	12	12	1.97×10^{7}	1.24×10^{7}
446.51	446.49	1	0.12	2.90	11	7	1.73×10^{7}	6.56×10^{6}
447.65	447.61	1	0.00	2.77	5	5	4.99×10^{7}	1.90×10^{7}
447.91	447.88	2	0.60	3.37	12	10	1.53×10^{7}	9.46×10^{6}
448.14	448.11	2	0.60	3.37	10	10	1.85×10^{7}	1.15×10^{7}
448.70	448.69	1	0.21	2.98	13	11	2.74×10^{7}	1.04×10^{7}
449.76	449.71	1	0.12	2.88	11	13	1.95×10^{7}	7.77×10^{6}
450.38	450.38	1	0.12	2.88	11	11	6.15×10^{6}	2.29×10^{6}
450.67	450.63	2	0.50	3.25	4	6	3.35×10^{7}	2.10×10^{7}
453.81	453.78	1	0.07	2.80	9	7	3.65×10^{7}	1.37×10^{7}
454.04	454.07	2	0.99	3.72	14	8	5.52×10^{7}	3.42×10^{7}
455.84	455.81	2	0.50	3.22	4	4	1.37×10^{7}	8.46×10^{6}
457.42	457.46	2	1.13	3.84	8	14	8.64×10^{6}	5.39×10^{6}
458.30	458.26	2	1.06	3.76	12	12	5.16×10^{7}	3.21×10^{7}
460.14	460.11	2	0.56	3.25	8	6	2.52×10^{7}	1.55×10^{7}
463.93	463.90	2	1.06	3.73	12	12	1.01×10^{7}	6.03×10^{6}

Table 13. Continued.

$\lambda_{Reported}$ (nm)	$\lambda_{Observed}$ (nm)	Ion	E_{low} (eV)	E_{upper} (eV)	g_{low}	g_{upper}	A (s^{-1})	Uncertainty (s^{-1})
465.39	465.38	2	1.10	3.76	10	12	1.22×10^{7}	7.66×10^{6}
465.52	465.50	2	0.56	3.22	8	4	8.63×10^{6}	5.39×10^{6}
467.15	467.15	2	0.73	3.38	14	6	9.11×10^{6}	5.86×10^{6}
468.73	468.70	1	0.88	3.53	11	19	2.67×10^{6}	1.00×10^{6}
470.26	470.25	2	0.82	3.45	16	12	9.87×10^{5}	6.29×10^{5}
470.36	470.33	2	0.66	3.30	12	8	3.30×10^{6}	2.08×10^{6}
471.03	471.03	2	1.13	3.76	8	12	8.92×10^{6}	5.69×10^{6}
472.89	472.85	2	1.10	3.72	10	10	2.03×10^{7}	1.24×10^{7}
473.30	473.26	2	1.10	3.72	10	8	3.69×10^{7}	2.32×10^{7}
473.62	473.63	2	0.60	3.22	10	4	1.80×10^{7}	1.13×10^{7}
474.96	474.99	1	0.79	3.40	5	9	1.00×10^{7}	3.88×10^{6}
475.90	475.92	1	0.92	3.53	7	19	2.80×10^{7}	1.04×10^{7}
478.72	478.69	2	1.13	3.72	8	10	1.69×10^{7}	1.05×10^{7}
480.14	480.11	2	1.13	3.72	8	6	2.55×10^{7}	1.56×10^{7}
484.84	484.82	2	0.66	3.22	12	4	8.74×10^{6}	5.57×10^{6}
489.45	489.43	2	1.17	3.70	4	4	2.51×10^{7}	1.61×10^{7}
491.28	491.28	1	0.84	3.36	9	7	7.61×10^{6}	2.88×10^{6}
491.96	491.99	1	0.81	3.33	7	15	1.48×10^{6}	6.72×10^{5}
492.39	492.39	1	0.84	3.36	9	1	1.14×10^{8}	4.48×10^{7}
493.05	493.03	2	1.53	4.04	8	12	1.62×10^{7}	1.02×10^{7}
493.45	493.42	2	1.13	3.64	12	14	8.43×10^{6}	5.25×10^{6}
499.05	499.06	1	0.88	3.36	11	7	4.57×10^{6}	1.93×10^{6}
499.90	499.90	1	0.92	3.40	7	9	2.17×10^{7}	8.54×10^{6}
501.54	501.51	2	1.23	3.70	12	4	1.49×10^{8}	9.33×10^{7}
502.36	502.35	1	0.90	3.36	9	7	8.61×10^{6}	3.12×10^{6}
503.18	503.14	1	0.79	3.25	5	7	2.69×10^{7}	1.01×10^{7}
507.56	507.54	1	0.81	3.25	7	7	2.47×10^{6}	9.39×10^{5}
509.89	509.89	2	0.82	3.25	16	6	9.23×10^{6}	5.68×10^{6}
510.39	510.35	1	0.99	3.41	15	17	4.68×10^{7}	1.70×10^{7}
510.93	510.99	2	1.62	4.04	6	12	3.39×10^{7}	2.05×10^{7}
513.07	513.07	1	0.88	3.30	11	5	2.73×10^{7}	1.15×10^{7}
514.13	514.16	1	0.92	3.33	7	15	1.26×10^{7}	4.92×10^{6}
517.67	517.63	2	1.06	3.45	12	12	1.55×10^{7}	9.55×10^{6}
518.76	518.75	1	0.94	3.33	5	3	5.61×10^{7}	2.12×10^{7}
519.82	519.78	1	0.88	3.27	11	13	2.33×10^{7}	8.89×10^{6}
525.19	525.12	1	1.05	3.41	17	17	2.69×10^{7}	9.58×10^{6}
528.35	528.31	1	0.99	3.33	15	15	3.29×10^{7}	1.24×10^{7}

Table 13. Continued.

$\lambda_{Reported}$ (nm)	$\lambda_{Observed}$ (nm)	Ion	E_{low} (eV)	E_{upper} (eV)	g_{low}	g_{upper}	A (s^{-1})	Uncertainty (s^{-1})
530.77	530.75	2	1.53	3.86	2	16	1.61×10^{7}	1.02×10^{7}
531.22	531.18	1	0.92	3.25	7	7	5.82×10^{6}	2.11×10^{6}
532.21	532.18	1	0.84	3.17	9	9	4.80×10^{7}	1.85×10^{7}
534.91	534.87	1	0.79	3.11	5	3	5.26×10^{7}	2.04×10^{7}
535.08	535.07	2	1.41	3.72	10	10	1.71×10^{7}	1.08×10^{7}
535.64	535.60	2	1.41	3.72	10	8	2.10×10^{6}	1.37×10^{6}
535.82	535.78	2	1.16	3.47	6	8	3.55×10^{6}	2.19×10^{6}
537.08	537.07	1	0.81	3.12	7	5	5.02×10^{7}	1.89×10^{7}
540.01	540.00	1	0.92	3.22	7	11	1.07×10^{7}	4.10×10^{6}
540.59	540.59	1	0.81	3.10	7	11	2.19×10^{6}	8.78×10^{5}
541.34	541.32	1	0.88	3.17	11	9	1.34×10^{7}	5.59×10^{6}
541.60	541.57	1	0.93	3.22	13	11	7.54×10^{6}	2.66×10^{6}
543.18	543.20	1	0.86	3.15	11	11	2.26×10^{6}	8.04×10^{5}
547.01	546.97	2	1.10	3.37	10	10	6.48×10^{6}	4.09×10^{6}
549.91	549.87	1	0.93	3.18	13	13	6.86×10^{5}	2.71×10^{5}
554.85	554.81	2	1.13	3.37	8	10	1.11×10^{6}	6.72×10^{5}
556.10	556.13	1	0.92	3.15	7	7	1.41×10^{7}	5.34×10^{6}
557.30	557.25	1	0.88	3.10	11	11	4.08×10^{6}	1.41×10^{6}
558.67	558.63	1	0.93	3.15	13	15	4.09×10^{6}	1.47×10^{6}
559.24	559.22	1	0.79	3.01	5	15	1.70×10^{6}	7.85×10^{5}
559.48	559.46	1	0.84	3.06	9	5	3.10×10^{6}	1.12×10^{6}
560.21	560.19	2	1.17	3.38	4	6	1.06×10^{6}	6.94×10^{5}
560.54	560.56	1	0.90	3.11	9	3	8.35×10^{6}	3.28×10^{6}
561.83	561.90	2	1.53	3.73	2	12	1.26×10^{7}	7.91×10^{6}
563.26	563.24	1	0.95	3.15	3	7	1.95×10^{7}	7.43×10^{6}
564.37	564.37	1	0.99	3.18	15	13	2.01×10^{7}	7.84×10^{6}
566.51	566.50	2	1.53	3.72	8	6	8.81×10^{5}	6.64×10^{5}
567.97	567.95	1	0.94	3.12	5	5	1.63×10^{6}	8.50×10^{5}
569.66	569.66	1	1.35	3.53	9	19	2.65×10^{7}	1.00×10^{7}
571.03	571.05	1	0.94	3.11	5	3	2.38×10^{7}	8.85×10^{6}
573.44	573.45	1	0.99	3.15	15	11	1.94×10^{7}	7.18×10^{6}
573.64	573.64	1	0.92	3.08	7	13	2.75×10^{6}	9.98×10^{5}
577.02	576.97	1	0.88	3.03	11	13	3.08×10^{6}	1.13×10^{6}
578.51	578.49	2	1.50	3.64	4	14	3.06×10^{5}	2.40×10^{5}
580.76	580.77	1	0.84	2.98	9	11	1.77×10^{7}	6.59×10^{6}
581.03	581.22	1	0.95	3.08	3	13	7.05×10^{5}	4.25×10^{5}
581.95	582.03	1	1.28	3.41	5	17	6.13×10^{6}	2.43×10^{6}

Table 13. Continued.

$\lambda_{Reported}$ (nm)	$\lambda_{Observed}$ (nm)	Ion	E_{low} (eV)	E_{upper} (eV)	g_{low}	g_{upper}	A (s^{-1})	Uncertainty (s^{-1})
583.17	583.15	2	1.17	3.30	4	8	5.67×10^{6}	3.60×10^{6}
584.90	584.87	1	0.94	3.06	5	5	9.51×10^{6}	3.66×10^{6}
585.68	585.64	2	1.62	3.73	6	12	2.84×10^{7}	1.82×10^{7}
591.40	591.38	1	1.05	3.15	17	7	1.76×10^{7}	6.74×10^{6}
611.46	611.41	1	1.05	3.08	17	9	3.69×10^{7}	1.40×10^{7}

A.7 Tb Estimated Transition Probabilities

Table 14. Tb transition probabilities and their associated energy level details.

$\lambda_{Reported}$ (nm)	$\lambda_{Observed}$ (nm)	Ion	E_{low} (eV)	E_{upper} (eV)	g_{low}	g_{upper}	A (s^{-1})	Uncertainty (s^{-1})
352.76	352.77	2	0.00	3.51	17	13	3.12×10^{6}	1.08×10^{6}
354.41	354.39	2	0.00	3.50	17	15	2.22×10^{7}	7.59×10^{6}
356.20	356.17	2	0.37	3.85	15	17	8.53×10^{7}	2.90×10^{7}
359.67	359.62	2	0.37	3.82	15	17	2.73×10^{7}	9.30×10^{6}
361.49	361.49	2	0.42	3.85	17	17	6.81×10^{6}	2.33×10^{6}
361.68	361.72	2	0.43	3.85	13	17	8.11×10^{6}	2.83×10^{6}
363.88	363.90	2	0.13	3.53	15	19	2.31×10^{7}	8.08×10^{6}
365.08	365.04	2	0.42	3.82	17	17	8.93×10^{7}	3.05×10^{7}
365.26	365.28	2	0.43	3.82	13	17	2.96×10^{7}	1.02×10^{7}
368.85	368.86	1	0.00	3.36	16	12	1.45×10^{7}	2.19×10^{6}
370.42	370.39	2	0.40	3.75	15	15	3.96×10^{7}	1.35×10^{7}
373.03	372.99	2	0.42	3.75	17	15	1.22×10^{7}	4.22×10^{6}
373.26	373.24	2	0.43	3.75	13	15	1.13×10^{7}	4.01×10^{6}
374.76	374.74	2	0.40	3.71	15	13	9.65×10^{7}	3.30×10^{7}
376.29	376.27	2	0.42	3.72	17	11	1.10×10^{7}	3.84×10^{6}
376.54	376.51	2	0.43	3.72	13	11	7.14×10^{7}	2.43×10^{7}
377.68	377.65	2	0.43	3.71	13	13	5.90×10^{7}	2.02×10^{7}
383.06	383.03	1	0.04	3.27	14	16	2.42×10^{7}	3.35×10^{6}
387.00	386.98	2	0.52	3.72	11	11	3.36×10^{7}	1.15×10^{7}
387.45	387.46	1	0.04	3.23	14	18	1.65×10^{8}	2.06×10^{7}
388.20	388.18	2	0.52	3.71	11	13	1.69×10^{7}	5.84×10^{6}
389.95	389.94	1	0.00	3.18	16	12	1.35×10^{8}	1.74×10^{7}
390.17	390.13	1	0.06	3.23	16	18	4.10×10^{7}	5.00×10^{6}
390.83	390.86	1	0.06	3.23	12	18	1.72×10^{7}	2.39×10^{6}
397.72	397.68	2	0.00	3.12	17	17	2.77×10^{7}	9.50×10^{6}
398.21	398.23	2	0.40	3.51	15	13	6.72×10^{7}	2.31×10^{7}

Table 14. Continued.

$\lambda_{Reported}$ (nm)	$\lambda_{Observed}$ (nm)	Ion	E_{low} (eV)	E_{upper} (eV)	g_{low}	g_{upper}	A (s^{-1})	Uncertainty (s^{-1})
398.67	398.67	1	0.00	3.11	16	16	1.03×10^{7}	1.62×10^{6}
400.28	400.30	2	0.40	3.50	15	15	4.27×10^{7}	1.47×10^{7}
400.58	400.55	2	0.13	3.22	15	17	3.00×10^{7}	1.02×10^{7}
403.31	403.34	2	0.42	3.50	17	15	7.73×10^{7}	2.63×10^{7}
403.66	403.62	2	0.43	3.50	13	15	8.46×10^{6}	3.00×10^{6}
410.57	410.62	1	0.17	3.19	10	14	3.52×10^{7}	4.42×10^{6}
413.47	413.44	2	0.52	3.51	11	13	4.32×10^{6}	1.48×10^{6}
414.47	414.44	2	0.13	3.12	15	17	3.56×10^{7}	1.22×10^{7}
417.14	417.13	1	0.30	3.27	8	16	1.76×10^{7}	2.55×10^{6}
427.55	427.54	1	0.46	3.36	14	12	2.14×10^{7}	3.07×10^{6}
428.56	428.55	1	0.29	3.18	12	12	3.37×10^{7}	5.10×10^{6}
428.74	428.78	1	0.34	3.23	14	18	1.97×10^{7}	2.77×10^{6}
430.02	430.04	1	0.35	3.23	10	18	7.02×10^{6}	1.06×10^{6}
431.92	431.88	1	0.00	2.87	16	16	4.03×10^{7}	5.04×10^{6}
432.66	432.65	1	0.00	2.86	16	18	7.75×10^{7}	1.03×10^{7}
435.71	435.68	1	0.34	3.19	14	14	6.80×10^{7}	8.60×10^{6}
437.26	437.28	1	0.04	2.87	14	16	1.09×10^{7}	1.43×10^{6}
438.63	438.58	2	0.37	3.20	15	15	1.12×10^{7}	3.88×10^{6}
441.66	441.61	1	0.06	2.87	12	16	1.35×10^{7}	1.78×10^{6}
442.35	442.41	1	0.06	2.86	12	18	1.20×10^{7}	1.65×10^{6}
446.97	446.95	1	0.46	3.23	14	18	7.94×10^{6}	1.38×10^{6}
456.41	456.43	2	0.40	3.12	15	17	3.69×10^{6}	1.28×10^{6}
464.57	464.53	2	0.00	2.67	17	15	6.35×10^{6}	2.18×10^{6}
470.27	470.31	1	0.47	3.11	8	16	2.07×10^{7}	3.02×10^{6}
475.29	475.25	2	0.00	2.61	17	17	1.19×10^{7}	4.09×10^{6}
476.28	476.26	1	0.58	3.18	18	12	7.35×10^{6}	9.66×10^{5}
476.49	476.52	2	0.52	3.12	11	17	2.68×10^{6}	9.29×10^{5}
491.63	491.62	1	0.34	2.86	14	18	6.08×10^{6}	7.80×10^{5}
492.44	492.43	1	0.84	3.36	6	12	5.42×10^{6}	1.07×10^{6}
493.22	493.16	1	0.34	2.86	14	14	6.55×10^{6}	8.76×10^{5}
493.56	493.61	1	0.85	3.36	4	12	6.00×10^{6}	9.39×10^{5}
494.85	494.83	1	0.35	2.86	10	14	1.92×10^{6}	4.23×10^{5}
504.24	504.19	1	0.78	3.23	2	18	1.07×10^{7}	1.45×10^{6}
508.80	508.75	1	0.77	3.20	10	16	3.42×10^{6}	5.60×10^{5}
510.25	510.26	1	0.68	3.11	4	16	2.36×10^{6}	4.28×10^{5}
519.93	519.89	1	0.80	3.19	8	14	7.61×10^{6}	1.04×10^{6}
530.51	530.47	1	0.04	2.37	14	18	8.95×10^{5}	1.40×10^{5}

Table 14. Continued.

$\lambda_{Reported}$ (nm)	$\lambda_{Observed}$ (nm)	Ion	E_{low} (eV)	E_{upper} (eV)	g_{low}	g_{upper}	A (s^{-1})	Uncertainty (s^{-1})
533.86	533.91	1	0.79	3.11	14	16	9.47×10^{6}	1.56×10^{6}
535.53	535.49	1	0.06	2.37	16	18	3.47×10^{6}	4.85×10^{5}
541.57	541.56	1	0.58	2.86	18	18	1.32×10^{6}	2.37×10^{5}
547.08	547.04	1	0.84	3.11	6	16	7.38×10^{6}	1.12×10^{6}
613.44	613.40	1	0.85	2.87	4	16	2.04×10^{6}	3.85×10^{5}

A.8 Dy Estimated Transition Probabilities

Table 15. Dy transition probabilities and their associated energy level details.

$\lambda_{Reported}$ (nm)	$\lambda_{Observed}$ (nm)	Ion	E_{low} (eV)	E_{upper} (eV)	g_{low}	g_{upper}	A (s^{-1})	Uncertainty (s^{-1})
353.59	353.60	2	0.54	4.04	16	18	3.04×10^{7}	7.51×10^{6}
353.85	353.85	2	0.00	3.50	18	18	1.88×10^{7}	4.62×10^{6}
356.33	356.31	2	0.10	3.58	16	16	1.83×10^{7}	4.63×10^{6}
359.16	359.16	1	0.00	3.45	17	15	5.37×10^{7}	1.32×10^{7}
363.02	363.02	2	0.54	3.95	16	18	2.39×10^{7}	6.23×10^{6}
368.57	368.57	2	0.59	3.95	14	18	3.75×10^{6}	9.27×10^{5}
383.64	383.65	2	0.54	3.77	16	16	2.55×10^{7}	6.53×10^{6}
397.85	397.85	2	0.93	4.04	14	18	5.59×10^{7}	1.44×10^{7}
398.38	398.37	2	0.54	3.65	16	16	3.35×10^{7}	8.97×10^{6}
405.05	405.06	2	0.59	3.65	14	16	1.80×10^{7}	4.78×10^{6}
414.31	414.31	2	0.59	3.58	14	16	1.73×10^{7}	4.66×10^{6}
432.24	432.22	2	0.59	3.46	14	16	2.02×10^{6}	5.11×10^{5}
435.85	435.89	2	0.93	3.77	12	16	4.97×10^{6}	1.31×10^{6}
469.68	469.67	2	1.31	3.95	18	18	3.28×10^{6}	8.75×10^{5}
481.88	481.85	1	0.51	3.08	15	11	7.18×10^{6}	1.58×10^{6}
499.78	499.75	2	1.17	3.65	10	16	6.70×10^{5}	1.68×10^{5}
513.63	513.60	2	1.22	3.64	12	18	7.90×10^{5}	3.06×10^{5}
513.96	513.91	2	1.17	3.58	10	16	5.23×10^{6}	1.45×10^{6}
514.14	514.12	2	1.36	3.77	8	16	5.80×10^{5}	2.97×10^{5}
515.13	515.11	2	1.36	3.76	8	14	1.85×10^{6}	5.87×10^{5}
530.52	530.57	2	1.31	3.65	18	16	6.52×10^{5}	2.68×10^{5}
531.19	531.19	2	1.17	3.50	10	18	5.38×10^{5}	1.89×10^{5}
536.36	536.34	1	1.14	3.45	11	17	1.45×10^{6}	4.77×10^{5}
538.63	538.62	2	1.46	3.76	10	14	1.09×10^{6}	3.14×10^{5}
540.92	540.90	2	1.36	3.65	8	16	9.13×10^{5}	2.87×10^{5}
541.00	540.96	1	1.52	3.82	11	13	4.76×10^{6}	1.52×10^{6}

A.9 Ho Estimated Transition Probabilities

Table 16. Ho transition probabilities and their associated energy level details.

$\lambda_{Reported}$ (nm)	$\lambda_{Observed}$ (nm)	Ion	E_{low} (eV)	E_{upper} (eV)	g_{low}	g_{upper}	A (s^{-1})	Uncertainty (s^{-1})
351.55	351.56	2	0.08	3.60	15	13	4.23×10^{7}	1.24×10^{7}
381.06	381.07	2	0.00	3.25	17	15	6.79×10^{7}	1.92×10^{7}
384.38	384.38	2	0.00	3.22	17	15	1.34×10^{7}	3.90×10^{6}
385.40	385.41	2	0.70	3.91	15	15	1.08×10^{8}	3.17×10^{7}
386.16	386.17	2	0.70	3.91	15	13	1.25×10^{8}	3.63×10^{7}
388.89	388.90	2	0.73	3.91	13	15	1.31×10^{8}	3.86×10^{7}
389.68	389.67	2	0.73	3.91	13	13	4.42×10^{7}	1.34×10^{7}
390.56	390.56	2	0.08	3.25	15	15	2.32×10^{7}	6.80×10^{6}
399.36	399.33	2	0.73	3.83	13	15	5.84×10^{6}	1.78×10^{6}
404.54	404.55	2	0.00	3.06	17	15	5.36×10^{7}	1.53×10^{7}
415.25	415.26	2	0.08	3.06	15	15	1.51×10^{7}	4.28×10^{6}
419.43	419.43	1	0.00	2.96	16	16	4.07×10^{6}	1.05×10^{6}
433.25	433.21	2	0.73	3.59	13	19	1.94×10^{6}	5.90×10^{5}
468.81	468.81	1	1.04	3.69	16	14	5.57×10^{6}	1.66×10^{6}
470.15	470.15	1	1.04	3.68	18	16	1.67×10^{7}	4.54×10^{6}
474.86	474.90	2	0.08	2.69	15	15	1.40×10^{6}	3.96×10^{5}
482.56	482.55	2	1.34	3.91	9	15	5.23×10^{6}	1.43×10^{6}
490.25	490.27	2	0.70	3.22	15	15	2.19×10^{6}	6.52×10^{5}
497.99	497.96	2	1.10	3.59	11	19	6.05×10^{6}	1.70×10^{6}
498.71	498.72	2	1.34	3.83	9	15	2.82×10^{6}	9.84×10^{5}
502.81	502.80	2	0.00	2.47	17	11	7.09×10^{4}	2.44×10^{4}
524.45	524.50	2	1.34	3.71	9	15	5.26×10^{6}	1.52×10^{6}
539.39	539.34	1	0.67	2.97	14	14	2.03×10^{6}	5.52×10^{5}
541.13	541.15	2	0.08	2.37	15	19	4.29×10^{5}	1.16×10^{5}
549.05	549.06	2	1.39	3.65	11	17	3.33×10^{5}	9.93×10^{4}
564.06	564.11	2	1.39	3.59	11	19	6.20×10^{5}	2.20×10^{5}
574.14	574.13	1	1.53	3.69	16	14	2.31×10^{6}	7.20×10^{5}
586.02	586.03	1	0.00	2.12	16	14	1.34×10^{6}	3.60×10^{5}
592.16	592.17	1	0.00	2.09	16	16	7.50×10^{5}	1.99×10^{5}
608.18	608.18	1	0.00	2.04	16	18	3.93×10^{5}	1.07×10^{5}
615.78	615.83	1	1.04	3.06	16	16	1.24×10^{6}	3.50×10^{5}
625.56	625.53	1	1.04	3.02	18	18	8.10×10^{5}	2.35×10^{5}
630.53	630.53	1	0.00	1.97	16	16	4.22×10^{5}	1.12×10^{5}

A.10 Er Estimated Transition Probabilities

Table 17. Er transition probabilities and their associated energy level details.

$\lambda_{Reported}$ (nm)	$\lambda_{Observed}$ (nm)	Ion	E_{low} (eV)	E_{upper} (eV)	g_{low}	g_{upper}	A (s^{-1})	Uncertainty (s^{-1})
363.34	363.35	2	0.00	3.41	14	14	6.61×10^{6}	2.49×10^{6}
380.80	380.80	2	0.64	3.89	10	12	3.18×10^{6}	1.21×10^{6}
384.80	384.77	2	0.67	3.89	8	12	5.23×10^{6}	1.98×10^{6}
392.18	392.22	2	0.64	3.80	10	14	7.18×10^{6}	2.67×10^{6}
393.87	393.86	2	0.00	3.15	14	12	1.51×10^{7}	5.70×10^{6}
397.46	397.47	2	0.05	3.17	12	12	7.42×10^{6}	2.94×10^{6}
402.04	402.05	1	0.86	3.95	11	13	4.00×10^{7}	1.50×10^{7}
423.49	423.48	2	0.67	3.60	8	10	2.73×10^{6}	1.07×10^{6}
441.08	441.04	2	0.85	3.66	16	12	1.04×10^{6}	4.22×10^{5}
444.83	444.84	1	1.16	3.95	17	13	9.91×10^{6}	3.59×10^{6}
467.31	467.32	1	0.00	2.65	13	11	1.18×10^{6}	4.34×10^{5}
479.54	479.60	1	0.62	3.21	9	13	6.09×10^{6}	2.35×10^{6}
484.87	484.84	1	0.00	2.56	13	9	4.16×10^{6}	1.57×10^{6}
488.60	488.63	2	0.64	3.17	10	12	7.26×10^{5}	2.80×10^{5}
495.17	495.19	2	0.67	3.17	8	12	5.17×10^{6}	2.00×10^{6}
514.03	514.10	1	1.53	3.95	7	13	6.31×10^{6}	2.53×10^{6}
527.57	527.58	2	0.89	3.24	12	14	1.61×10^{5}	6.09×10^{4}
531.00	531.06	2	1.32	3.66	14	12	1.71×10^{6}	6.48×10^{5}
537.49	537.53	2	1.35	3.66	8	12	5.30×10^{5}	2.01×10^{5}
551.85	551.81	2	1.35	3.60	8	10	2.54×10^{6}	9.56×10^{5}
562.64	562.69	1	0.89	3.09	13	15	1.69×10^{6}	6.40×10^{5}
571.31	571.31	1	0.86	3.03	11	13	4.31×10^{5}	1.62×10^{5}
576.27	576.28	1	0.00	2.15	13	11	1.29×10^{6}	5.13×10^{5}
585.51	585.53	1	0.00	2.12	13	13	5.32×10^{5}	1.96×10^{5}
604.36	604.35	1	1.07	3.12	19	11	1.90×10^{5}	8.56×10^{4}
630.87	630.88	1	0.00	1.96	13	15	3.43×10^{5}	1.36×10^{5}

A.11 Tm Estimated Transition Probabilities

Table 18. Tm transition probabilities and their associated energy level details.

$\lambda_{Reported}$ (nm)	$\lambda_{Observed}$ (nm)	Ion	E_{low} (eV)	E_{upper} (eV)	g_{low}	g_{upper}	A (s^{-1})	Uncertainty (s^{-1})
366.80	366.81	2	0.00	3.38	9	9	3.51×10^{6}	8.51×10^{5}
373.40	373.41	2	0.03	3.35	7	9	1.05×10^{7}	2.28×10^{6}
391.64	391.65	1	1.09	4.25	6	8	1.99×10^{7}	4.57×10^{6}

Table 18. Continued.

$\lambda_{Reported}$ (nm)	$\lambda_{Observed}$ (nm)	Ion	E_{low} (eV)	E_{upper} (eV)	g_{low}	g_{upper}	A (s^{-1})	Uncertainty (s^{-1})
413.82	413.78	1	0.00	3.00	8	2	4.66×10^{6}	1.12×10^{6}
419.99	419.99	2	0.00	2.95	9	9	2.07×10^{6}	4.94×10^{5}
448.12	448.13	2	0.00	2.77	9	9	1.84×10^{6}	4.32×10^{5}
452.93	452.94	2	0.03	2.77	7	9	4.85×10^{5}	1.21×10^{5}
454.84	454.86	2	0.00	2.72	9	5	3.66×10^{5}	1.06×10^{5}
462.64	462.66	2	0.00	2.68	9	7	1.22×10^{6}	2.92×10^{5}
465.50	465.49	2	0.03	2.69	7	7	4.06×10^{5}	1.02×10^{5}
475.85	475.84	2	1.11	3.72	7	5	5.34×10^{5}	1.67×10^{5}
537.30	537.31	1	1.09	3.39	6	14	2.93×10^{5}	8.11×10^{4}
570.99	570.95	2	1.54	3.72	13	5	5.79×10^{6}	1.36×10^{6}
646.02	646.02	1	1.09	3.01	6	8	1.23×10^{6}	3.29×10^{5}

A.12 Yb Estimated Transition Probabilities

Table 19. Yb transition probabilities and their associated energy level details.

$\lambda_{Reported}$ (nm)	$\lambda_{Observed}$ (nm)	Ion	E_{low} (eV)	E_{upper} (eV)	g_{low}	g_{upper}	A (s^{-1})	Uncertainty (s^{-1})
373.46	373.47	1	2.23	5.55	3	5	2.21×10^{7}	2.35×10^{6}
377.00	377.01	1	2.14	5.43	1	3	3.96×10^{7}	3.32×10^{6}
381.62	381.61	2	3.91	7.16	6	10	2.15×10^{8}	2.14×10^{7}
387.27	387.29	1	2.23	5.43	3	3	1.72×10^{7}	2.33×10^{6}
399.07	399.09	1	2.44	5.55	5	5	2.68×10^{7}	3.53×10^{6}
414.89	414.91	1	2.44	5.43	5	3	4.82×10^{7}	4.40×10^{6}
443.91	443.92	1	2.14	4.94	1	3	1.98×10^{7}	2.00×10^{6}
457.61	457.62	1	2.23	4.94	3	5	2.48×10^{7}	2.58×10^{6}
458.23	458.24	1	2.23	4.94	3	3	1.49×10^{7}	1.71×10^{6}
478.66	478.66	1	2.14	4.73	1	3	6.93×10^{7}	6.09×10^{6}
485.11	485.11	2	3.02	5.57	6	4	9.06×10^{6}	1.89×10^{6}
491.25	491.24	1	2.44	4.97	5	5	2.76×10^{6}	3.12×10^{5}
493.54	493.55	1	2.44	4.96	5	7	2.31×10^{7}	2.53×10^{6}
507.22	507.21	1	0.00	2.44	1	5	1.82×10^{4}	2.12×10^{3}
514.70	514.72	1	2.23	4.64	3	3	4.83×10^{6}	4.20×10^{5}
533.51	533.55	1	3.11	5.43	3	3	1.37×10^{8}	1.25×10^{7}
535.29	535.31	2	3.36	5.67	2	4	2.99×10^{8}	2.90×10^{7}
558.84	558.81	1	2.14	4.36	1	11	1.83×10^{6}	1.82×10^{5}
573.00	573.06	1	3.39	5.55	13	5	1.18×10^{7}	9.96×10^{5}
583.71	583.75	1	3.04	5.16	3	3	2.15×10^{7}	2.11×10^{6}

Table 19. Continued.

$\lambda_{Reported}$ (nm)	$\lambda_{Observed}$ (nm)	Ion	E_{low} (eV)	E_{upper} (eV)	g_{low}	g_{upper}	A (s^{-1})	Uncertainty (s^{-1})
585.46	585.45	1	3.21	5.32	11	11	2.75×10^{6}	3.07×10^{5}
626.08	626.09	1	3.21	5.19	11	7	6.28×10^{6}	5.07×10^{5}
648.91	648.91	1	2.14	4.05	1	3	1.02×10^{7}	1.12×10^{6}

A.13 Lu Estimated Transition Probabilities

Table 20. Lu transition probabilities and their associated energy level details.

$\lambda_{Reported}$ (nm)	$\lambda_{Observed}$ (nm)	Ion	E_{low} (eV)	E_{upper} (eV)	g_{low}	g_{upper}	A (s^{-1})	Uncertainty (s^{-1})
355.43	355.44	2	2.15	5.64	5	5	1.16×10^{8}	3.54×10^{7}
362.39	362.40	2	2.15	5.57	5	7	1.81×10^{7}	5.46×10^{6}
364.77	364.78	1	0.51	3.91	2	4	2.18×10^{7}	6.55×10^{6}
375.67	375.68	1	0.51	3.81	2	2	6.25×10^{6}	1.94×10^{6}
387.66	387.66	2	1.54	4.74	5	3	2.05×10^{7}	6.32×10^{6}
392.52	392.48	1	0.51	3.67	2	4	2.90×10^{6}	9.24×10^{5}
405.44	405.44	1	0.51	3.57	2	2	1.29×10^{7}	3.91×10^{6}
412.46	412.47	1	0.93	3.93	4	6	2.48×10^{7}	7.51×10^{6}
415.40	415.41	1	0.93	3.91	4	4	6.02×10^{6}	1.91×10^{6}
418.42	418.43	2	2.15	5.11	5	5	5.91×10^{7}	1.79×10^{7}
426.19	426.20	2	5.65	8.55	3	1	1.22×10^{9}	3.66×10^{8}
429.59	429.60	1	0.93	3.81	4	2	1.01×10^{7}	3.18×10^{6}
434.20	434.20	2	4.48	7.33	5	3	2.05×10^{8}	6.21×10^{7}
443.02	443.03	2	4.53	7.33	3	3	1.46×10^{8}	4.30×10^{7}
445.07	445.08	1	0.93	3.71	4	4	2.79×10^{6}	8.58×10^{5}
458.68	458.69	2	3.65	6.35	5	5	2.39×10^{6}	7.86×10^{5}
483.95	483.96	2	1.46	4.02	3	5	1.15×10^{6}	3.62×10^{5}
490.48	490.49	1	0.51	3.04	2	4	3.91×10^{6}	1.21×10^{6}
499.41	499.41	2	1.54	4.02	5	5	9.31×10^{6}	2.84×10^{6}
542.18	542.19	1	0.25	2.53	6	8	4.37×10^{5}	1.34×10^{5}
543.78	543.79	1	0.93	3.21	4	6	9.71×10^{5}	3.01×10^{5}
547.66	547.67	2	1.76	4.02	7	5	2.08×10^{7}	6.12×10^{6}
566.50	566.49	2	3.83	6.02	7	9	4.65×10^{6}	1.38×10^{6}
571.34	571.35	2	3.65	5.82	5	5	6.26×10^{6}	1.87×10^{6}
580.04	580.06	1	0.93	3.06	4	6	3.68×10^{5}	1.10×10^{5}
598.38	598.39	2	1.46	3.53	3	3	8.37×10^{6}	2.53×10^{6}
615.99	615.99	2	4.03	6.04	9	7	7.97×10^{7}	2.44×10^{7}
619.96	619.96	2	3.65	5.65	5	3	6.84×10^{7}	2.10×10^{7}

Table 20. Continued.

$\lambda_{Reported}$ (nm)	$\lambda_{Observed}$ (nm)	Ion	E_{low} (eV)	E_{upper} (eV)	g_{low}	g_{upper}	A (s^{-1})	Uncertainty (s^{-1})
622.80	622.81	2	3.65	5.64	5	5	6.78×10^{6}	2.13×10^{6}
623.54	623.53	2	4.03	6.02	9	9	2.68×10^{7}	8.29×10^{6}
624.23	624.23	2	3.83	5.82	7	5	5.68×10^{7}	1.73×10^{7}
646.30	646.31	2	1.46	3.38	3	1	2.17×10^{7}	6.57×10^{6}

Vita

Sawyer Blue Irvine was born on December 5th, 1996, in Knoxville, TN. He attended public school until grade 5 when he was homeschooled until middle school. At the end of middle school, he attended freshmen year at the STEM academy in Knoxville and then returned to homeschool after the freshmen year to finish high school. He attended Pellissippi State Community College during high school.

He graduated with a Bachelor of Science in Chemistry and a minor in Physics from Brigham Young University – Idaho. He performed various research projects during his undergraduate program with Dr. Heywood and Dr. Becerril. During his senior year at BYU-Idaho he was accepted into the Department of Nuclear Engineering at University of Tennessee – Knoxville for graduate school.

He attended graduate school while doing research under Dr. Jamie Coble, Dr. Kristian Myhre, and Dr. Hunter Andrews. He plans on obtaining a Master of Science from the Nuclear Engineering department in August of 2022 and has accepted an offer from ORNL as a Radioisotope Production and Separations Technical Professional.